YEDITEPE UNIVERSITY
GRADUATE SCHOOL OF NATURAL AND APPLIED SCIENCES

THE ANTI-CANCER ACTIVITY OF SOY LECITHIN-BASED LIPOSOMAL CURCUMIN IN PROSTATE CANCER

A Dissertation Submitted
by
Selen Tiryaki

In Partial Fulfillment
of the Requirements for the Degree of
Doctor of Philosophy
in
Biotechnology

Supervisor
Prof. Dr. Dilek Telci Temeltaş

Co-Supervisor
Assist. Prof. Dr. Gülengül Duman

Istanbul - 2025

THE ANTI-CANCER ACTIVITY OF SOY LECITHIN-BASED LIPOSOMAL CURCUMIN IN PROSTATE CANCER

by

Selen Tiryaki

Approved by:

Prof. Dr. Dilek Telci Temeltaş
(Yeditepe University) .....
(Thesis Supervisor)

Assist. Prof. Dr. Gülengül Duman
(Yeditepe University)
(Co-Supervisor)

Prof. Dr. Gamze Torun Köse
(Yeditepe University) .....

Assoc. Prof. Dr. Ayşegül Doğan
(Yeditepe University) .....

Prof. Dr. Ceren Çıracı Muğan
(Istanbul Technical University) .....

Assist. Prof. Dr. Derya Dilek Kançağı
(Fenerbahce University) .....

DATE OF APPROVAL: ..../..../20...

DECLARATION OF ORIGINALITY

I hereby declare that this thesis is my own work and that all information in this thesis has been obtained and presented following academic rules and ethical conduct. I have fully cited and referenced all material and results as required by these rules and conduct, and this thesis study does not contain any plagiarism. The necessary permissions have been obtained if any material used in the thesis requires copyright. No material from this thesis has been used to award another degree.

To the best of my knowledge and belief, it contains no material previously published or written by another person nor material accepted for the award of any other degree except where due acknowledgment has been made in the text.

I accept all kinds of legal liability that may arise in cases contrary to these situations.

Selen Tiryaki

Signature

ABSTRACT

THE ANTI-CANCER ACTIVITY OF SOY LECITHIN-BASED LIPOSOMAL CURCUMIN IN PROSTATE CANCER

Prostate cancer ranks as one of the most prevalent cancers among males and ranks second in cancer-related deaths. Recently, there is an increasing emphasis on designing cancer-specific targets and developing drug delivery systems aimed at these targets to prevent cancer formation and progression. Curcumin, a phenolic phytochemical derived from the *Curcuma longa* plant's roots, has been used for traditional treatments for many centuries. Various research has demonstrated that curcumin displays antioxidant, anti-mutagenic, anti-inflammatory, anti-proliferative, and anti-cancer properties by regulating numerous molecular pathways. Although *in vivo* research has revealed that curcumin has a function as a tumor suppressor and inhibits tumor growth, its limited solubility in water (resulting in reduced bioavailability), poor pharmacokinetics, and easy degradation in neutral to basic pH conditions limit its effectiveness and hinder its use as a chemotherapeutic agent and chemosensitizer. One approach to enhance curcumin's bioavailability is encapsulating it in a highly water-soluble carrier form. Based on this concept, a formulation of soy lecithin-based encapsulated curcumin ($_{SLC}$CUR) was developed. *In vitro* experiments revealed that encapsulation in soy lecithin-based carriers significantly improved curcumin's solubility. The studies demonstrated that the intracellular uptake of $_{SLC}$CUR was 15-fold higher than $_{F}$CUR and exhibited high targeting efficiency in androgen receptor-positive (AR+) prostate cancer cells (22Rv1 and LNCaP), along with normal prostate epithelial cells (PNT1A). Moreover, greater apoptotic activity was shown in $_{SLC}$CUR-treated prostate cancer cells relative to those treated with free curcumin ($_{F}$CUR). In a Foxn1$^{nu/nu}$ mutant nude mice 22Rv1 xenograft model, the administration of $_{SLC}$CUR showed a 10-fold higher reduction in tumor size compared to $_{F}$CUR, indicating that the anticancer efficacy of curcumin is significantly enhanced when encapsulated in soy lecithin-based carriers. The research was supported by TÜBİTAK under project number 123S225.

ÖZET

PROSTAT KANSERİNDE SOYA LESİTİN BAZLI LİPOZOMAL KURKUMİNİN ANTİ-KANSER AKTİVİTESİNİN İNCELENMESİ

Prostat kanseri, erkekler arasında en yaygın kanser türlerinden biridir. Prostat kanseri, kanserle ilişkili ölümlerde ikinci olarak yer almaktadır. Kanser oluşumunu ve ilerlemesini önlemek amacıyla kansere özel hedefler ve bu hedeflere yönelik ilaç dağıtım sistemleri tasarımı üzerine çalışmalar son yıllarda önem kazanmıştır. Kurkumin, *Curcuma longa* bitkisinin köklerinden ekstrakt edilen fenolik bir fitokimyasaldır ve yüzyıllardır geleneksel tıpta kullanılmaktadır. Farklı çalışmalarla kurkuminin çok sayıda sinyal yolağını modüle eden bir anti-oksidan, anti-mutajenik, anti-inflamatuar, anti-proliferatif ve anti-kanser özelliklerine sahip olduğu ve tümör baskılayıcı bir ajan olarak görev yaptığı ve tümör büyümesini inhibe ettiği gösterilmiştir. Kurkuminin suda düşük çözünürlüğü (dolayısıyla düşük biyoyararlanımı) ve zayıf farmakokinetik yapısı kurkuminin etkinliğini kısıtlamakta kullanımını sınırlamaktadır. Kurkuminin düşük biyoyararlanımının arttırılması için kullanılan yöntemlerinden biri suda çözünürlüğü yüksek taşıyıcı bir formun içerisine enkapsüle edilerek kullanılmasıdır. Bu noktadan hareketle, bu çalışmada soya lesitini bazlı enkapsüle kurkuminin formülasyonu geliştirilmiş olup, yapılan *in vitro* deneylerde soya lesitin bazlı enkapsülasyon ile kurkuminin çözünürlüğünün arttırıldığı gösterilmiştir. *In vitro* deneylerde soya lesitini bazlı enkapsüle kurkuminin hücre içine alımının serbest formdaki kurkumine kıyasla hem 15 kat daha yüksek olduğu hem de yüksek hedefleme etkinliği gösterdiği androjen reseptörü pozitif (AR+) prostat kanseri hücre hatları 22Rv1 ve LNCaP ve normal prostat epitel hücreleri PNT1A üzerinde yapılan deneylerle gösterilmiştir. Ayrıca, $_{SLC}$CUR ile tedavi edilen kanser hücrelerinde, serbest kurkumin ($_{F}$CUR) ile tedavi edilenlere kıyasla daha fazla apoptotik aktivite gözlenmiştir. Foxn1$^{nu/nu}$ mutant nude fare 22Rv1 ksenograft modelinde, $_{SLC}$CUR uygulaması $_{F}$CUR'a kıyasla tümör boyutunda 10 kat daha fazla azalma göstermiştir; bu da kurkuminin antikanser etkinliğinin soya lesitini bazlı taşıyıcılarda kapsüllendiğinde önemli ölçüde arttığını göstermektedir. Bu araştırma 123S225 numaralı proje kapsamında TÜBİTAK tarafından desteklenmiştir.

This thesis is dedicated to my beloved babies

Reisco, Ayşesu, Sidsu, Zisu & Göceksu, Cafer, and Goldy…

ACKNOWLEDGEMENTS

First and foremost, I am deeply grateful to my advisor, Prof. Dr. Dilek Telci Temeltaş, for her unwavering support, guidance, and the invaluable opportunities she provided throughout my PhD journey. Her mentorship shaped both my research and who I became as a scientist.

My sincere thanks to my co-supervisor, Assist. Prof. Dr. Gülengül Duman and to my committee members Prof. Dr. Fikrettin Şahin, Prof. Dr. Gamze Torun Köse, Assoc. Prof. Ayşegül Doğan, Assoc. Prof. Ceren Çıracı Muğan, and Assist. Prof. Derya Dilek Kançağı for their valuable feedback and support.

I would like to thank Prof. Dr. Itır Ebru Zemheri for the histopathological analyses, and Dr. Engin Sümer and Dr. Burcu Can for their help during the animal studies. Heartfelt thanks to Dr. Pınar Akkuş Süt, whose steady encouragement helped me stand back up whenever I lost.

Warm thanks to all members of the DT Lab for being part of this journey. Special thanks to Dr. İnci Kurt Celep, whose calm guidance and sisterly presence were a constant light. To Ayça Ece Nezir, for turning lab days into lifelong friendship and always listening to my endless questions. To İpek Bedir, for lighting up even the quietest days and always being a call away to share my chaos. To Halime İlhan Sığınç, for her kind heart and constant support. To Ürün Ukan, for a friendship that feels timeless, even from afar. To Duygu Orak, for being a true friend no matter the distance. And to Alican Kuşoğlu, whose quiet support always found its way to me.

To the love of my life, Baran Çolak, your belief in me made me shine. I am endlessly grateful and excited for everything we will build together.

Finally, my deepest thanks to my family, Gönül, Sedat Tiryaki, Feriha, Ayla, Mert, and Çınar Kopuk for standing by me through everything. And to my sister, Gizem Tiryaki, my best friend, my anchor, and the most precious soul in my life.

This study was funded by the Scientific and Technological Research Council of Turkey (TÜBİTAK) (Project No. 123S225) and Yeditepe University (Project No. HD-24035).

TABLE OF CONTENTS

LIST OF FIGURES

LIST OF TABLES

LIST OF ABBREVIATIONS

°C	Degree Celsius
kDa	Kilodalton
mA	Milliampere
mL	Milliliter
mM	Millimolar
nm	Nanometer
V	Volt
v/v	Volume per volume
w/v	Weight per volume
x*g*	Times gravity
ADT	Androgen deprivation therapy
ADP	Adenosine diphosphate
AIPC	Androgen-independent prostate cancer
AKT	Protein kinase B
AR	Androgen receptor
APAF-1	Apoptotic peptidase activating factor 1
APS	Ammonium persulfate
AP-1	Activator protein 1
ATCC	American type culture collection
BSA	Bovine serum albumin
BPH	Benign prostatic hyperplasia
CAR-T	Chimeric antigen receptor T-cell
Cas9	CRISPR-associated protein 9
CBP	Cyclic adenosine monophosphate response element binding protein
CRISPR	Clustered regularly interspaced short palindromic repeats
CRPC	Castration-resistant prostate cancer
CUR	Curcumin
DISC	Death-inducing signaling complex
DHT	Dihydrotestosterone
DLS	Dynamic light scattering

DMSO	Dimethyl sulfoxide
DNA	Deoxyribonucleic acid
DTT	Dithiothreitol
EDTA	Ethylenediamine tetraacetic acid
EGTA	Ethylene glycol tetraacetic acid
EGFR	Epidermal growth factor receptor
EPR	Enhanced permeability and retention
ER	Endoplasmic reticulum
ERG	Ets-related gene
FADD	Fas-associated death domain protein
FBS	Fetal bovine serum
FDA	Food and drug administration
FT-IR	Fourier transform infrared spectroscopy
GE	Gel electrophoresis
GRAS	Generally recognized as a safe
GnRH	Gonadotropin-releasing hormone
HG-PIN	High grade-prostatic intraepithelial neoplasia
HIV	Human immunodeficiency virus
HL-60	Human leukemia 60
MAPK	Mitogen activated protein kinase
MDR	Multidrug resistance
NF-κB	Nuclear factor kappa-B
PA	Polyacrylamide
PARP	Poly ADP-ribose polymerase
PBS	Phosphate buffered saline
PCa	Prostate cancer
PDI	Polydispersity index
pH	Power of hydrogen
PIN	Prostatic intraepithelial neoplasia
PI3K	Phosphoinositide 3-kinase
PLGA	Poly(lactic co-glycolic acid
PMSF	Phenylmethanesulfonylfluoride
PSA	Prostate specific antigen

PTEN	Phosphatase and tensin homolog
RPMI-1640	Roswell Park Memorial Institute 1640
SDS	Sodium dodecyl sulfate
STAT	Signal transducer and activator of transcription
TEMED	Tetramethyl ethylenediamine
TMPRSS2	Transmembrane protease, serine 2
TNF	Tumor necrosis factor
TNM	Tumor node metastases
TRAIL	Tumor necrosis factor related apoptosis inducing ligand
TUNEL	Terminal deoxynucleotidyl transferase dUTP nick-end labeling
VEGFR	Vascular endothelial growth factor receptor
ZP	Zeta potential

1. INTRODUCTION

1.1. PROSTATE

The prostate is an exocrine gland within the reproductive system in men, with an approximate weight of 11 grams. It is in the pelvic area and is found in all mammals and some vertebrates [1]. Its anatomy, pathology, and biochemistry differ among species, highlighting its unique role in reproduction. The prostate is covered with muscles and smooth muscle fibers that contract during ejaculation to expel prostatic fluid (Figure 1.1). The prostate produces a fluid that substantially increases semen volume, improves sperm motility, provides protective functions, and extends sperm survival [2]. This fluid is rich in citric acid and proteolytic enzymes, which nourish sperm—the male reproductive cells—and prevent their coagulation in the vagina during sexual intercourse. This fluid, along with sperm, is excreted as semen after ejaculation. Neutralizing the urethral acidity improves sperm mobility and viability, facilitating successful fertilization [3]. The growth and function of the prostate are influenced by endocrine glands, particularly by serum testosterone, which supports its development and maintains its size [4].

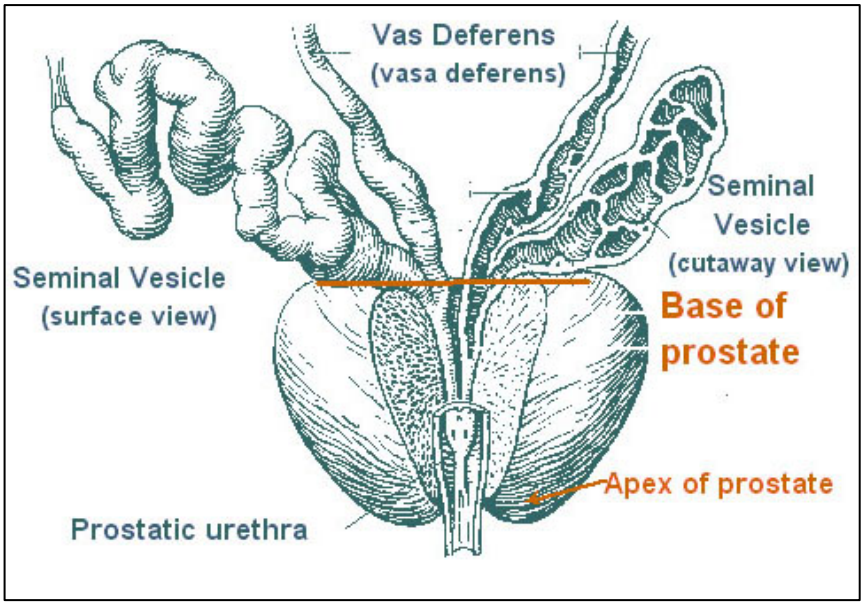

Figure 1.1. Anterior view of the pelvis of a male. The prostate gland, an essential element of the male reproductive system, is anatomically positioned directly below the urine bladder. and anterior to the rectum [2].

An essential prostate function is its connection to the excretory system. The prostate encompasses the part of the urethra placed closely under the urine bladder, and this anatomical position is crucial for regulating urinary flow and retention. [5]. The ideal prostate development and the regular growth depends on androgens, especially androgen 5-alpha-dihydrotestosterone (DHT), which affect glandular production and cell differentiation [6]. 5-alpha reductase enzyme catalyzes the conversion of testosterone to its more potent derivative dihydrotestosterone (DHT), which is essential for the development and proliferation of prostate cells [7]. Increased DHT levels may induce the atypical proliferation of the cells in the prostate, potentially resulting in cancer formation [8]. Furthermore, certain studies indicate that 5-alpha reductase inhibitors may diminish the prostate cancer risk. [9,10]. However, the impact of 5-alpha reductase on prostate carcinoma is complicated, as further studies suggest that inhibitors may not effectively restrict cancer progression [11,12].

The structure and function of the prostate are greatly impacted by several changes that occur as men age [13]. Androgen receptors and growth factors, which regulate the cell proliferation and differentiation, are processes by which prostate cells react to hormonal changes [14]. These variables work together to produce the aberrant growth patterns linked to benign prostatic hyperplasia (BPH), known as a prostate expansion and is among the most prevalent age-related disorders [15]. BPH is frequently associated with changes in cellular growth factors as well as long-term hormonal abnormalities, specifically the rise in estrogen and fall in testosterone [16–18]. Furthermore, the accumulation of these cellular alterations raises the risk of prostate cancer, another age-related illness that can result from comparable hormonal imbalances [19].

1.1.1. Cellular Constituents of the Prostate

The adult prostate tissue comprises two primary cell types, stromal and epithelial, each performing an essential part in preserving the gland's integrity and functionality [20]. Among epithelial cells, basal cells provide structural support, luminal cells is linked to releasing of prostate-specific antigen (PSA), and intermediate cells transition between these states [21]. Neuroendocrine cells, though rare, contribute to hormonal regulation within the prostate [22].

PSA, a key biomarker for prostate health, is released by luminal cells to facilitate semen liquefaction [23]. Surrounding the epithelial tissue, stromal cells consist of smooth muscle and fibroblast cells that provide structural integrity and support (Figure 1.2). Additionally, the adult prostate contains a complex network of blood vessels, ganglia, peripheral nerves, and white blood cells, which contribute to tissue nourishment, signal transmission, and immune defense [22].

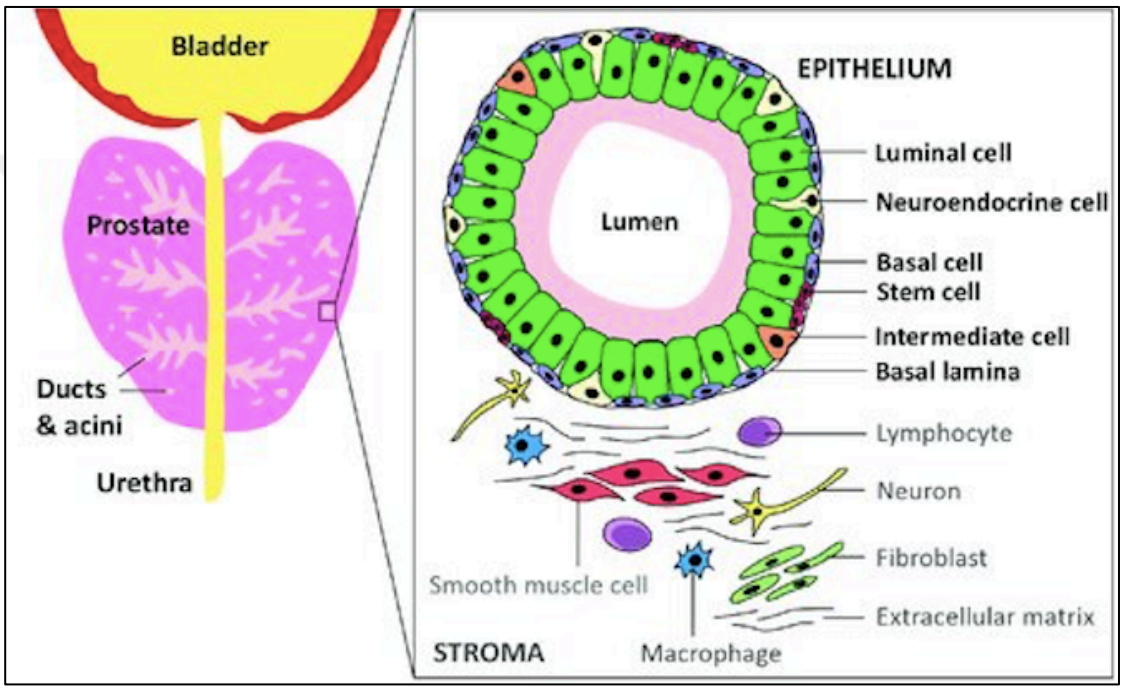

Figure 1.2. Schematic anatomy of the prostate highlighting differentiation between stromal and epithelial cells. Epithelial cells, located above the basement membrane, include basal cells that provide structural support and are critical for the prostate's epithelial layer. Stromal cells, on the other hand, are composed of fibroblasts, smooth muscle cells, vascular components, and neural elements, which collectively maintain the structural integrity, contractility, and signaling functions of the prostate [24].

Prostate cells are participating in the production and secretion of many different biological molecules critical to their function, including spermine, zinc, prostaglandins, citric acid, cholesterol, seminine, and PSA. These molecules play essential roles in processes such as sperm motility, immune defense, and glandular health [25]. Prostate diseases—such as

cancer, hypertrophy, inflammation, and infection—can disrupt the production or activity of these substances, leading to functional impairments and disease progression [26].

1.2. PROSTATE CANCER

1.2.1. Characteristics of the Prostate Cancer

Prostate cancer is not only the second most prevalent cancer among men but also comes as the fourth cancer with mortality in the world, representing around 7.3% of all newly diagnosed cancers (Figure 1.3) [27,28]. The prevalence and mortality rates of prostate cancer are significantly associated with advancing age with the average age at diagnosis being 66 years. The risk of prostate cancer significantly rises beyond the age of 50, particularly in developed countries such as North America and Europe, where prostate cancer screenings are more prevalent [29]. In the initial phases of prostate cancer, symptoms may be absent, pain may be nonexistent, and there may be little to no requirement for therapy [30]. In advanced stages, symptoms may include back pain, urine retention, and urinating difficulties. The principal technique for identifying prostate cancer involves measuring PSA levels, which, while indicative, lack specificity as they may also be raised in other disorders, including benign prostatic hyperplasia [31]. A tissue biopsy is generally necessary to validate a cancer diagnosis. Regardless of the cancer's location, current treatments are limited by the disease's tendency to progress from androgen-dependent to androgen-independent variants, limiting therapeutic options [32]. The progression of castration-resistant prostate cancer (CRPC) poses a considerable challenge in treatment, necessitating more aggressive interventions such as chemotherapy or innovative androgen receptor-targeted treatments [33]. Surgery and radiation therapy are the primary treatment for localized prostate carcinoma, frequently yielding a 10-year disease-free survival rate [34]. Nonetheless, these therapies may result in significant adverse effects, including urine incontinence and sexual malfunction that may affect the patient's life quality [35].

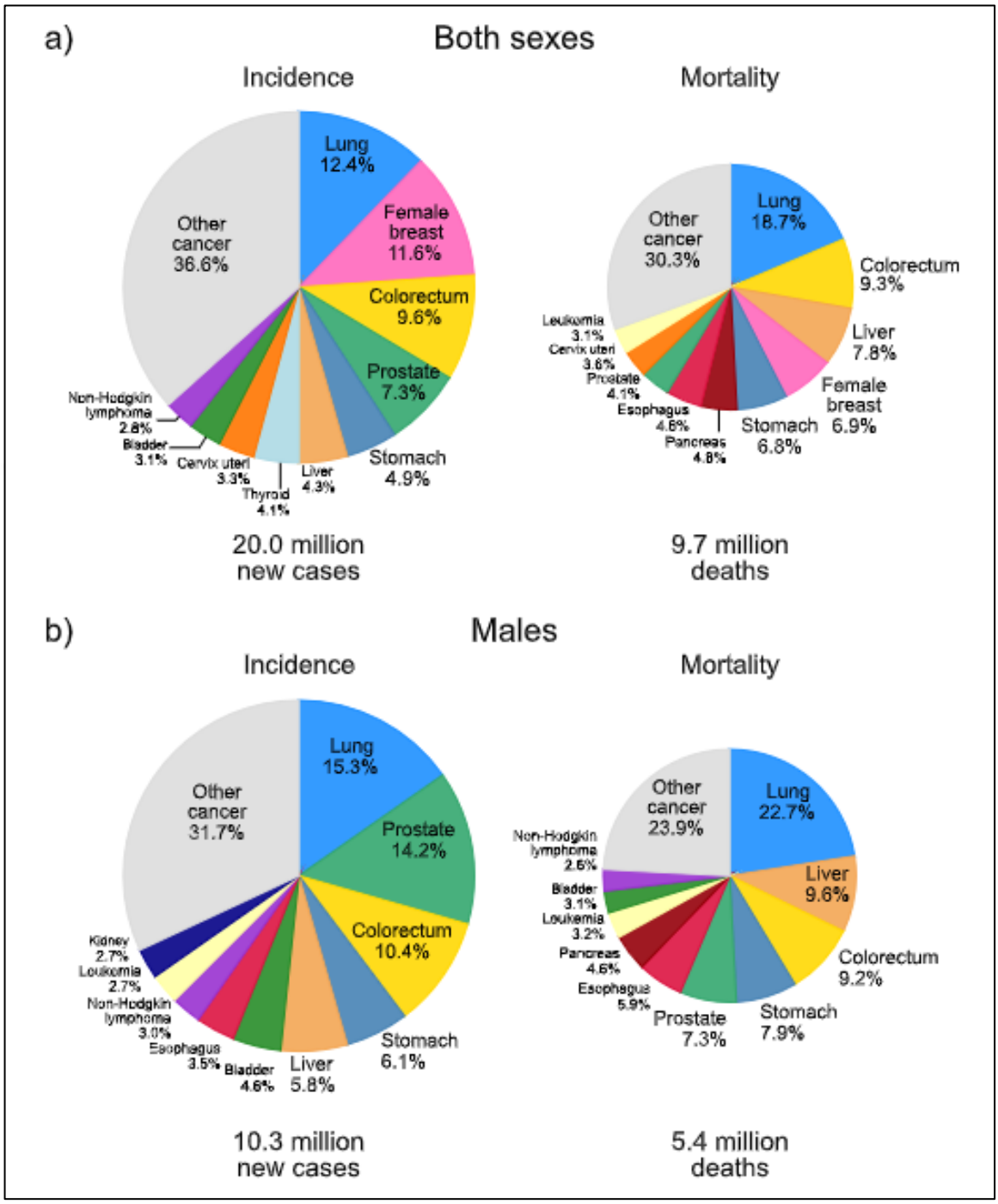

Figure 1.3. The division of deaths and cases for the five most prevalent malignancies in 2022. Pie charts for (a) both sexes and (b) males. Prostate cancer (PCa) is the fourth most prevalent malignancy in terms of incidence, accounting for 7.3% of new cases. The area of each segment in the pie chart corresponds to the percentage of cases or deaths [28].

1.2.2. Prostate Cancer Progression

Research on prostate carcinoma primarily concentrates on acquired mutations and the identification of genes implicated in its development [36]. Genetic alterations, particularly in oncogenes as well as tumor suppressor genes, are crucial in the development of prostate cancer [37]. The process is influenced by genetic mutations in addition to epigenetic changes that modulate gene expression without modifying the DNA sequence [38]. The interplay of these changes with environmental factors affects androgen metabolism, DNA repair mechanisms, cancer metabolism, and inflammation pathways, all of which participate in the initiation and prostate cancer progression [39,40]. Altered DNA repair mechanisms can lead to the accumulation of the genetic mutations, whereas inflammation within the prostate microenvironment may facilitate cancer cell proliferation and metastasis [41]. The androgen receptor (AR) signaling mechanism is important in the prostate cancer development, as androgen-dependent tumors are driven by AR activation [42]. Changes in the AR gene or its regulatory elements may lead to androgen-independent prostate cancer (AIPC), a more aggressive variant of the disease that exhibits reduced responsiveness to standard treatments [43]. Prostatic intraepithelial neoplasia (PIN), especially high-grade PIN (HG-PIN), represents the initial histological precursor to prostate cancer, marked by the destruction of basal and secretory formations alongside the thickening of the epithelial layer [44]. The transition from PIN to invasive cancer is frequently linked to chromosomal abnormalities, including gene amplifications and deletions, which contribute to the carcinogenic process (Figure 1.4) [45]. The tumor microenvironment, characterized by an invasion of immune cells and chronic inflammation, significantly influences prostate carcinogenesis, promoting tumor progression and resistance to therapies [46]. The multifocality of prostate cancer, marked by various areas of prostatic intraepithelial neoplasia and carcinoma, highlights the disease's heterogeneity and the complex genetic and cellular changes that occur during tumor progression [47].

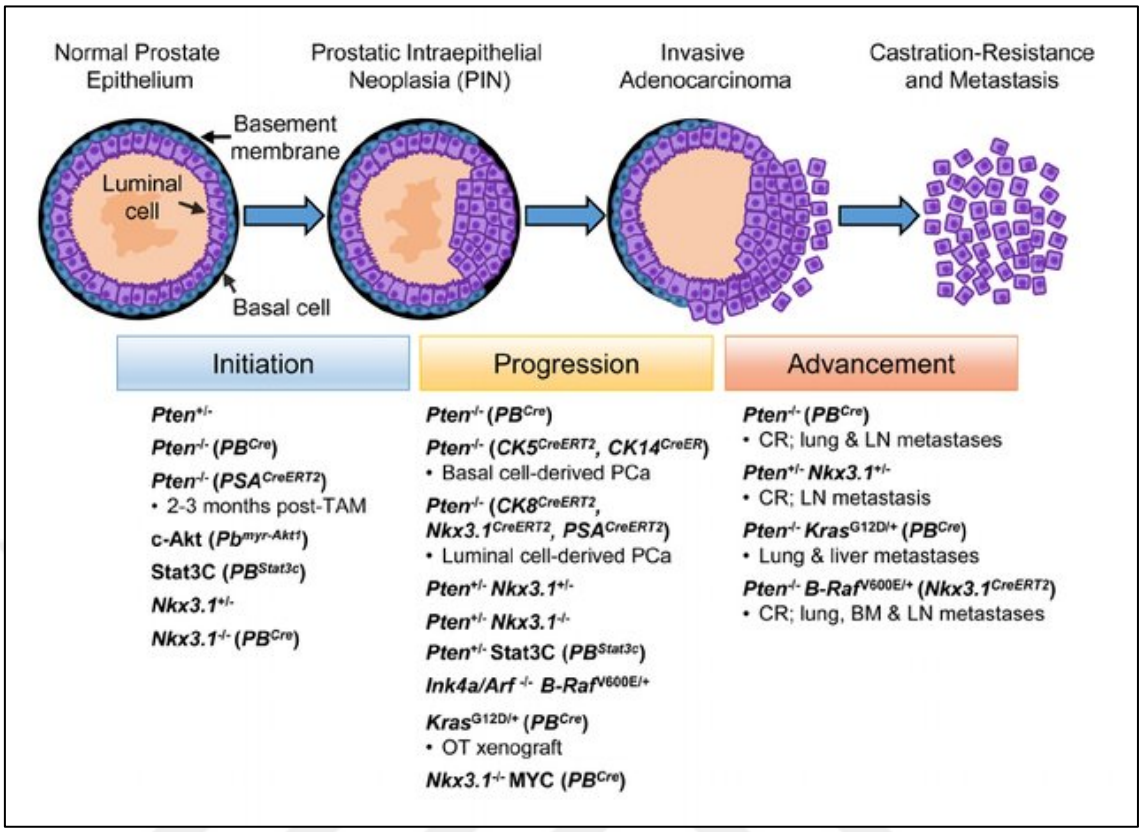

Figure 1.4. The prostate cancer progression and corresponding management or therapy approaches. Aggressive tumors in prostate cancer alter the strategies for treatment and management of cancer progression [24].

The development and advancement of prostate cancer is considerably affected by molecular mechanisms [48]. The TMPRSS2-ERG gene fusion represents a prevalent genetic alteration in prostate cancer, arising from the fusion of the TMPRSS2 gene, which is usually controlled through androgen signaling, with the ERG gene, an ETS transcription factor family member [49]. This fusion results in ERG overexpression, which promotes tumorigenesis by disrupting the normal differentiation of prostate epithelial cells and activating cancer signaling pathways [50]. Moreover, the loss of PTEN (phosphatase and tensin homolog) represents other typical genetic alterations in prostate cancer [51]. PTEN functions as a tumor suppressor by restricting the PI3K/AKT signaling, essential for the controlling of cell growth and survival [52]. The absence of PTEN leads to uncontrolled cell growth and defense against programmed cell death, which contributes to the aggressive characteristics of prostate cancer [53]. Another significant alteration in prostate cancer occurs in the p53 gene, which is an essential regulator of the cell cycle and programmed cell death [54].

Mutations in p53 correlate with the advancement of prostate cancer to more severe and aggressive stages, including metastasis, by compromising its capacity to induce cell cycle arrest or apoptotic death in response to DNA damage [55].

The interplay of genetic alterations, environmental influences, and hormonal factors establishes a complex tumor microenvironment that facilitates the progression and metastasis of prostate cancer [56]. Comprehending these molecular mechanisms offers significant knowledge on possible treatment targets for prostate cancer, especially in cases resistant to standard therapies.

1.2.3. Grading of Prostate Cancer

The grading and staging of prostate cancer are essential for assessing prediction and informing therapy choices [57]. The Gleason score is a prevalent method for evaluating the aggressiveness of prostate cancer, examining the tumor's architectural pattern through histological inspection [58]. The Gleason grading method allocates scores from 2 to 10, where elevated scores signify more aggressive cancer with an increased probability of progression and metastasis [59]. The score is calculated by evaluating the two most prevalent patterns of cancer cell differentiation in a biopsy sample and aggregating their results. A Gleason score of 6 or lower is generally regarded as low-grade, but scores of 7 or higher signify intermediate to high-grade disease, with values of 8 or above linked to a markedly poorer prognosis [60].

The Tumor Nodes Metastases (TNM) staging system, together with the Gleason score, is employed to specify the level of cancer progression [61]. The TNM system evaluates the dimensions of the primary neoplasm or tumor (T), the degree of lymphatic involvement or nodes (N), and the existence of distant metastases (M) [62]. This staging method is essential for assessing cancer's local progression and distant metastasis, which subsequently affects the treatment selection, encompassing localized interventions (e.g., surgery, radiation) and systemic therapies (e.g., chemotherapy, androgen deprivation therapy) [63]. The Gleason score and TNM staging collectively provide a thorough evaluation of prostate cancer, assisting clinicians in predicting patient outcomes and customizing treatment approaches [64].

The International Society of Urological Pathology (ISUP) grading system is a systematic framework for classifying prostate cancer according to histological patterns seen in tissue specimens. This methodology, established in 2014 as an enhancement of the conventional Gleason scoring method, classifies prostate cancer into five grade groups, from grade group 1 (less aggressive, aligned with Gleason score ≤6) to grade group 5 (the most aggressive, aligned with Gleason scores 9–10). The ISUP approach enhances risk stratification and prognostication by providing a more clinically useful and efficient evaluation of tumor aggressiveness. It is especially beneficial in informing treatment choices, differentiating candidates for active surveillance from those need more intensive therapy. The repeatability and predictive precision of the ISUP grading system have established it as the chosen standard in modern clinical practice and research. The significance of these categorization systems resides in their capacity to predict prognosis and their function in enhancing clinical decision-making, thereby ensuring patients receive the most suitable and effective treatment for their cancer stage and grade [65].

1.2.4. Therapies for Prostate Cancer Treatment

Conventional chemotherapy is frequently employed for instances of CRPC, wherein the malignancy has advanced to an androgen-independent condition [66,67]. Chemotherapy is commonly constrained by its significant toxicity, resulting in severe adverse effects, and its efficiency is diminished in certain patients due to multidrug resistance (MDR) mechanisms [68]. This resistance is associated with alterations in drug transporters, increased drug efflux, and enhanced DNA repair, all of which reduce the effectiveness of chemotherapy. Consequently, there is an urgent demand for new effective medications with minimized adverse effects, including targeted therapies and customized medicine [69]. Recent advancements involve the utilization of nanoparticles for targeted drug administration, encapsulating drugs within carriers such as lipids, peptides, or antibodies to enhance treatment specificity and minimize systemic toxicity [70]. These strategies improve treatment accuracy and reduce the adverse effects linked to traditional chemotherapy [71].

The capacity of prostate cancer to undergo a transition from androgen-dependent to androgen-independent condition creates limitations for current therapy approaches (Figure 1.5). Surgical intervention and radiotherapy are the favored therapies for localized prostate cancer, offering a high 10-year disease-free survival rate for several patients [73]. These

methods are frequently integrated with androgen deprivation therapy (ADT), and it diminishes androgen receptor signaling to suppress prostate cancer cell proliferation [74]. The androgen receptor signaling pathway is initially fundamental for survival of patients with prostate cancer [75]. Most prostate cancers are androgen-sensitive, which increases the activity of the androgen receptors [76].

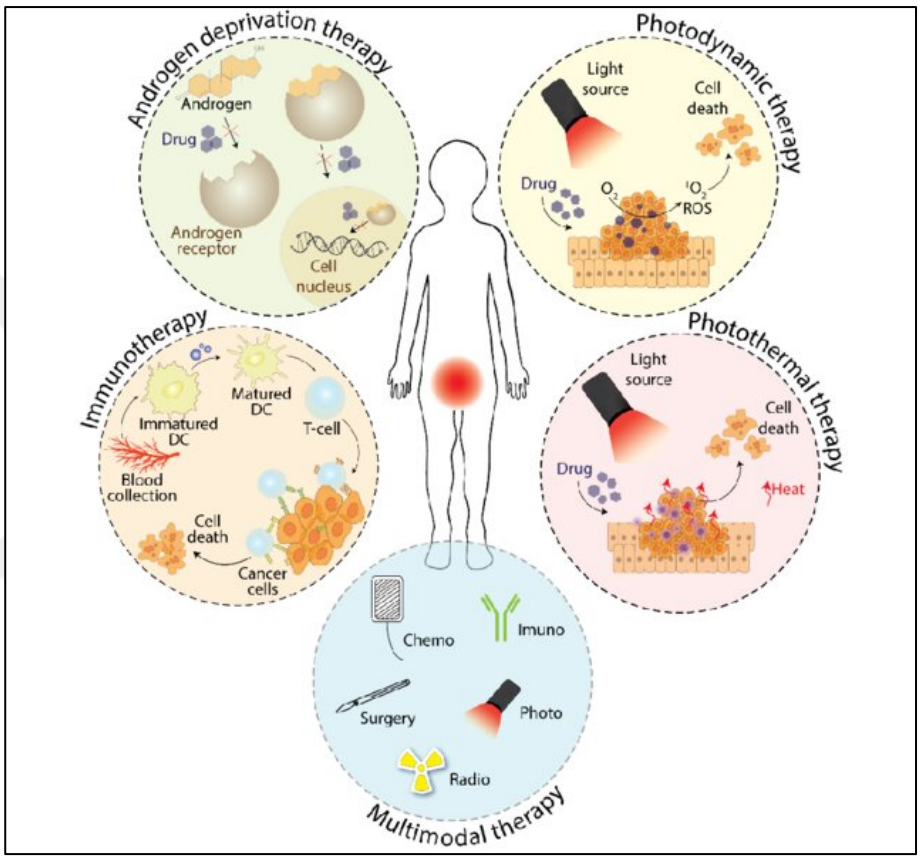

Figure 1.5. Representative schematic of treatment approaches for advanced prostate carcinoma [72].

Numerous androgen receptor (AR) antagonists and steroidal agents have been formulated to inhibit androgen signaling in prostate cancer (Figure 1.6). Flutamide, bicalutamide, and enzalutamide are non-steroidal antiandrogens that competitively restrict androgen binding to the androgen receptor, thereby inhibiting androgen receptor-mediated transcription and tumor development. Spironolactone, mifepristone, and cyproterone acetate are steroidal compounds exhibiting antiandrogenic characteristics that disrupt androgen production or receptor interaction. These drugs, in conjunction with natural androgens like testosterone

and dihydrotestosterone (DHT), illustrate the complex nature of androgen receptor signaling modulation. Focusing on this route is fundamental to prostate cancer therapy, particularly in androgen-sensitive and castration-resistant phases [77-79].

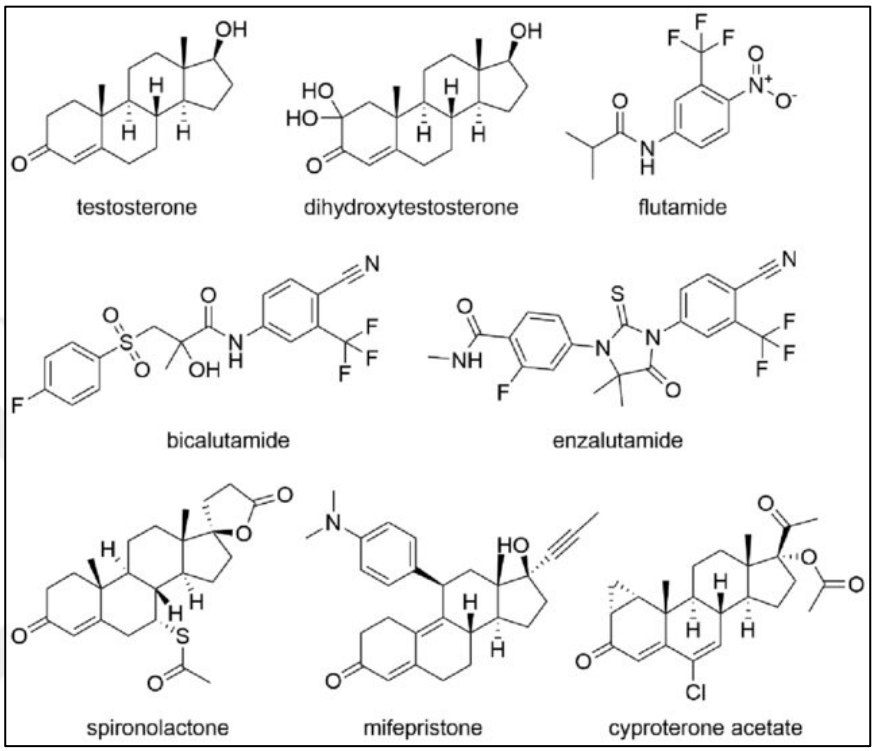

Figure 1.6. The names and chemical structures of androgens and anti-androgens used in prostate cancer treatment [77].

Despite these treatments, ADT ultimately becomes inefficient in CRPC, where cancer adapts and proliferates despite reduced circulating testosterone levels [82]. In many cases, novel therapeutic methods are emerging to overcome resistance. Immunotherapy, including immune checkpoint inhibitors and PARP inhibitors, has shown promising outcomes in clinical studies for CRPC patients by addressing the genetic defects of the malignancy [83,84]. Recent research indicates that genomic targeting by gene editing technologies, such as CRISPR-Cas9, may effectively modify cancer DNA and can reverse resistance to ADT [85]. Moreover, CAR-T cell therapy (Chimeric Antigen Receptor T-cell) is under investigation as a promising treatment for advanced prostate carcinoma, providing a possible method to stimulate the immune system to more effectively target and eradicate prostate cancer cells [86].

Curcumin has been known as an exciting anticancer drug in recent years because of its advantageous safety profile. Curcumin as a natural substance, functions as an androgen receptor antagonist and suppresses NKX3.1 expression, diminishing androgen response element binding activity and downregulating genes such as AR and PSA in the prostate cancer cells [80]. Curcumin diminishes NF-κB (Nuclear Factor kappa-B) activation and the production of proteins such as CBP and AP-1, which contribute to the development of cancer cells [81].

1.3. CURCUMIN

Phytochemicals, which are plant-derived compounds, are being extensively researched for their possible role in disease prevention, including cancer [87]. Curcumin, a golden-colored polyphenol extracted from the *Curcuma longa* plant roots, is a natural polyphenolic material with the chemical formula $C_{21}H_{20}O_6$ with a molecular weight of 368.37 g/mol [92]. The chemical structure comprises a beta-diketone molecule, including two aromatic rings interconnected, comprising a seven-carbon chain. Each of these aromatic rings comprise hydroxyl and methoxy groups, enhancing its significant biological activity (Figure 1.7) [93]. The particular chemical profile of curcumin provides anti-inflammatory, antioxidant, and anticancer properties, resulting in a favorable candidate for medicinal applications [94].

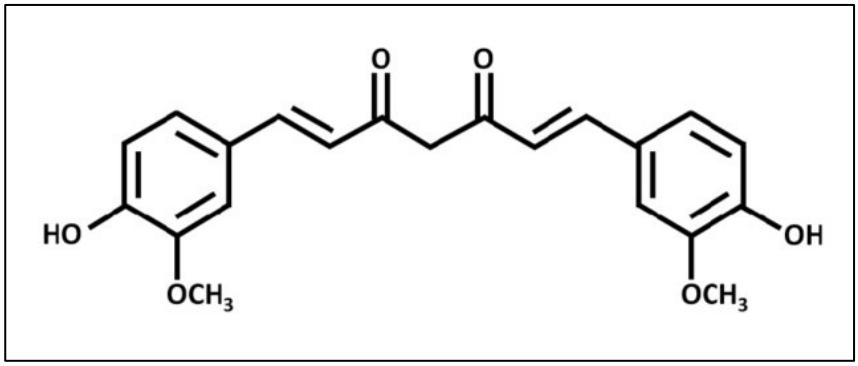

Figure 1.7. The chemical structure of curcumin. The structure is a beta-diketone molecule consisting of two aromatic rings comprising a seven-carbon chain. Each of these aromatic rings have hydroxyl and methyl groups [93].

Curcumin is known as its anti-inflammatory, anti-mutagenic, antibacterial, and anti-tumor attributes [88,89]. It has been an essential component of conventional medicine in Asian countries for centuries, used in both oral and topical applications for its therapeutic advantages (Figure 1.8).

Figure 1.8. Various activities of curcumin highlighting its pharmacological effects. These include anti-diabetic, anti-tumor, anti-fibrotic, antioxidant, anti-viral, anti-inflammatory, anti-pathogenic, and cardiovascular protective properties [91].

Curcumin exhibits a comprehensive range of biological actions, including the regulation of several cellular functions critical to cancer formation, like inflammation, apoptosis, angiogenesis, and metastasis [90-94]. Curcumin is soluble in organic solvents like acetone and ethanol, and dimethyl sulfoxide (DMSO), but is virtually insoluble in water [95]. The limited solubility significantly restricts its therapeutic applicability by impacting its bioavailability [96].

Despite its potential, curcumin overcomes limitations associated with fast metabolism and poor absorption in the body, hence limiting its effectiveness when administered orally [97].

Researchers have developed various nanoformulations, including liposomes, micelles, nanogels, nanoparticles, and cyclodextrins, to enhance the water solubility and bioavailability of the curcumin [98–100]. These formulations safeguard curcumin against metabolic breakdown and enable targeted delivery to cancerous cells, therefore increasing its therapeutic efficiency, particularly in prostate carcinoma treatment [101,102].

Due to curcumin's significant health benefits, curcumin is employed globally in many forms, including tablets, capsules, supplements, soaps, and cosmetics [103]. Its anti-inflammatory and antioxidant characteristics have established it as a fundamental component in both traditional and modern therapy [98]. The U.S. Food and Drug Administration (FDA) has classified curcumin as Generally Recognized as Safe (GRAS) and has been involved in a variety of clinical studies, indicating that curcumin is a safe at doses that exceed 10 g/day, with no evidence of dose-limiting toxicity [104]. Enhancing the biological availability of curcumin is a significant emphasis of ongoing research to optimize its therapeutic efficiency, particularly in prostate cancer treatment [105].

1.3.1. Anti-Cancer and Anti-Tumor Activity of Curcumin

Curcumin has been known as an exciting anticancer treatment in recent years because of its advantageous safety profile [106]. It has been documented to influence many signaling pathways and demonstrate a wide range of biological activity, involving antioxidant, anti-mutagenic, anti-inflammatory, anti-proliferative, and anti-cancer effects [107]. Curcumin is an established antioxidant that may inhibit angiogenesis, promote apoptosis, reduce the synthesis of anti-apoptotic proteins in cancer cells, and limit cellular proliferation [108]. These pathways establish curcumin as a crucial compound in cancer research and treatment (Figure 1.9) [109]. Curcumin specifically interacts with essential signaling molecules involved in cancer progression, demonstrating significant cellular activity in both *in vitro* and *in vivo* models [110]. It is shown to inhibit angiogenesis and cell-cell adhesion by affecting specific signaling pathways, including NF-κB, STAT3 (Signal Transducer and Activator of Transcription 3), and MAPK (Mitogen-Activated Protein Kinase), which are generally dysregulated in cancer cells [111]. Furthermore, curcumin can hinder tumor cell proliferation, prevent tumor growth, and inhibit metastasis, which are critical factors in cancer treatment and prevention [112].

Studies demonstrate that curcumin, even at elevated doses, can augment the effectiveness of chemotherapeutic drugs while exerting low or no detrimental effects on healthy tissues, rendering it a significant adjunct in cancer therapy [113]. It has also been indicated to facilitate the loss of pre-malignant lesions in multiple organs [114]. The effects of curcumin are enhanced when it is taken with other drugs or phytochemicals [115,116]. Research indicates that curcumin amplifies the anti-cancer efficacy of chemicals like quercetin, resveratrol, epigallocatechin gallate, and ursolic acid, resulting in synergistic effects across multiple types of cancer, involving breast, colorectal, and prostate malignancies [117–121].

The synergistic effects indicate that curcumin may provide a more efficacious therapeutic approach when used in conjunction with other medications, especially in prostate cancer, where its capacity to influence androgen receptor signaling and other pathways can enhance patient outcomes [122–126].

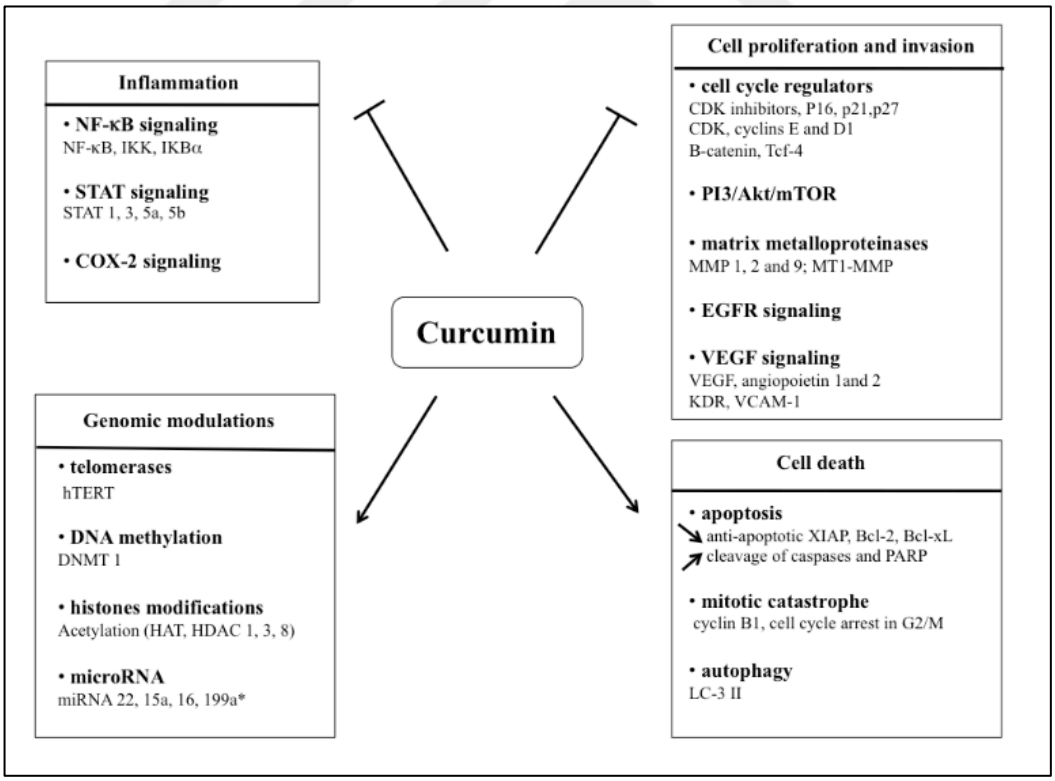

Figure 1.9. The molecular targets regulated by curcumin. Cancer cell death or carcinogenesis occurs following these modulations. Arrows and blunt-ended lines indicate the initiation and inhibition of the pathways [127].

Many chemotherapeutic agents, such as plant-derived taxol and vincristine, may cause significant damage to healthy cells while promoting death in malignant cells. However, curcumin has shown safety [128]. Curcumin promotes apoptosis in cancerous cells and suppresses cellular growth [129]. It affects both p53-dependent and -independent molecular pathways and leading to apoptosis via intrinsic or extrinsic pathway (Figure 1.10) [130]. Curcumin-induced DNA damage or stress factors initiate the intrinsic apoptotic pathway, leading to the overexpression of pro-apoptotic proteins (e.g., Bax, Bim, Bak, Puma, and Noxa) and the downregulation of anti-apoptotic proteins (e.g., Bcl-2, cFLIP, and Bcl-xL) [131].

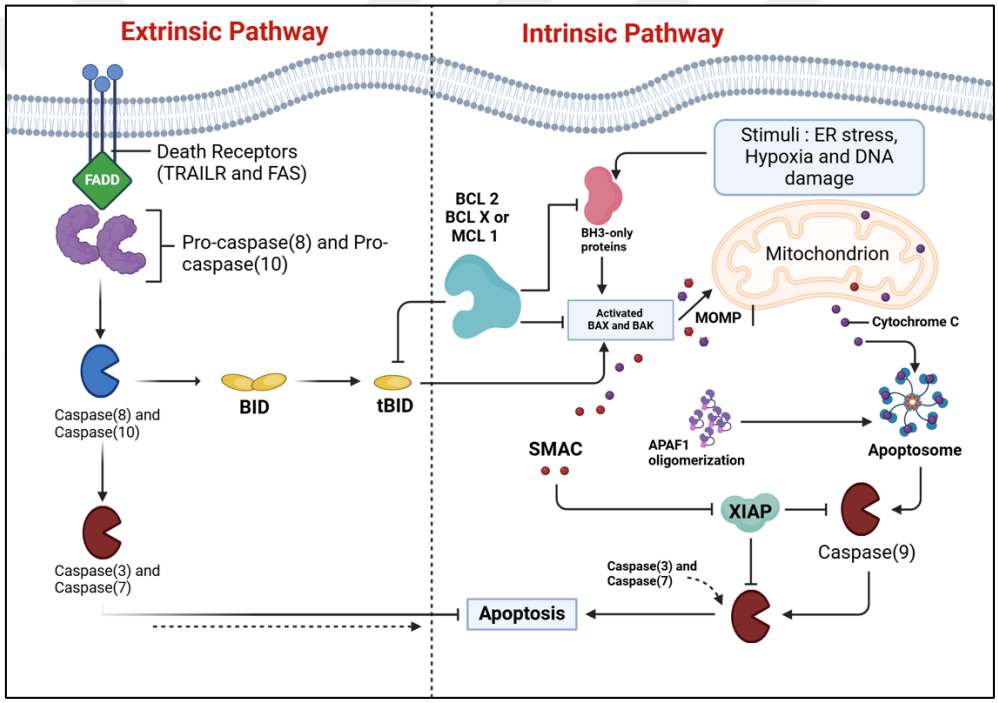

Figure 1.10. The intrinsic and extrinsic molecular pathways of apoptosis. The intrinsic pathway occurs via mitochondria-mediated mechanisms, while the extrinsic pathway occurs via the death receptor-mediated signaling [130].

The modulation of Bcl-2 family proteins leads to the release of the cytochrome from the mitochondria, the development of apoptosome (comprising APAF-1 (Apoptotic Protease Activating Factor 1), caspase 9, and cytochrome c), and eventually, cell death through apoptosis [132–134]. In the extrinsic pathway, curcumin activates Fas and TRAIL (Tumor Necrosis Factor-Related Apoptosis Inducing Ligand) receptors located on the cell membrane

[135]. This results in the generation of death-inducing signaling Complex (DISC), which includes Fas, Fas-associated protein with death domain (FADD), caspase-8, and caspase-10. Caspase-8 and caspase-10 interact with the intrinsic pathway by Bid cleavage, facilitating cytochrome c release and triggering the caspase cascade (Figure 1.11) [106].

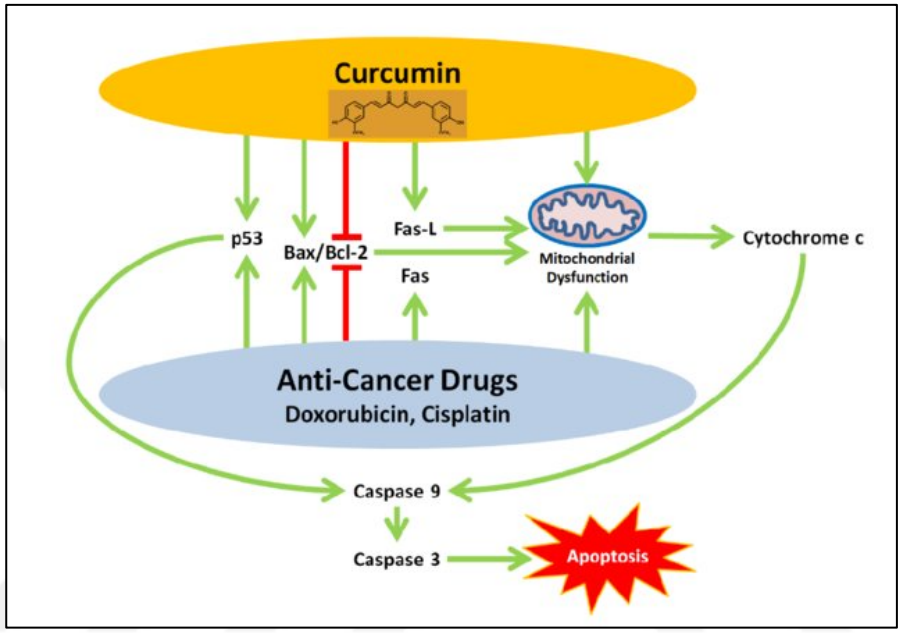

Figure 1.11. Signaling pathways associated with curcumin and the chemotherapeutic drugs doxorubicin and cisplatin. All three, cisplatin, doxorubicin, and curcumin, induce the Bax upregulation and downregulate Bcl-2. Curcumin leads to the induction of the Fas signaling pathway. Together, these pathways activate the caspase cascade and promote apoptosis. Molecular targets and signaling pathways activated by curcumin are shown by the arrow (→), while inhibition is indicated by the symbol (⊣) [106].

Research demonstrates that curcumin facilitates Poly (ADP-ribose) polymerase (PARP) cleavage, and the generation of apoptotic bodies while downregulating anti-apoptotic Bcl-2 family proteins [136]. Moreover, curcumin enhances endoplasmic reticulum stress and triggers apoptosis via both intrinsic and extrinsic pathways. It is shown that curcumin triggers pro-apoptotic endoplasmic reticulum stress in the HL-60 human leukemia cells [137]. Moreover, curcumin can reversibly inhibit non-malignant cells in the G0 phase without causing apoptosis, while it induces apoptosis in malignant cells [138].

1.3.2. Anti-Cancer Activity of Curcumin in Prostate Cancer

Prostate cancer cells frequently acquire resistance to therapies and are governed by many anti-apoptotic proteins that facilitate their survival and growth [139, 140]. Curcumin has been shown to trigger apoptosis in prostate cancer cells in both androgen-dependent and androgen-independent contexts as a promising chemoprotective and chemotherapeutic agent [141]. Curcumin displays its anti-cancer properties in prostate cancer by influencing various critical molecular targets associated with abnormal signaling pathways [142]. This involves the suppression of androgen receptor (AR) signaling, AP-1, NF-κB, Bcl-2, PI3K/Akt, Cyclin D1, and Wnt/β-catenin pathways, all of which are fundamentally linked to the evolution of prostate cancer. Through this multifaceted mechanism, curcumin disrupts both proliferation and survival signals, demonstrating its potential as a therapeutic agent (Figure 1.12) [143].

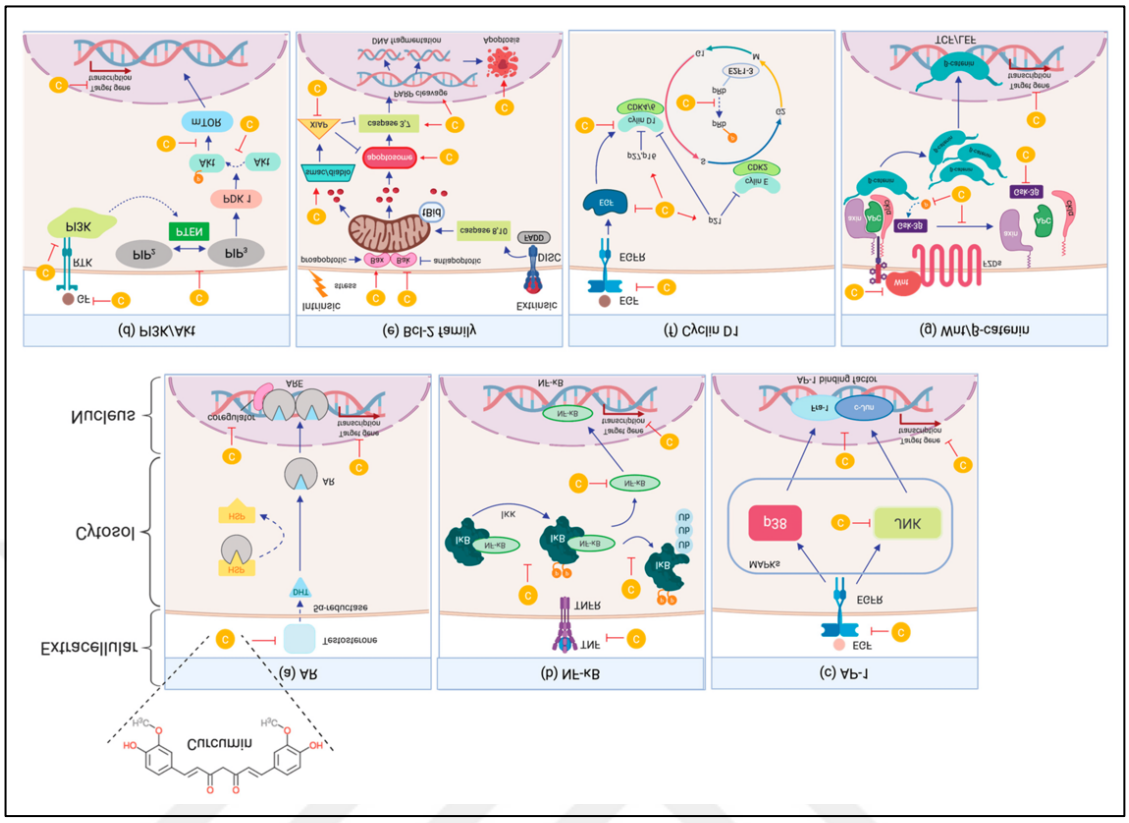

Figure 1.12. Mechanisms of action of curcumin as an anti-cancer potential on critical molecular targets in dysregulated signaling pathways of prostate cancer. Curcumin demonstrates anti-cancer characteristics by inhibiting various signaling pathways and molecular targets: (a) Androgen receptor (AR) signaling, (b) Nuclear factor kappa-B (NF-κB) signaling, ,(c) Activating protein-1 (AP-1) signaling, (d) Phosphatidylinositol 3 kinases/serine/threonine kinase (PI3K/Akt) signaling, (e) B-cell lymphoma 2 (Bcl-2) signaling, (f) Cyclin D1, and (g) Wingless (Wnt)/ß-catenin signaling. Molecular targets and signaling pathways activated by curcumin are shown by the arrow (→), while inhibition is indicated by the symbol (⊣) [143].

Curcumin's chemopreventive potential has shown beneficial effects in androgen-dependent LNCaP and 22Rv1 human prostate cancer cells, in addition to in androgen-independent prostate cancer cell lines, comprising PC-3 human prostate adenocarcinoma cells, DU-145 human prostate cancer cells, and the LNCaP-derivative C4-2B cells human prostate cancer cells [144]. Curcumin's capacity to regulate androgen receptor signaling pathways

establishes it as a prospective treatment approach for androgen-independent prostate cancer, where conventional hormone therapies frequently prove ineffective [145].

1.3.3. Nanoformulations of the Curcumin

Curcumin received significant interest as a cancer therapeutic due to its safety profile, making it a promising anti-cancer strategy in recent years [146]. Research demonstrates that curcumin enhances the efficacy of chemotherapeutic drugs and, even at high dosages, does not harm or negatively impact healthy organs, positioning it as a potential adjunct in cancer therapy [147,148]. Curcumin exhibits combined suppressive effects on the proliferation and viability of prostate, breast, and colorectal cancer cells, especially when used in conjunction with other natural substances [149–151]. As curcumin has poor pharmacokinetic characteristics, restricting its effectiveness as a chemosensitizer and chemotherapeutic agent, nanotechnology has appeared as a possible answer to overcome these constraints [152, 153]. Encapsulating curcumin in nanocarriers significantly improves its solubility and bioavailability, hence increasing its therapeutic effectiveness (Figure 1.13) [154].

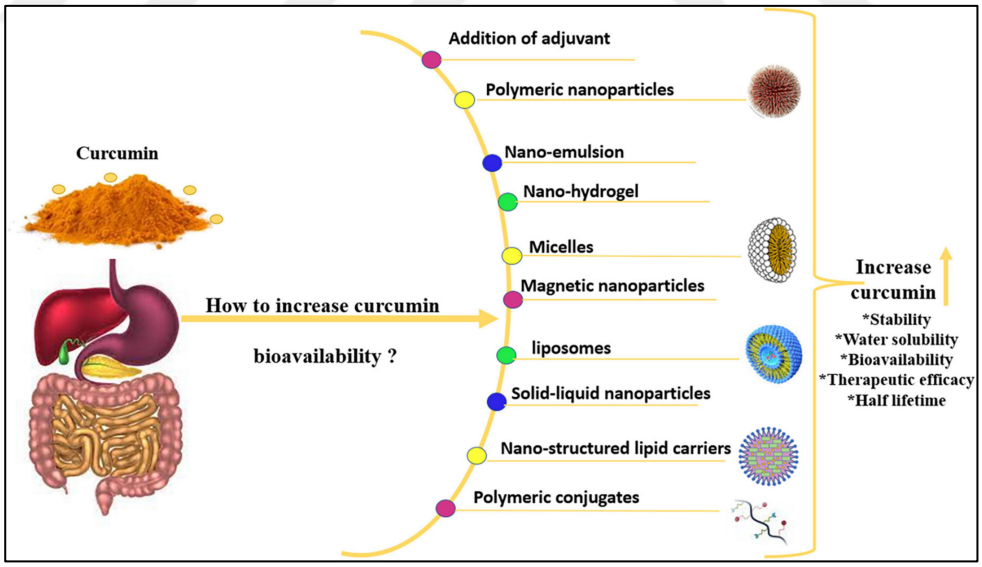

Figure 1.13. Recent methods developed to enhance the bioavailability of curcumin [164].

Liposomes are commonly used as nanocarriers due to their ability to encapsulate hydrophobic substances like curcumin, and their potential ability to carry substantial amounts of chemotherapeutic agents, improve drug stability, and promote prolonged circulation in the bloodstream [155]. These characteristics are particularly advantageous for

prostate cancer therapy, as curcumin's hydrophobic qualities may be successfully managed through liposomal encapsulation [156,157]. Poly (lactic co-glycolic acid) and curcumin nanoparticles (PLGA-CUR) have demonstrated encouraging results in the treatment of prostate carcinoma. Research demonstrates that curcumin, administered via PLGA nanoparticles, is more efficacious in preventing the proliferation of prostate cancer cells than free curcumin [101]. PLGA nanoparticles effectively transport curcumin into cancer cells, releasing it directly into the cytoplasm and thereby enhancing its anti-cancer properties. This research indicates that PLGA-CUR nanoparticles markedly diminish tumor size in animal models. Additionally, it is revealed that PLGA-CUR nanoparticles suppressed androgen receptor expression, downregulated nuclear β-catenin in tumor xenograft tissues, and stimulated cleavage of PARP [158]. Also, PLGA-CUR nanoparticles induced apoptosis by suppressing Bcl-xL and diminishing Akt and STAT3 phosphorylation, which are critical regulators of cell survival and proliferation [159,160]. These findings emphasize the efficiency of curcumin nanoparticles as a treatment agent for prostate cancer [161–163].

1.3.4. Soy Lecithin-Based Formulations

Lecithin is a phospholipid commonly used as a safe and biocompatible substance in the food and pharmaceutical industries [165]. It contains components necessary to maintain cell membrane fluidity, which enhances the absorption and increases the bioavailability of drugs [166]. Research indicates that lecithin-based docetaxel nanoparticles markedly enhance the anti-tumor efficacy of docetaxel, facilitating improved transport and more effective targeting of cancer cells [167]. This research demonstrated that soy lecithin-based nanoparticles exhibited a prolonged releasing profile, releasing 80% of docetaxel within the 72 hours, with higher bioavailability compared to docetaxel alone (8.75% vs. 2.40%) [168]. Thus, lecithin-based nanoparticle formulations have been proven to enhance the therapeutic effectiveness of pharmaceuticals with low oral bioavailability [169]. The continuous release feature, along with improved bioavailability, makes lecithin-based formulations an effective solution for the challenges associated with the oral absorption of poorly soluble drugs [147]. Moreover, lecithin's amphiphilic properties enhance the cellular targeting of therapeutic agents, hence increasing the effectiveness of anticancer treatments [170]. Lecithin-based carriers have shown the capacity to enhance cellular uptake of hydrophobic drugs like curcumin and docetaxel, hence improving their therapeutic effectiveness in cancer therapy [171].

2. AIM OF THE STUDY

Curcumin, a natural polyphenol, is distinguished for its anti-proliferative, antioxidant, anti-mutagenic, and anti-cancer features, however, the low bioavailability of the curcumin through oral administration limits its therapeutic efficacy. This study aimed to observe the *in vitro* anticancer efficacy of soy lecithin-based encapsulated curcumin ($_{SLC}$CUR) on 22Rv1 and LNCaP prostate cancer cells, using the normal prostate epithelial cells PNT1A as a reference. The *in vitro* findings were further validated *in vivo* using a 22Rv1 xenograft mouse model of prostate cancer.

3. MATERIALS

3.1. INSTRUMENTS

3.1.1. Instruments for Characterization of the $_{SLC}$CUR Particles

High-speed homogenizer (Hidolf, Germany), Lyophilizer (Labconco, USA), Zetasizer (Nano ZST, Mallvern Instruments Ltd., UK), Transmission Electron Microscope (TEM, JEM-2100 Plus, JOEL, Japan), Scanning Electron Microscope (SEM, Zeiss Evo40 (Zeiss, Heidelberg, Germany), Atomic Force Microscope (AFM, XE-1000 AFM, Park Systems, Korea), Fourier Transform Infrared Spectroscopy (FT-IR, Perkin Elmer FTIR System Spectra BX, USA).

3.1.2. Instruments for Cell Culture Experiments

Laminar flow (ESCO Lab Class II Biohazard Safety Cabinet, Singapore), CO_2 Cell Culture Incubator (NU-5800, NuAire, USA), Centrifugator (Sigma, England), Carl Zeiss Primo Vert Microscopy with AxioCam-1050 color (GmbH 3708, Göttingen, Germany), 80 °C freezer (ThermoForma -80°C ULTC Freezer, USA), Centrifuge (MICRO-22R, Germany), Flourescence Microscope (Nikon 80 Eclipse Fluorescence Microscope), pH meter (Hanna Instrument PH2112, Germany), Benchtop Vortex (Stuart SA, UK), Stirrer (Heidolph MR2, Germany), Stirrer and Heater (Bio-mer, M1023, China), SpectraMax Paradigm (Molecular Devices Multi Mode Detection, USA).

3.1.3. Instruments for SDS-PAGE and Western Blotting Experiments

Chemi-DOC XRS, Gel Imaging System (Bio Rad, USA), Weigher (Shimadzu Corporation TW423L, Japan), Centrifuge (MICRO 22R, Hettich, Germany), Gyro-Rocker (Stuart, UK), Centrifuge (Sigma, England), SpectraMax Paradigm (Molecular Devices Multi Mode Detection, USA).

3.2. EQUIPMENTS

Cell Culture Flasks (T25, T75, and T150, SPL Life Science, South Korea), Polypropylene Eppendorf (0.5 mL and 1.5 mL Isolab Universal, Germany), Falcon tube (15 mL and 50 mL,

Isolab, Germany), Sterile Filter (0.22 µm and 0.45 µm, Sartorius Stedim Biotech, Germany), Cell Culture multi-well plates (6-well, 24-well, 96-well, TPP, Switzerland), Pipette Tips (Isolab, Germany), Sterile Serological Pipettes (Isolab, Germany), Electronic Pipette (CAPP Aid, Denmark), Bright-Line Hemacytometer (Sigma Aldrich, Germany), Micropipettes (Eppendorf, Germany), Cover Slip (Sigma, Germany), Graduated Cylinder (Isolab, Germany), Erlenmeyer Flasks (Isolab, Germany).

3.3. CHEMICALS

3.3.1. Cell Lines

Normal Epithelial Prostate Cells (PNT1A, #95012614, Sigma Aldrich, USA), Human Epithelial Prostate Carcinoma Cells (22Rv1 ATCC #CRL-2505), Lymph Node Carcinoma of Prostate Cells (LNCaP, ATCC #CRL-1740), Transgenic Mouse Adenocarcinoma Cells (TRAMP-C2, ATCC #CRL-2731).

3.3.2. Cell Culture Media

Roswell Park Memorial Institute 1640 growth medium (RPMI-1640, Gibco #11875093, Thermo Fisher Scientific, USA), Dulbecco's Modified Eagle's Medium (DMEM, high glucose, Gibco #11965092, Thermo Fisher Scientific, USA).

3.3.3. Cell Culture Growth Supplements

Fetal Bovine Serum (FBS, Sigma, #F9665), Penicillin/Streptomycin (100 U/mL/100 µg/mL) (Sigma, #p4333, 6SLBJ7114U), L-glutamine Solution (Sigma Aldrich G7513, Germany).

3.3.4. Other Chemicals for Cell Culture

WST-1 Cell Proliferation Reagent (Roche, 11644807001, Switzerland), Trypsin 10x (Lonza, BE02-007E, Switzerland), DMSO (Dimethyl Sulfoxide, Santa Cruz Biotechnology, 202581, USA).

3.3.5. Chemicals for Cellular Uptake Experiments

HEPES (4-(2 hydroxyethyl)-1 piperazinethanesulfonic acid) (Merck, Germany), Dimethyl Sulfoxide (Merck, Germany), Phosphate Buffered Saline (PBS) (PAN Biotechnology, P04-5350, Germany), Ethylene Glycol Tetraacetic Acid (EGTA) (Fluka 037792, USA), 10X concentrated PBS (10X) (Lonza, BE117-517Q, Belgium), Sodium Orthovanadate (Na_3VO_4) (Sigma, S6508, USA), Mounting Media (F4680-25, Sigma, USA), Ethylenediamine Tetraacetic Acid (EDTA) (Merck, K401732186 946, Germany), Dithiothreitol (DTT) (Applichem A1101, USA), Phenylmethanesulfonylfluoride (PMSF) (Sigma 78830, USA).

3.3.6. Chemicals for SDS-PAGE and Western Blotting

Acrylamide/Bis-acrylamide (Merck, A3574, Germany), Sodium Dodecyl Sulfate (Sigma, L3771, Germany), Laemmli Buffer 5X (Sigma, S3401, Germany), Ammonium persulfate (APS) (Sigma, A3678, Germany), B-Mercaptoethanol (Merck, 805740, Germany), Methanol, pure (Sigma, 34885, Germany, Nitrocellulose membrane (0.22 μm) (GE Healthcare RPN3032D, USA), Albumin, Bovine Serum (Bioshop, ALB001, Canada), Protein Assay Reagent A and B (Bio Rad 50001135, 50001145 USA), Whatman 3MM CHR Blotting Paper (GE Health Care3030-917, USA), RIPA Lysis Buffer (SC Biotechnology, USA), Tris Ultra-Pure (Merck 819623, Germany), Tween-20 Detergent (Merck, 655204, Germany), WesternBright Sirius (Advansta K12043, USA), 2-Propanol (Sigma Aldrich 24137, Germany).

3.3.7. Antibodies

3.3.7.1. Primary Antibodies

Caspase-9 (CST, 9502S, USA), C-Caspase-3 CST, 9664S, USA), PARP (CST, 9542P, USA), B-Actin (Sigma, A53164, Germany)

3.3.7.2. Secondary Antibodies

Anti-mouse IgG Antibody (Sigma, A44161, Germany), Mouse IgG Antibody (Santa Cruz Biotechnology, 2025, USA), Rabbit IgG Antibody (Santa Cruz Biotechnology 2027, USA) Anti-rabbit IgG Antibody (CST, 7074S, USA).

3.4. KITS AND SOLUTIONS

In-Situ Cell Death Detection Fluorescein Kit (Terminal Deoxynucleotidyl Transferase dUTP Nick End Labeling (TUNEL) Assay, Roche, #11684795910).

4. METHODS

4.1. SYNTHESIS OF THE PARTICLES

4.1.1. Preparation of SLC Particles

To prepare the soy lecithin (SLC) particles, a 2% (v/w) dispersion of soy lecithin was prepared first. Soy lecithin was combined with sterile water for injection in a high-speed homogenizer (21000 rpm) for 15-30 minutes. The resulting dispersion was further stirred using a sonicator (70 kHz at 70% vibration) for a total time of 15 minutes, in 5-minute intervals, to reduce the particle size. Following the measurement of particle size and zeta potential (ZP) via dynamic light scattering (DLS), the sample was subjected to freezing and lyophilization at a pressure of 0.1 millibar and a temperature of −50°C. Upon obtaining the powder form, it was stored in a vacuum oven for one hour and thereafter placed in firmly sealed containers within the refrigerator.

4.1.2. Preparation of $_{SLC}$CUR Particles

To prepare the soy lecithin-based encapsulated curcumin ($_{SLC}$CUR) particles, 300 mg of SLC particles and 100 mg of free curcumin ($_{F}$CUR) were weighed in a 3:1 ratio and mixed with sterile water for injection using a high-speed homogenizer (21000 rpm). The dispersion was further stirred using a sonicator (70 kHz at 70% vibration) for a total time of 45 minutes, in 5-minute intervals, to reduce the particle size. The resultant curcumin nanoparticle dispersion was subjected to freezing and lyophilization at 0.1 millibar pressure and -50 °C. Thereafter, the lyophilized powder was mixed with sterile water, and the mixture was subjected to sonication again for a further 45 minutes, according to the same conditions (5-minute intervals, 70 kHz power, and 70% amplitude). The mixture was subsequently frozen again and lyophilized under identical conditions. The particle size and ZP were obtained by DLS. The resulting nanoparticle suspension was frozen and dried in a lyophilizer at 0.1 millibar pressure and -50 °C. Next, the sample was kept in a vacuum oven for 1 hour and stored in tightly closed containers in the refrigerator.

4.1.3. Characterization of $_{SLC}$CUR Particles

The size, ZP values, and polydispersity index (PDI) results were obtained from the DLS instrument to characterize the $_{SLC}$CUR particles. DLS revealed the size distribution of the nanoparticle formulations, while ZP assessed the surface charge of the particles. The particle size, PDI, and ZP were obtained using a DLS instrument, with each sample evaluated at least three times. For the determination of the encapsulation efficiency (EE), the formulation undergoes lyophilization for 48 hours. The quantity of curcumin loaded into soy lecithin was indirectly evaluated by examining the curcumin alone and the soy lecithin-curcumin mixture using a spectrofluorometer at an absorption wavelength of 425 nm. The EE was determined by following equation:

$$EE\ (\%) = \frac{(amount\ of\ SLCCUR\ in\ the\ mixture)}{(initial\ amount\ of\ FCUR\ in\ the\ mixture)} x100 \quad (4.1)$$

A transmission electron microscopy (TEM) analysis was used for the comprehensive morphological analysis of the $_{SLC}$CUR particles For the TEM analysis, a droplet of the $_{SLC}$CUR sample was positioned onto a carbon coated copper grid with a 200-mesh size and leaved to air-dry for one hour before imaging. The $_{SLC}$CUR sample was subsequently stained using a 2% uranyl acetate alternative for negative staining. The sample was subsequently investigated using TEM. The images were acquired at an accelerating voltage of 200 kV. A scanning electron microscopy (SEM) analysis was employed to evaluate the morphological properties of the $_{SLC}$CUR particles. The dried $_{SLC}$CUR sample was coated with gold prior to SEM analysis, and the sample was examined at a magnification of 5.00 KX. Furthermore, atomic force microscopy (AFM) analysis was done to examine the surface topography of the $_{SLC}$CUR particles. The sample was placed on a carbon disc and dried at room temperature before imaging. Fields of 4 × 4 μm² on all surfaces were analyzed utilizing XEI software (version 1.18). Serum stability experiments of the $_{SLC}$CUR particles were done in a PBS solution (pH 7.4) enriched with 10% (v/v) fetal bovine serum (FBS). The $_{SLC}$CUR solution was incubated at the 37 °C, and the particle size (nm), ZP (mV), and PDI of the formulation were assessed at specific time intervals. The pH was around 7.4 for all media used in the characterization analysis, including water, buffers, and serum-containing PBS. Additionally, molecular bond characterization of SLC, $_{SLC}$CUR, and $_{F}$CUR was demonstrated by FT-IR.

All these FT-IR analyses were done in the transmittance mode, covering the range of 4500–450 cm−1.

4.2. CELL CULTURE

4.2.1. Cell Growth and Maintenance Conditions

PNT1A, 22Rv1, and LNCaP cells were routinely cultured in the RPMI-1640 medium and supplied with 10% (v/v) FBS, 100 µg/mL streptomycin & 100 U/mL penicillin.

4.2.2. Cell Subculturing

For subculturing, the monolayer of the cell was rinsed with 2 mL of 1X PBS (pH=7.4) before trypsin/EDTA (0.05% (v/v) trypsin and 0.02% EDTA) treatment for 5 minutes. Following the collection of cells in 2x FBS containing growth medium, cells were subjected to 5 minutes at 300 x*g* centrifugation. The cell pellet was next resuspended with an appropriate cell culture medium and seeded in a flask in an incubator at 37 °C, 5% (v/v) CO_2, with a humidified air until they reach to an 80-90% confluency.

4.2.3. Determination of the Cell Numbers

After the subculturing of cells (explained in the Section 4.1.2), 10 µL cell suspension was placed on each mirror grid of the hemocytometer. Two different grids of the hemocytometer were counted using phase-contrast light microscopy. The cell number was calculated using Equation 4.1, which is given below.

$$(Cell\ number)/mL = Counted\ cell\ number\ x\ Dilution\ factor\ x\ Depth\ of\ hemocytometer \quad (4.2)$$

4.2.4. Cell Freezing

For the cryopreservation of the cells, 90 % (v/v) FBS and 10% (v/v) DMSO were mixed to prepare cell freezing solution. Cells were collected and washed once as described above (Section 4.2.2), and the pellet was resuspended with 1 mL cell freezing solution to be

transferred to cryo-preservation tubes. Next, they were then placed at -80°C immediately for short-term preservation. The vials were put in the liquid nitrogen-containing tanks for the long-term preservation.

4.3. DETERMINATION OF CELLULAR TOXICITY

4.3.1. Determination of the Cellular Toxicity of SLC

To determine the cellular toxicity of the empty carrier SLC, a WST-1 proliferation test was done for PNT1A cells. In this assay, 5000 cells were inoculated into 96-well plates and left for attachment to the monolayer overnight. After allowing for the cell attachment, the cells were treated with 0, 25, 50, and 75 µg/mL of SLC for periods ranging from 24 to 72 hours at 37 °C. At every 24-hour interval, WST-1 reagent was applied onto the cells according to the manufacturer's instructions. The methodology was based on the tetrazolium salts that cleaved to the formazan molecules through mitochondrial enzymes. The viable cell numbers are related to the number of metabolically active cells. Tetrazolium salts are generally colorless, and the activity of the mitochondria in the alive cells on tetrazolium provides the colored products. The absorbance of the plate was observed at 450 and 630 nm, and the percentage of viable cells were determined by normalizing the absorbance readings of non-treated cells to 100 %. The cell numbers were calculated by measuring the absorbance of $25x10^2$ to $2x10^4$ cells as standards at 24 hours and generating a linear model.

4.3.2. Determination of the Cellular Toxicity of $_{SLC}$CUR

To determine the cellular toxicity of $_{SLC}$CUR, a WST-1 proliferation test was done for PNT1A, 22Rv1, and LNCaP cells. In this assay, 5000 cells were inoculated into 96-well plates and left for attachment to the monolayer overnight. After allowing for the cell attachment, cells underwent treatment with 0, 25, 50, and 75 µg/mL of $_{SLC}$CUR for 24 to 72 hours at 37 °C. At every 24-hour interval, WST-1 reagent was applied to the cells according to the manufacturer's instructions. Then, the absorbance was observed at 450 and 630 nm, and the viability of the cells was calculated by normalizing the absorbance readings of non-treated cells to 100 %. The cell numbers were calculated by measuring the absorbance of $25x10^2$ to $2x10^4$ cells as standards at 24 hours and generating a linear model.

4.3.3. Determination of the Cellular Toxicity of $_{SLC}$CUR and $_{F}$CUR

To determine the cellular toxicity of $_{SLC}$CUR and $_{F}$CUR, a WST-1 proliferation test was done for PNT1A, 22Rv1, and LNCaP cells. In this assay, 5000 cells were seeded into 96-well plates and left for attachment to the monolayer overnight. After allowing for the cell attachment, cells underwent treatment at 37 °C with 0, 6.25, 12.5, and 25µg/mL of $_{SLC}$CUR and 0, 2.08, 4.16, and 8.33 µg/mL of $_{F}$CUR for 24 to 72 hours at 37 °C. At every 24-hour interval, the WST-1 reagent was applied onto the cells according to the manufacturer's instructions. Next, the absorbance was obtained at 450 and 630 nm, and the viable cells were calculated by normalizing the absorbance readings of the non-treated cells to 100 %. The cell numbers were calculated by measuring the absorbance of $25x10^2$ to $2x10^4$ cells as standards at 24 hours and generating a linear model.

4.4. DETERMINATION OF CELLULAR UPTAKE

To determine the intracellular uptake of $_{SLC}$CUR and $_{F}$CUR in PNT1A, 22Rv1 and LNCaP cells the fluorescence intensity of the curcumin was detected in the cell. Cells were inoculated in the 6-well plate as $3x10^5$ cells/well and they were allowed to attach at 37 °C overnight. The next day, the cells were treated with 25 µg/mL of $_{SLC}$CUR and 8.33 µg/mL of $_{F}$CUR for 4 hours. Following cell harvesting, the hypotonic solution was added to the pellets, and they were vortexed before placing them on ice (the composition of the hypotonic solution is seen in Table 4.1. Then, Nonidet NP-40 was added to samples to reach a final concentration of 1% (v/v). Lastly, the fluorescence intensity was obtained by the Varioskan Lux Spectrophotometer at 420 nm excitation/550 nm emission wavelength.

Table 4.1. Components of the hypotonic solution

Component	Stock Concentration	Final Concentration
HEPES	40 mM	10 mM
EDTA	100 mM	0.1 mM
EGTA	10 mM	0.1 mM
DTT	100 mM	0.1 mM
NaF	500 mM	50 mM
Na_3VO_4	100 mM	1 mM
PMSF	100 mM	0.5 mM
B-glycerophosphate	300 mM	30 mM
Aprotinin	1 mg/mL	10 µg/mL
Leupeptine	1 mg/mL	10 µg/mL
Pepstatin	1 mg/mL	10 µg/mL
dH_2O	-	

EGTA, Ethylene Glycol Tetraacetic Acid; EDTA, Ethylenediaminetetraacetic Acid; DTT, Dithiothreitol; PMSF, phenylmethylsulfonyl fluoride; dH_2o, distilled water.

The cellular uptake of $_{SLC}$CUR and $_{F}$CUR in PNT1A, 22Rv1, and LNCaP cells was assessed. 25 µg/mL of $_{SLC}$CUR and 8.33 µg/mL of $_{F}$CUR was applied to the cells for 48 hours. The cells were then fixed and stained for imaging. Fixation was done using 4% paraformaldehyde (PFA) in PBS at RT for 15 minutes. Following fixation, cells were washed three times with PBS to eliminate any remaining fixative. Nuclei were stained with DAPI (blue). Images were obtained with a fluorescence microscope equipped with suitable filters for the fluorophores.

4.5. DETECTION OF APOPTOTIC CELL DEATH

4.5.1. Detection of Apoptotic Cell Death by TUNEL Assay

The apoptotic populations of PNT1A, 22Rv1, LNCaP, and TRAMP-C2 cells were determined by TUNEL assay. For this purpose, the cells were inoculated in 8-well chamber slides at a density of $5x10^4$ cells/well and allowed to attach overnight. Next day, cells were treated with 25 µg/mL of $_{SLC}$CUR and 8.33 µg/mL of $_{F}$CUR for 48 hours. After collecting cells, the pellet was resuspended with 4% (v/v) PFA and incubated for 1 hour at 37 °C. Then, the supernatant was discarded, and the remaining solution was resuspended with the pellet and added onto the 8-well chamber slides for air-dry. After drying, the samples were

incubated with the TUNEL reaction mixture (comprising label and enzyme mix) at 37°C. Following the incubation, the TUNEL reaction mixture was removed from the samples, and the slides were analyzed by fluorescent microscope at an excitation/emission wavelength of 515-565 nm (green).

4.5.2. Western Blotting for the Detection of Apoptotic Cell Death

4.5.2.1. Protein Isolation

PNT1A, 22Rv1, and LNCaP cells were inoculated into 6-well plates at a density of $3x10^5$ cells per well. Following cell attachment, the cells were subjected to treatment with 25 µg/mL of $_{SLC}$CUR and 8.33 µg/mL of $_{F}$CUR for 48 hours. After the treatment, dead cells in the cell culture medium were collected at 350 x*g* centrifugation for 5 minutes at 4°C. Then, 100 µL of supernatant was kept, while the remaining volume was discarded, and the pellet was resuspended in 1X PBS. The centrifugation process was repeated under the same conditions. Meanwhile, the cells in culture flasks were washed with 1X PBS. Following the washing of cells and completely draining PBS, 30 µl of RIPA buffer, supplemented with Protease Inhibitor, was added into each well. The cell monolayer of each well was scraped with a scraper and collected into the Eppendorf tubes. The centrifuged cells were also combined with the scraped cell lysates. The combined cell lysates were cooled on ice and subjected to sonication at 60 kHz for three cycles, followed by centrifugation at 1000 xg at 4°C for one minute to remove cellular debris. The supernatant was obtained to fresh tubes and placed at -80°C until required.

4.5.2.2. Protein Content Assay

A detergent-compatible protein assay was employed to evaluate the protein content. First, a 500 µg/mL of bovine serum albumin (BSA) working stock was prepared. The stock solution underwent heat inactivation at 57°C for 1 h. Next, protein standards of 0.1 mg/mL, 0.25 mg/mL, 0.5 mg/mL, 0.75 mg/mL, and 1 mg/mL were prepared through serial dilution. Protein samples obtained from cells were diluted at a ratio of 1:10 in dH_2O. In a 96-well plate, 5 µL each of the standard and protein samples were combined with 25 µL of Protein Assay Reagent A and 200 µL of Protein Assay Reagent B in triplicate. The samples were incubated in the dark at RT for 15 minutes. Absorbance values were observed

at 750 nm by microplate reader, and protein concentrations were obtained from the BSA calibration curve generated by BSA standards.

4.5.2.3. Sodium Dodecyl Sulfate-Polyacrylamide Gel Electrophoresis (SDS-PAGE) and Western Blotting

The protein lysates were denatured in Laemmli buffer for 5 minutes at 95°C and loaded into the 12% of sodium dodecyl sulfate-polyacrylamide (SDS-PA) gels as described in Table 4.2, and the separating and stacking gels were prepared as described in Table 4.3. First, a separating gel was prepared between the casting gel glasses, and the gel top was covered with isopropanol for the protection of any air contact and to help the gel polymerize. After the gel's polymerization, isopropanol was poured out between the glasses, and the surface of the gel was rinsed with dH_2O to remove the remaining isopropanol. Stacking gel was prepared and poured on the polymerized separating gel surface. A 1 mm thick 10-well comb was placed on the surface of the stacking gel, and it was allowed to be polymerized. After polymerization, the comb was removed from the surface of the gel, and the gel was positioned in the GE apparatus, which was filled with the 1X running buffer. Then, the protein samples were carefully loaded in the wells and run by GE at 75 V for approximately 3 hours. The running buffer (10X, pH 8.5) was prepared according to Table 4.4. The running buffer was diluted to 1X in dH_2O and cooled at 4 °C before use. The Mini-PROTEAN Tetra Handcast System and PowerPac™ Basic Power Supply (BioRad) were used for gel preparation and operation.

Table 4.2. SDS-PA gel buffers.

	4X Tris-SDS (lower gel buffer)	**4X Tris-SDS (upper gel buffer)**
Tris Base	1.5 M	0.5 M
SDS	0.4% (w/v)	0.4% (w/v)
pH	8.8	6.8

SDS, sodium dodecyl sulfate.

Table 4.3. SDS-PA gel compositions.

	Separating Gel	Stacking Gel
Acrylamide/bis-acrylamide	6 ml	0.65 ml
Lower buffer	3.75 ml	-
Upper buffer	-	1.25 ml
APS	50 µl	25 µl
TEMED	10 µl	5 µl
dH_2O	5.20 ml	3.25 ml

APS, ammonium persulfate; TEMED, tetramethyl ethylenediamine.

SDS-PA gel electrophoresis was followed by Western blotting to transfer protein samples onto nitrocellulose membranes featuring pore diameters of 0.22 or 0.45 µm, based on the molecular weight of the target protein. The wet transfer was done at 175 mA for 1.5 h using Mini Trans Blot Module (Bio Rad) for proteins of approximately 30- 150 kDa. Transfer buffer (10X, pH 8.3) was prepared described in Table 4.5. The transfer buffer was diluted to 1X in dH_2O with 20% (v/v) methanol and cooled at 4 °C before use.

Table 4.4. Running and transfer buffer recipes.

	10X Running buffer	10X Transfer buffer
Tris base	0.25 M	0.25 M
Glycine	1.92 M	1.92 M
SDS	1% (w/v)	-
pH	8.5	8.3

SDS sodium dodecyl sulfate.

Membrane blocking was performed for 1 hour in the 5 % (w/v) of non-fat milk powder in Tris-buffered saline (1X TBS, given in Table 4.5), and 0.5 % (v/v) Tween-20 (TBS-T) at RT. Following the blocking, the membranes were treated overnight with primary antibodies for β-Actin (Sigma Aldrich 5316, USA), PARP (CST 9542P, USA), and cleaved caspase 9 (CST 9502S, USA) at 1:1000 dilution in the 5% (w/v) of milk at 4°C. After the incubation, the membrane washing was done with 1X TBS-T two times for 5 minutes. Next, HRP-conjugated anti-rabbit (CST #7074) or anti-mouse secondary antibodies were used based on the source organism of each antibody at 1:3000 dilution in 5% (w/v) of milk for 2 hours at RT. The membranes underwent three washes in the TBS-T for 10 minutes each, from

blocking to imaging, except for the last wash, which utilized 1X TBS. To obtain the luminescence, the blots were incubated with WesternBright Sirius HRP-Conjugate Substrate at RT for 1 minute and the bands were visualized with the chemiluminescence module of the ChemiDoc XRS+Gel Imaging System and ImageLab software.

Table 4.5. Preparation of 10X TBS (pH 7.6).

Component	Concentration
Tris base	0.2 M
NaCl	0.15 M

NaCl, sodium chloride.

4.6. EVALUATION OF THE *IN VIVO* ANTI-TUMOR ACTIVITY IN 22RV1 XENOGRAFT TUMOR MODEL

4.6.1. Animals

For *in vivo* anti-tumor activity experiments, homozygous nude ($Foxn1^{nu}/Foxn1^{nu}$, 007850) male mice (6-8-week-old) weighing 22±2g obtained from Yeditepe University Experimental Research Center (YÜDETAM) (Yeditepe University, Istanbul, Turkey) and performed at Yeditepe University. The homozygous nude mice were housed in filtered and sterilized cages and the cages were maintained at an ideal temperature of 23±10 °C and humidity of 60±10 %. Then, the mice were kept under 12 hours in light/dark cycles, and they were provided with specialized meals for nude mice and given water *ad libitum*. All animal treatments and studies were done in accordance with the rules authorized by the Yeditepe University Institutional Animal Care and Welfare Committee (Istanbul, Turkey).

4.6.2. Development of 22Rv1 Xenograft Prostate Cancer Model in Homozygous Nude ($Foxn1^{nu}/Foxn1^{nu}$) Male Mice

To determine the anti-cancer activity of the $_{SLC}$CUR, a 22Rv1 prostate cancer xenograft tumor model was created in homozygous nude ($Foxn1^{nu}/Foxn1^{nu}$, 007850) mice. For this purpose, animal groups were established, the necessary concentrations and amounts of SLC,

$_{F}$CUR, and $_{SLC}$CUR were determined, and the sample size for the animal studies was estimated using power analysis. Our research group has utilized and optimized the 22Rv1 xenograft tumor model with homozygous nude mice in previously published studies [172]. These studies will be taken into consideration while doing animal research. Using the previously developed method by our group, a 22Rv1 xenograft tumor model will be generated in 6–8 weeks old homozygous nude (Foxn1^{nu}/Foxn1^{nu}) male mice. In this context, 12x10^{6} 22Rv1 cells grew in the RPMI-1640 with 10 % (v/v) FBS, 100 U/mL penicillin, and 100 µg/mL streptomycin were dissolved in matrigel at a ratio of 1:3. They were injected subcutaneously from the dorsal region of the mice. After seven days following the implantation of cancer cells, the animals were separated randomly into four groups: (i) Group to be given sterile PBS, (ii) SLC (Dosage to be applied: 1.5 g/kg, intraperitoneal), (iii) $_{F}$CUR (Dosage to be applied: 500 mg/kg, intraperitoneal) (iv) $_{SLC}$CUR (Dosage to be applied: 1.5 g/kg, intraperitoneal). Control groups received the same volume of PBS as the treated groups (vehicle control). The dose to be applied was determined based on the literature research [124,125,151]. Beginning on the third day following inoculation of the tumor cells, mice were administered intraperitoneal injections every three days, resulting in eight injections. Each animal's weight was obtained before each injection. Also, mice were monitored for mortality and morbidity until the conclusion of the study. Following 24 days of treatment, the mice were euthanized via cervical dislocation, and the tumor volumes were measured. The Yeditepe University Animal Care and Welfare Committee (HADYEK) authorized the study protocol (decision #2023/17), and all studies followed to the ARRIVE guidelines.

4.6.3. Histopathological Examination

Formalin fixed paraffin embedded organ and tumor samples were prepared for examination by a specialized pathologist by collecting and preserving tissues from the heart, lung, kidney, liver, spleen, stomach, and intestine in 10% (v/v) formalin. The samples were then analyzed at the Ümraniye Training and Research Hospital Pathology Department using hematoxylin and eosin (H&E) staining [173]. Tumor tissue samples were evaluated for necrosis, inflammation, and fibrosis, with each factor classified on a scale from 0 to 3, where 0 indicates absence, 1 defines mild presence, 2 implies moderate presence, and 3 represents severe presence.

4.6.4. Measurements of the Tumor Volume

The size and volume of the tumor for each animal were assessed following tumor resection. A caliper measured tumor sizes and tumor volumes were obtained by the formula given below [174]:

$$Tumor\ Volume = Length\ x\ (Width)^2 \tag{4.3}$$

4.7. STATISTICAL ANALYSIS

All results determined from the three separate experiments were represented as the means ± standard deviation (SD). Student t-test was employed to assess group mean differences. One way analysis of variance (ANOVA) was performed to conduct multiple comparisons. *p*-value below 0.05 was assessed as statistically significant (* $P \leq 0.05$, ** $P \leq 0.01$, *** $P \leq 0.001$, **** $P \leq 0.0001$). All analyses were done utilizing Microsoft Excel (Version 2020), and graphs were generated with GraphPad Prism (Version 8.4.4; GraphPad Software, USA, obtained via free trial from www.graphpad.com).

5. RESULTS

5.1. SYNTHESIS AND CHARACTERIZATION OF $_{SLC}$CUR PARTICLES

The particle size distribution, ZP, PDI, and encapsulation efficiency of the $_{SLC}$CUR were assessed to characterize the $_{SLC}$CUR particles using DLS (Table 5.1). The results showed that the $_{SLC}$CUR particle size was roughly 120 nm with a PDI of 0.3 (Figure 5.1), indicating that the particles were within the nanoscale range, displaying distinct particles with homogeneous distribution and consistent dispersion. The stability of the $_{SLC}$CUR formulation was confirmed by the ZP measurement of −20.25 ± 1.2 (Figure 5.2), suggesting appropriate colloidal stability. Encapsulation efficiency (EE) was determined using Equation (1) and expressed as mean ± standard deviation, resulting in a value of 78.3% ± 0.1% (Table 5.1).

Table 5.1. Mean values of the particle size diameter, polydispersity index, zeta potential and the percentage of encapsulation efficiency.

Formulation	Particle Size (nm)	Polydispersity Index	Zeta Potential	Encapsulation Efficiency (%)
$_{SLC}$CUR	119.5 ± 0.93	0.31 ± 0.09	−20.25 ± 1.2	78.3 ± 0.1

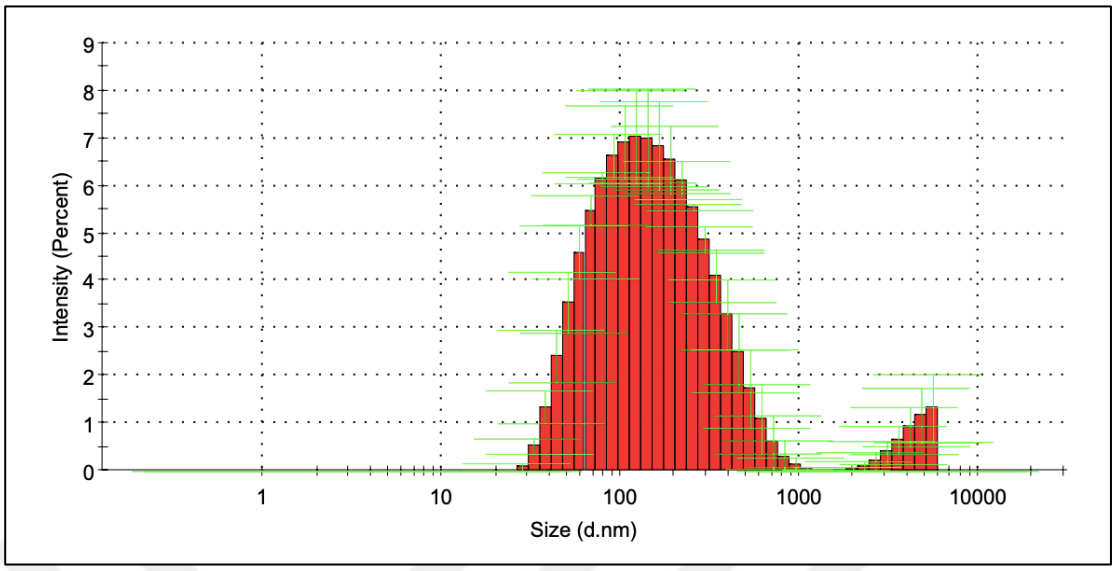

Figure 5.1. The particle size distribution of $_{SLC}$CUR. The particle size was obtained by dynamic light scattering. Each sample was evaluated at least three times.

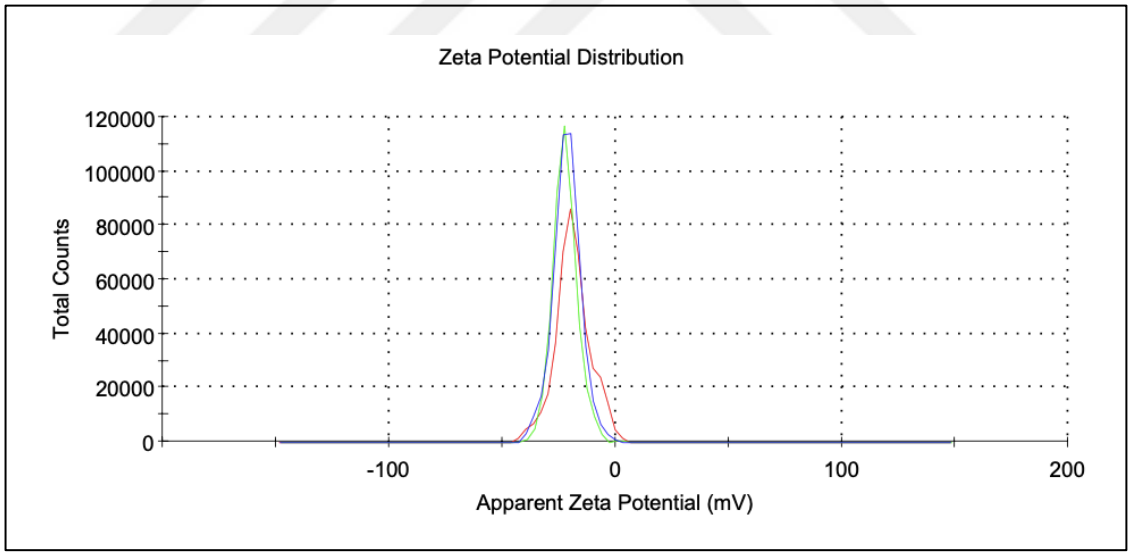

Figure 5.2. The zeta potential of $_{SLC}$CUR particles. The zeta potential was measured by the Zetasizer instrument. The green, blue, and red diagrams show independent measurements of the sample, indicating that the measurement was done a minimum of three repeats for accuracy and repeatability.

The morphology and surface characteristics of the particles were next analyzed using TEM and SEM instruments. The TEM investigation revealed that the $_{SLC}$CUR particles were equally distributed, displayed a spherical shape, and they were in range of the nanometric size (Figure 5.3), which was consistent with the findings obtained from DLS measurements. In TEM images, the $_{SLC}$CUR particles were identified as separate individual particles, while SEM analysis confirmed their spherical morphology, showing agglomeration and variation in particle sizes, covering both smaller and slightly larger particles (Figure 5.4).

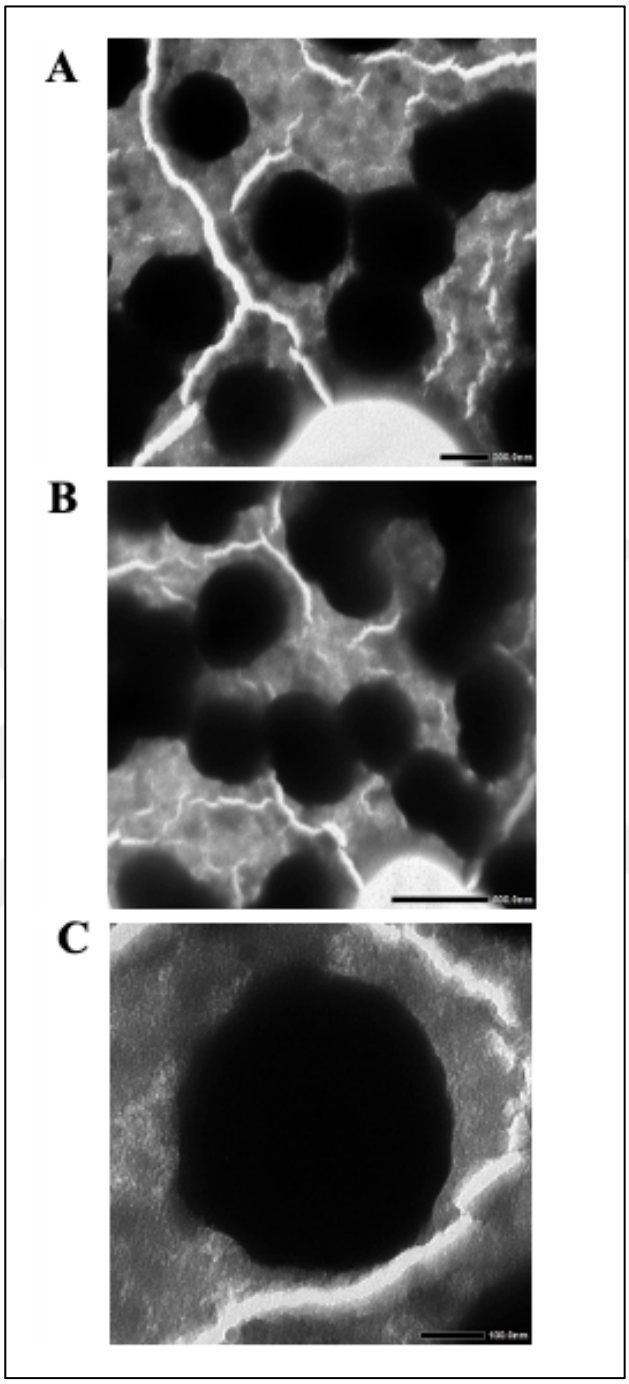

Figure 5.3. Transmission electron microscope (TEM) images of $_{SLC}$CUR particles. The images were obtained at (a) 500 nm scale, (b) 200 nm scale, and (c) 100 nm scale. A droplet of the $_{SLC}$CUR sample was positioned on a carbon coated copper grid with a 200-mesh size and permitted to air-dry for 1 hour prior to imaging for TEM examination. The samples were then stained with a 2% uranyl acetate alternative (Ted Pella, USA) for negative staining. Images were captured at 200 kV accelerating voltage. Uniformly dispersed, spherical-shaped $_{SLC}$CUR was observed.

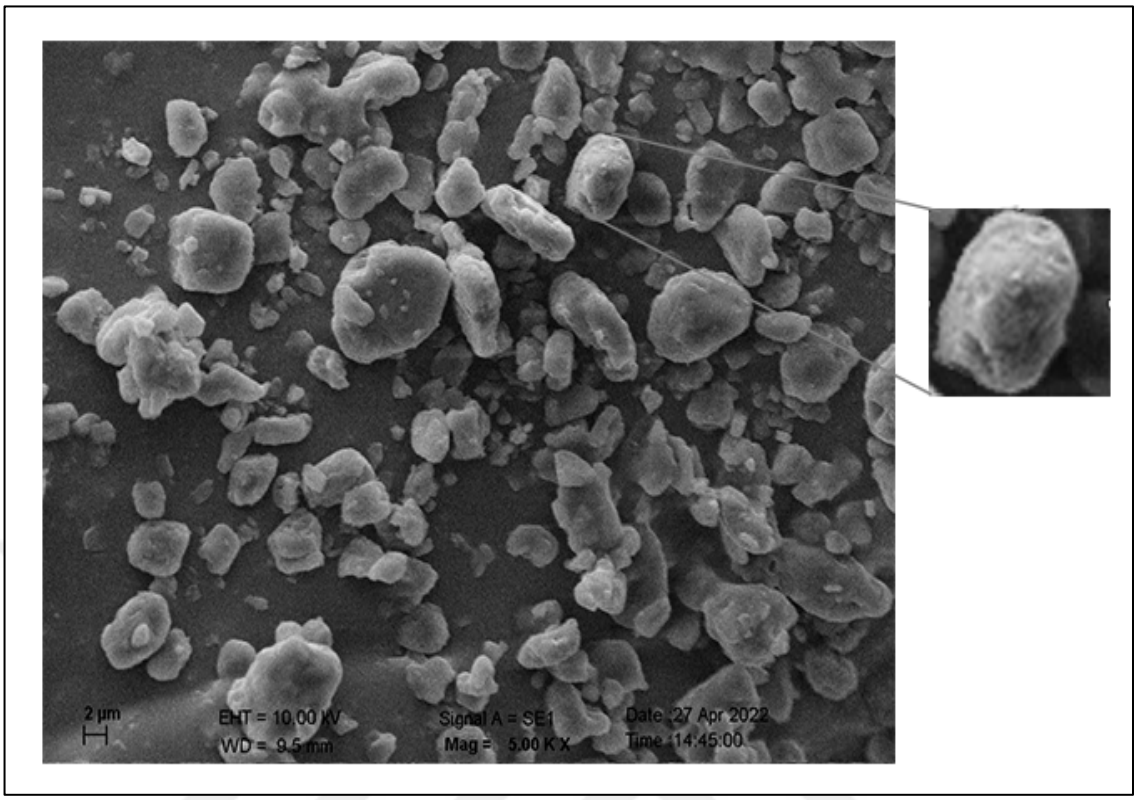

Figure 5.4. Scanning electron microscope (SEM) image of the SLCCUR particles. The dried SLCCUR sample was coated with gold before the SEM examination. The spherical shape and aggregation of SLCCUR were detected. The magnification is 5.00 KX, and the scale bar is 2 µm.

Following TEM data, AFM investigation was performed to obtain the surface topography of the SLCCUR particles. The quantification of AFM results revealed that the particles exhibited spherical morphologies, with a clearly visible nanometer-scale size distribution, ranging from around 150 to 180 nm (Figure 5.5).

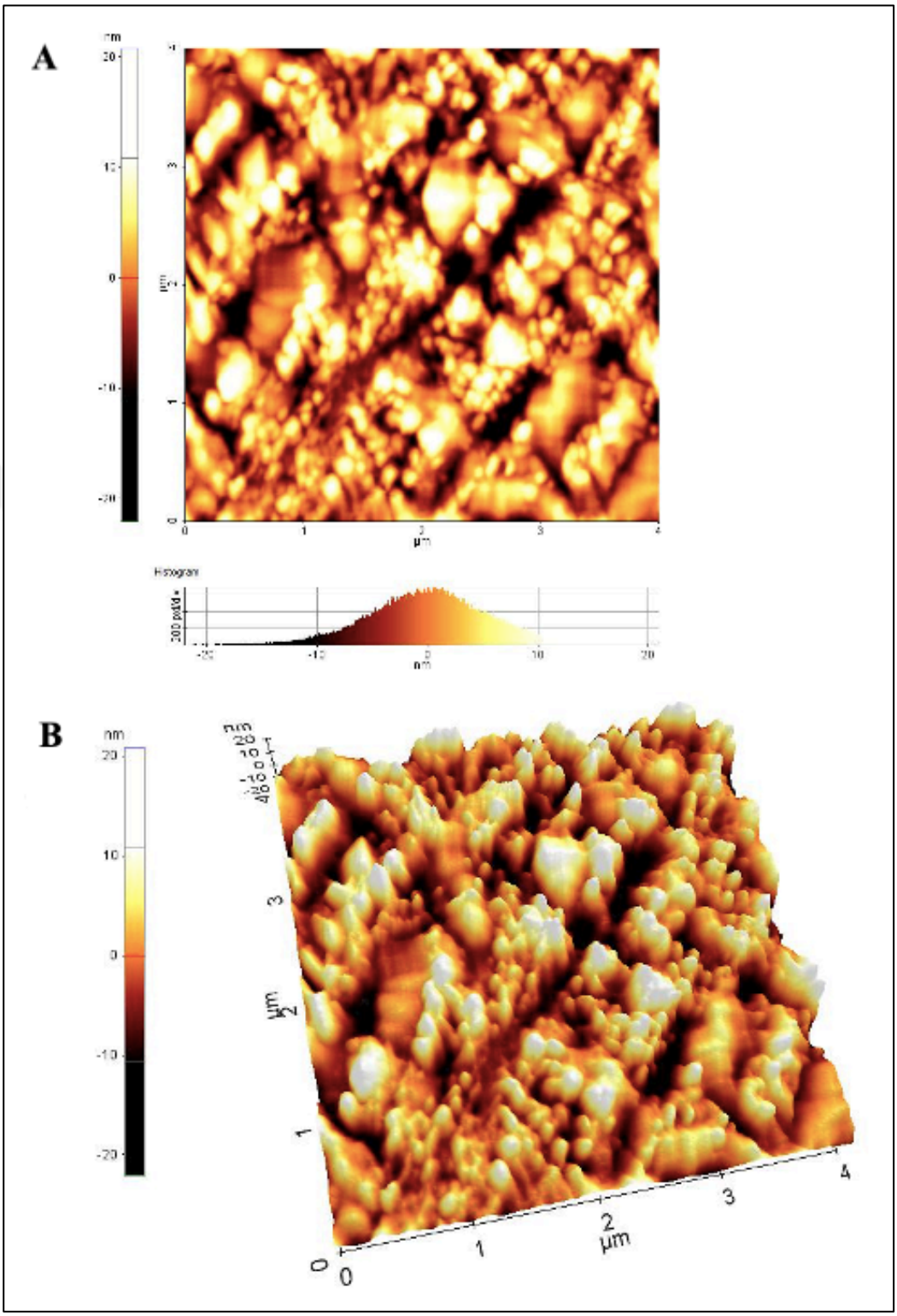

Figure 5.5. Atomic force microscope (AFM) image of the $_{SLC}$CUR particles. (a) Two-dimensional and (b) Three-dimensional perspectives were shown. The sample was positioned on a carbon disc and dried at room temperature before imaging. Fields of 4 × 4 µm² on all surfaces were analyzed utilizing XEI software (version 1.18).

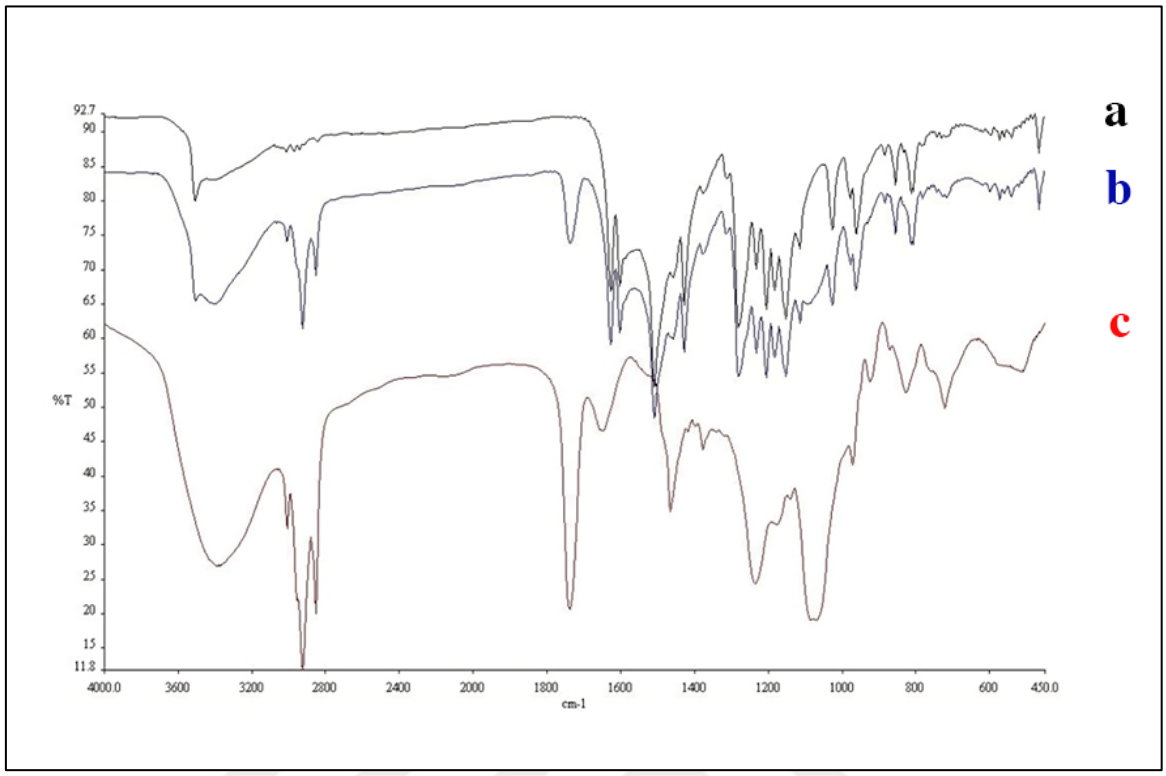

Figure 5.6. FT-IR spectrum of $_{SLC}$CUR particles. a) free curcumin ($_{F}$CUR), b) soy lecithin (SLC), and c) soy lecithin-based curcumin ($_{SLC}$CUR) molecular bond characterization was carried out using FT-IR, with measurements obtained on a Perkin Elmer FT-IR System Spectra BX in transmittance mode, covering the range of 4500-450 cm^{-1}.

To evaluate the serum stability and define the physicochemical characteristics of $_{SLC}$CUR particles, they were incubated in PBS (pH 7.4) comprising 10% (v/v) FBS at 37°C. The average particle size, PDI, and ZP were evaluated at particular time intervals (0, 1, 2, 3, 4, 6, 8, 12, and 24 hours) to examine possible changes in particle stability with time. No important changes in the average particle size were found after 24 hours of incubation under these conditions, indicating the good colloidal stability of the $_{SLC}$CUR particle in a serum-containing environment (Figure 5.7).

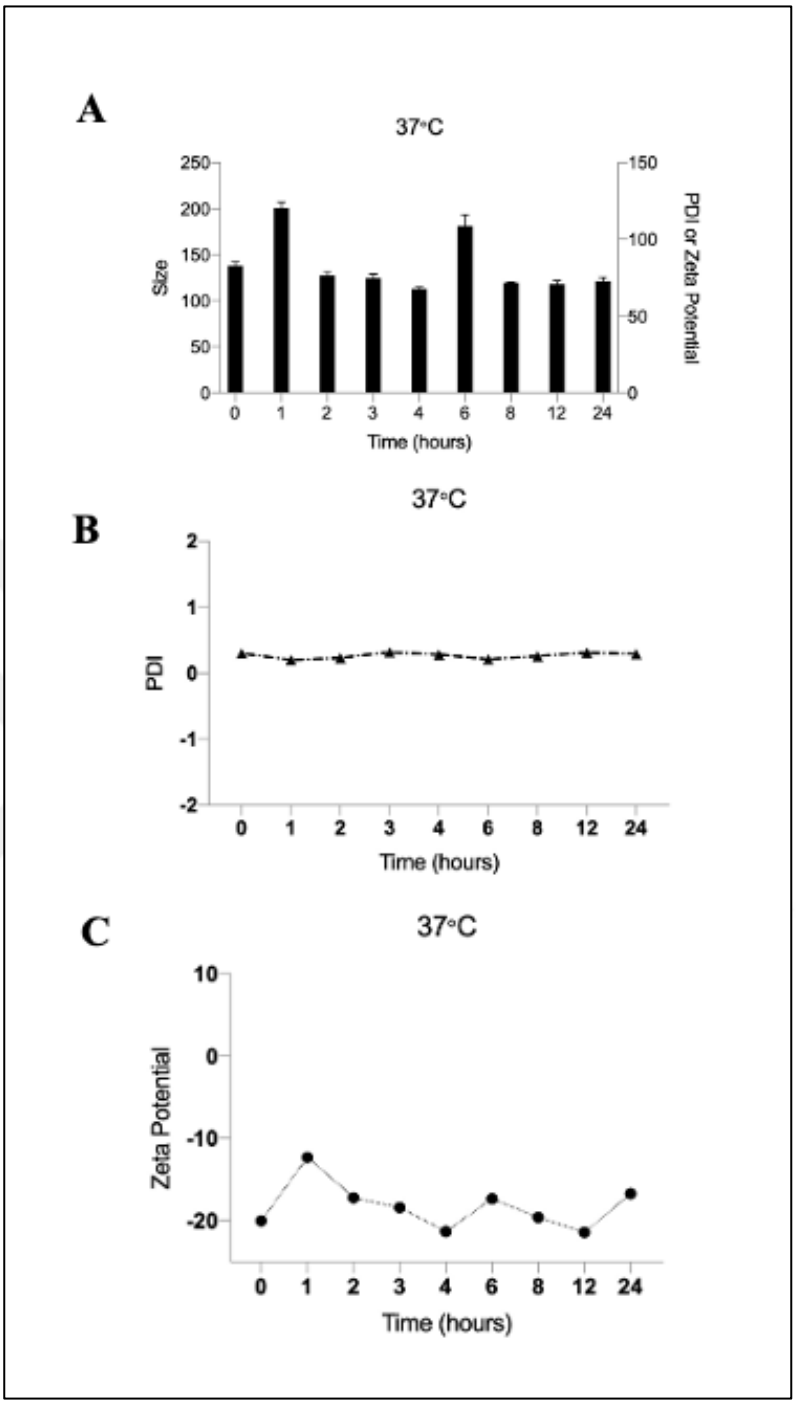

Figure 5.7. Serum stability of $_{SLC}$CUR particles. The $_{SLC}$CUR particles were incubated in PBS with 10% (v/v) FBS at 37°C for 24 h, during which the (a) particle size, (b) polydispersity index (PDI), and (c) zeta potential was assessed at specific time intervals.

5.2. EFFECT OF SLC, $_{SLC}$CUR, AND $_{F}$CUR ON CELL PROLIFERATION

5.2.1. Determination of the Cellular Toxicity of SLC

In order to determine whether curcumin can exhibit a cytotoxic effect when encapsulated in SLC, an experimental setup was established that employed androgen-responsive human prostate carcinoma 22Rv1 and LNCaP cells, as well as normal epithelial cells PNT1A. For this purpose, the cytotoxicity of the empty carrier, SLC, was initially determined on all cell lines at the concentrations of 25, 50, and 75 µg/mL over 24 to 72 hours. The WST-1 cell proliferation assay was employed to investigate the potential cytotoxic effects of the SLC carrier system on cell viability. In PNT1A cells, minimal inhibitory effects on the cell proliferation were obtained after treatment with 25 µg/mL of SLC at 24, 48, and 72 hours, with cell counts observed at 6166, 5566, and 8033, respectively (Figure 5.8). A cytostatic effect was seen at 72 hours following treatment with 50 µg/mL SLC, resulting in a decrease in cell count to 5191. Treatment with 75 µg/mL of empty SLC significantly decreased cell proliferation compared to untreated controls, with cell counts dropping from the initial seeding number of 5000 to 4863, 3641, and 2975 at 24, 48, and 72 hours, respectively. Similarly, no inhibitory effect on cell proliferation was noted in 22Rv1 and LNCaP cells after treatment with 25 µg/mL of SLC for 24 to 72 hours. A cytostatic response was observed at 50 µg/mL of SLC, with cell counts of 4541 and 5520 for 22Rv1, and 4125 and 5141 for LNCaP cells at 24 and 48 hours, respectively. After 72 hours, treatment with 75 µg/mL of SLC resulted in a substantial decrease in cell number in both the 22Rv1 and LNCaP cells compared to untreated controls. The findings indicate that SLC concentrations over 25 µg/mL induce non-specific cytotoxic effects, probably independent of the encapsulated cargo. A dose-dependent increment in cytotoxicity was noted at higher doses (50 and 75 µg/mL), indicating the importance of careful dose determination. Thus, 25 µg/mL was determined as the maximal safe and non-toxic quantity under the conditions applied in this study and was chosen for the following treatments.

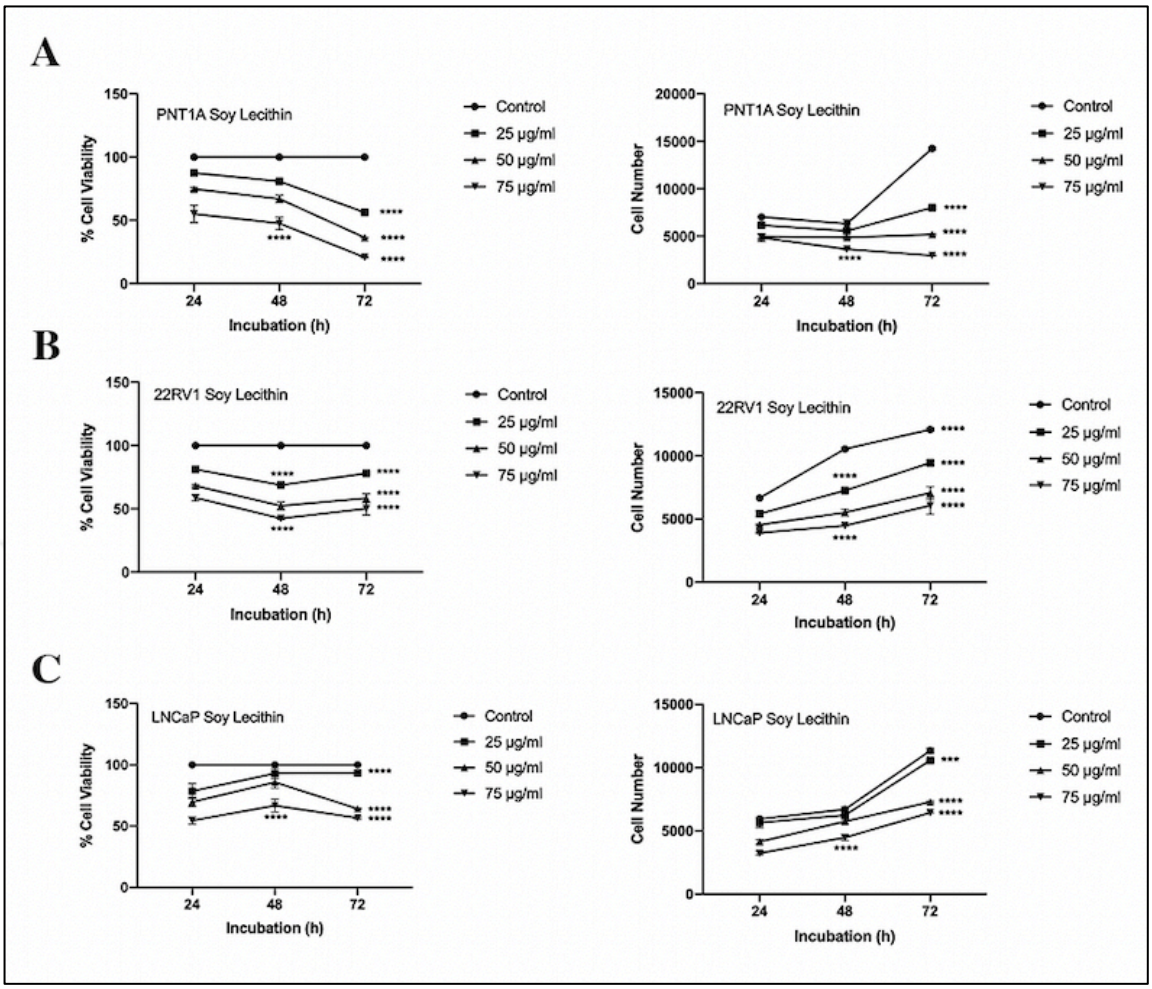

Figure 5.8. Effects of SLC on prostate cells proliferation. (a) PNT1A, (b) 22Rv1, and (c) LNCaP cell proliferation was observed after the cells were administered to treatment with 0 (control), 25, 50, and 75 µg/mL of SLC for 24 to 72 hours. Cell viability and total number of cells were evaluated the ending of each 24 hours. The cell viability of untreated cells (0 µg/mL) was defined as 100% to determine the comparative viability for each condition (n = 3). Data is defined as mean ± standard deviation (SD). Statistically significant reductions in cell number relative to the control are represented as $***p \leq 0.001$ and $**p \leq 0.0001$.

5.2.2. Determination of the Cellular Toxicity of $_{SLC}$CUR and $_{F}$CUR

The cytotoxic impacts of $_{SLC}$CUR and $_{F}$CUR on prostate cells were evaluated in a dose- and time-dependent approach (Figure 5.9). No significant decrease in cell number was noted in PNT1A cells after treatment with $_{SLC}$CUR at concentrations of 6.25, 12.5, or 25 µg/mL for

24 hours. Likewise, $_{F}$CUR administration at corresponding curcumin dosages (2.08, 4.16, and 8.33 μg/mL) did not show notable changes in cell proliferation. In 22Rv1 cells, $_{SLC}$CUR treatment led to a concentration-dependent reduction in cellular viability. After 24 hours, a concentration of 6.25 μg/mL produced a cytostatic effect (4967 cells), whereas treatments with 12.5 and 25 μg/mL reduced cell numbers to 2934 and 1500, respectively. The effect was more significant at 48 and 72 hours, with cell numbers of 1967 and 5183 for 12.5 μg/mL, and 950 and 983 for 25 μg/mL, respectively. $_{F}$CUR treatment at 48 hours resulted in decreased cell numbers (4533, 2617, and 1817 for concentrations of 2.08, 4.16, and 8.33 μg/mL, respectively); however, this decrease was not maintained after 72 hours, as cell numbers reached the initial seeding density of 5000 cells. In LNCaP cells, administration of 25 μg/mL $_{SLC}$CUR led to a significant decrease in cell numbers to 4217, 1783, and 2100 at 24, 48, and 72 hours, respectively. $_{F}$CUR at the equivalent dosage (8.33 μg/mL) did not result in an important inhibitory effect on LNCaP cell proliferation at any examined time point.

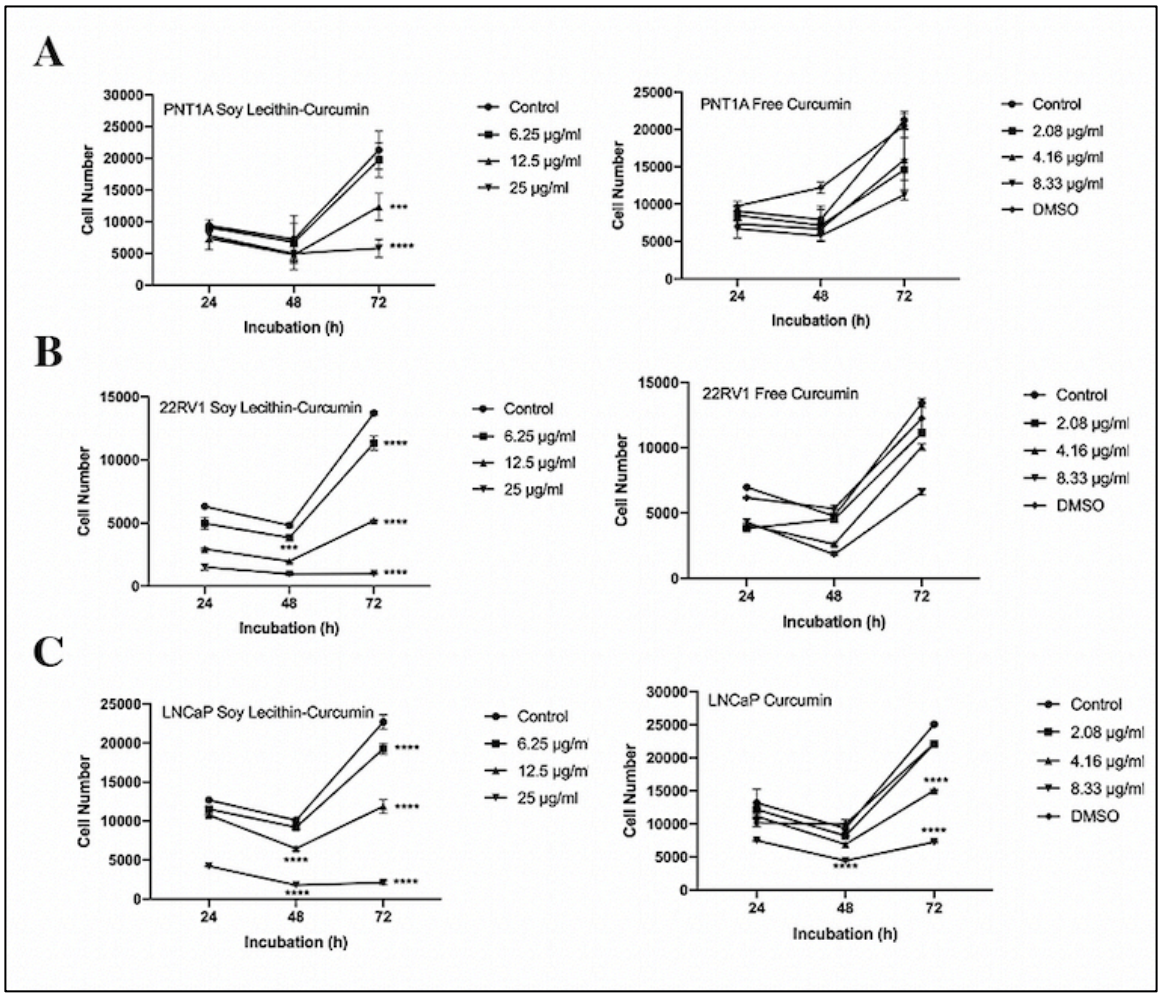

Figure 5.9. Effects of $_{SLC}$CUR and $_{F}$CUR on prostate cells proliferation. (a) PNT1A, (b) 22Rv1, and (c) LNCaP cell proliferation was observed after the cells were administered to treatment with 0 (control),6.25, 12.5, and 25 µg/mL of $_{SLC}$CUR and 0 (control), 2.08, 4.16, and 8.33 µg/mL of $_{F}$CUR for 24 to 72 h. The soy lecithin:curcumin ratio in the $_{SLC}$CUR was 3:1. Curcumin was dissolved in 1:1000 DMSO-containing cell culture medium. Cell viability and total number of cells were evaluated ending of each 24 hours. The cell viability of untreated cells (0 µg/mL) was defined as 100% to determine the comparative viability for each treatment condition (n = 3). Data are showed as mean ± standard deviation (SD). Statistically significant reductions in cell number relative to the control are indicated as ***$p \leq 0.001$ and **$p \leq 0.0001$.

5.3. DETERMINATION OF INTRACELLULAR UPTAKE OF $_{SLC}$CUR

The intracellular absorption of curcumin was examined by measuring fluorescence intensity in PNT1A, 22Rv1, and LNCaP cells after treatment with $_{SLC}$CUR at 6.25, 12.5, and 25 µg/mL concentrations, and $_{F}$CUR at 2.08, 4.16, and 8.33 µg/mL for 48 hours. Fluorescence microscopy images demonstrated that curcumin was visibly internalized only in cells treated with $_{SLC}$CUR, while no measurable fluorescence was detected in cells treated with $_{F}$CUR (Figure 5.10).

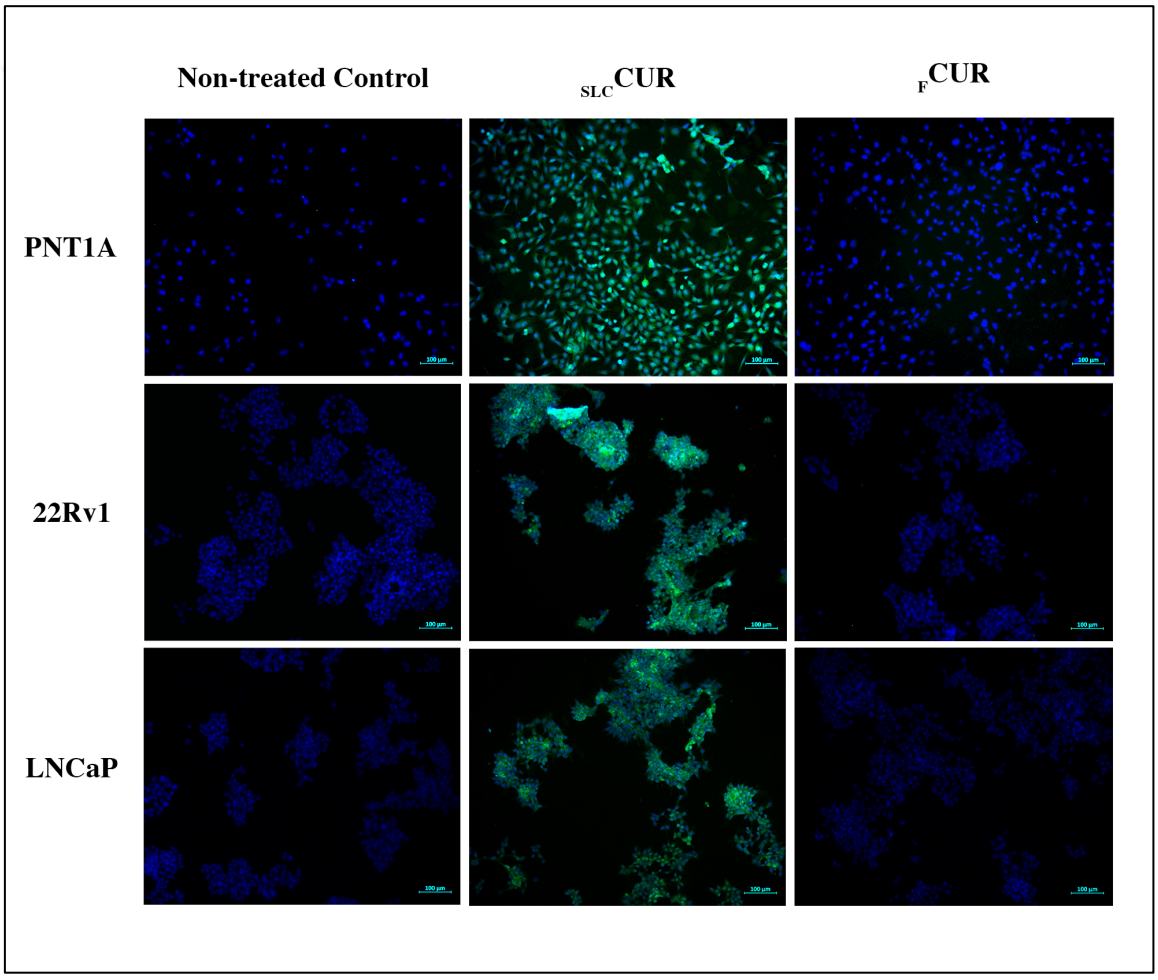

Figure 5.10. Evaluation of the cellular uptake of $_{SLC}$CUR and $_{F}$CUR in prostate cells. Cells were subjected to treatment with 25 µg/mL $_{SLC}$CUR and 8.33 µg/mL $_{F}$CUR for 48 hours and examined under a fluorescent microscope at 20X. Cells were stained with DAPI (blue) for nuclear imaging. Untreated cells were determined as a control. The overlay shows the determination of $_{SLC}$CUR uptake in the cells. The scale bar measures 100 µm.

Fluorescence intensity was further measured to evaluate curcumin uptake in lysed PNT1A, 22Rv1, and LNCaP cells with a fluorescence reader (Figure 5.11). In PNT1A cells, $_{SLC}$CUR treatment resulted in fluorescence intensity increments of 8.7-, 13.7-, and 16-fold at the corresponding doses. However, any statistically significant changes in fluorescence intensity were detected in PNT1A cells subjected to $_{F}$CUR treatment. In 22Rv1 cells, $_{SLC}$CUR treatment caused significant increases in fluorescence intensity, showing 5.34-, 16.53-, and 28.9-fold at increasing doses. However, $_{F}$CUR treatment at similar concentrations increased only 0.71, 0.67, and 1.23-fold. Like 22Rv1, in LNCaP cells, $_{SLC}$CUR induced a rise in fluorescence intensity of 6.74-, 14.9-, and 27.66-fold, whereas $_{F}$CUR induced increases only 1.62-, 1.87-, and 2.87-fold, respectively. These results indicate that the intracellular uptake of $_{SLC}$CUR in 22Rv1 and LNCaP prostate cancer cells was almost 15-fold higher than the uptake of $_{F}$CUR. Furthermore, the fluorescence intensity fold changes in 22Rv1 and LNCaP prostate cancer cells were significantly higher than in PNT1A normal prostate epithelial cells.

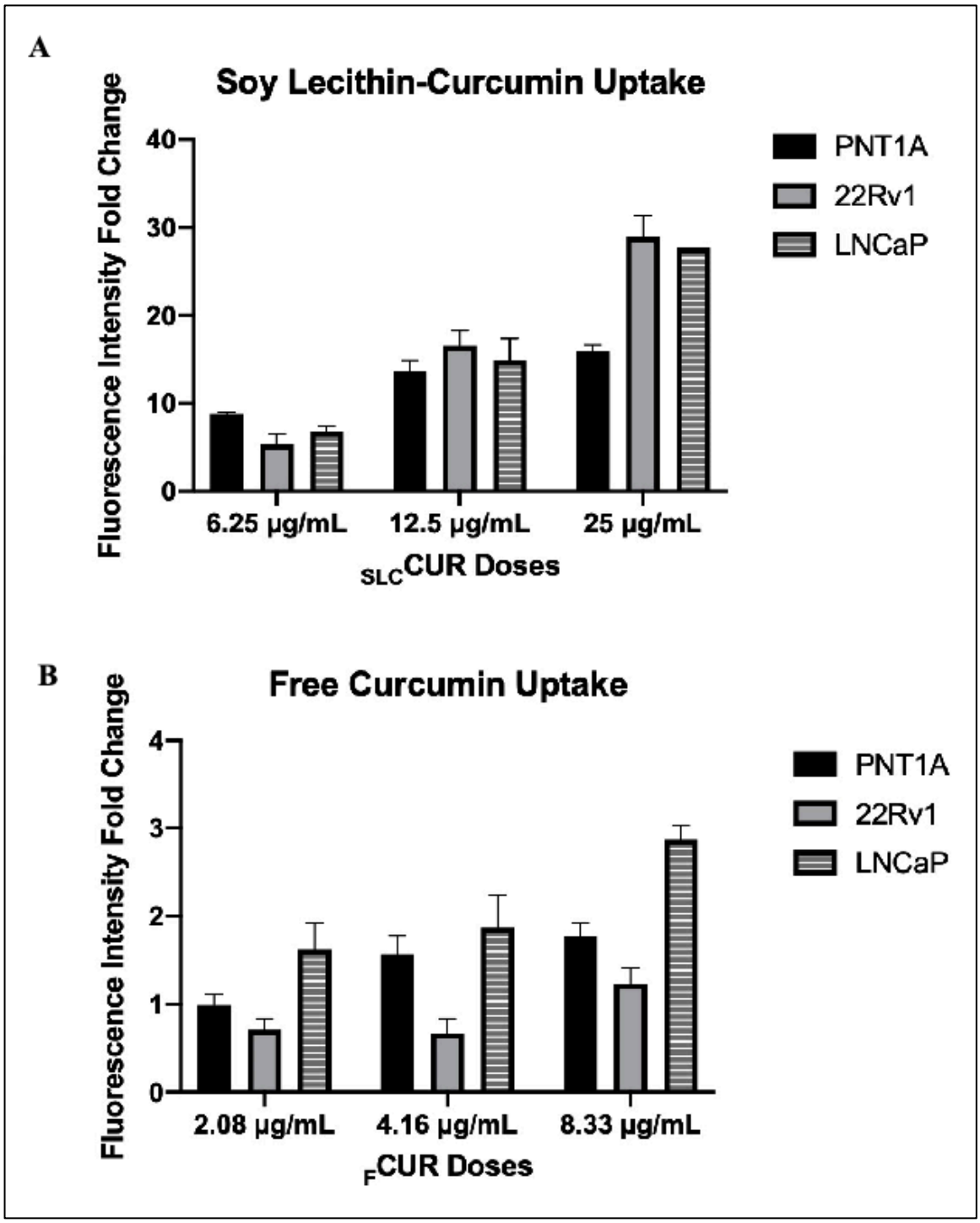

Figure 5.11. Investigation of cellular uptake of $_{SLC}$CUR in the cells. (a) $_{SLC}$CUR and (b) $_{F}$CUR in PNT1A, 22Rv1, and LNCaP cells. Cells were subjected to 6.25, 12.5, and 25 µg/mL of $_{SLC}$CUR treatment and 2.08, 4.16, and 8.33 µg/mL of $_{F}$CUR for 48 hours, after which fluorescence intensity values were determined after the cell lysis at an excitation/emission wavelength of 420/550 nm. The fluorescence intensity levels were normalized to untreated control cells.

5.4. DETERMINATION OF CELL DEATH INDUCED BY $_{SLC}$CUR

5.4.1. Analysis of Apoptotic Markers by Western Blot

Considering that curcumin has been accepted for its ability to regulate either intrinsic or extrinsic apoptotic pathways by inhibiting survival-promoting proteins and activating essential mediators that induce apoptotic cell death, we subsequently aimed to examine the activation of critical apoptotic markers after treatment with $_{SLC}$CUR and $_{F}$CUR. Following the cell viability results, a 48-hour incubation time was chosen to determine the cell death and the activation of apoptotic markers. Protein lysates were extracted from PNT1A, 22Rv1, and LNCaP cells subjected to 25 µg/mL $_{SLC}$CUR and 8.33 µg/mL $_{F}$CUR, and subsequently examined for caspase-9 and PARP cleavage. The findings indicated that $_{SLC}$CUR treatment resulted in full cleavage of caspase-9 and PARP, confirming an effective activation of apoptosis (Figure 5.12). On the other hand, $_{F}$CUR induced only partial cleavage of caspase-9. A 1-fold and 2.5-fold increase in PARP cleavage was found in 22Rv1 and LNCaP cells after $_{SLC}$CUR treatment compared to $_{F}$CUR.

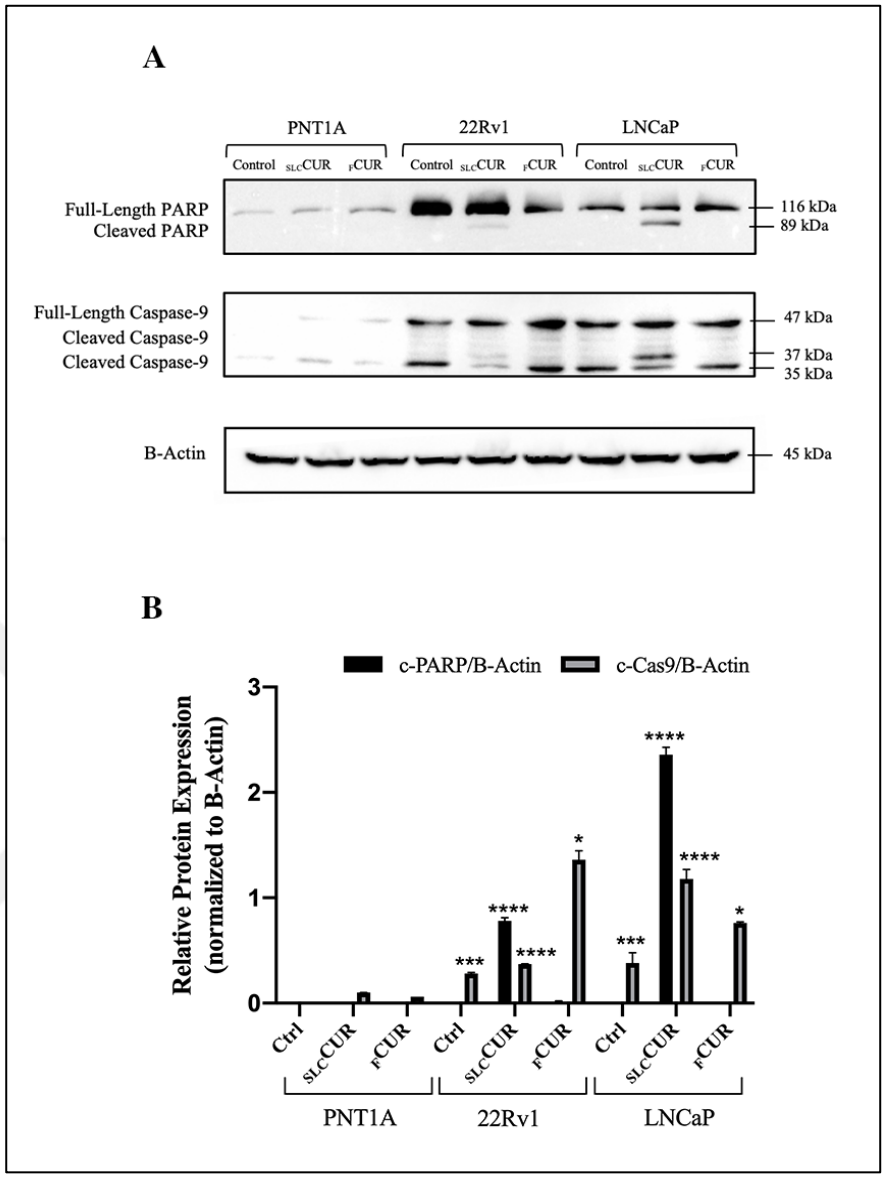

Figure 5.12. Analysis of the apoptosis in PNT1A, 22Rv1, and LNCaP cells. The cells were treated with 25 μg/mL of $_{SLC}$CUR and 8.33 μg/mL of $_{F}$CUR for 48-hour and the protein levels were analyzed using Western blot. (a) Protein lysates were analyzed for apoptotic markers, specifically cleaved caspase-9 (c-Cas9) (47, 37 and 35 kDa) and cleaved PARP (c-PARP) (116 and 89 kDa), by Western blot. The blots shown are three separate experiments, with β-actin (45 kDa) as a loading control for normalization. (b) Densitometric analysis of c-PARP and c-Cas9 band intensities. Quantification was performed using ImageJ software and normalized to β-actin and the untreated control group. Data are displayed as mean ± SD. *$p \leq 0.05$, ***$p \leq 0.001$, ****$p \leq 0.0001$.

5.4.2. Detection of DNA Fragmentation by TUNEL Assay

Apoptotic cell death was further assessed using the TUNEL assay in 22Rv1 and LNCaP cells after treatment with $_{SLC}$CUR and $_{F}$CUR. Figure 5.13 illustrates the treatment-induced changes in cell morphology, coupled with corresponding fluorescent TUNEL staining. The fluorescence intensities obtained following $_{SLC}$CUR and $_{F}$CUR treatments were compared to those induced by the positive control, staurosporine. $_{SLC}$CUR treatment induced significant apoptotic cell death in 22Rv1 and LNCaP cells, but $_{F}$CUR treatment did not produce a comparable apoptotic response. The quantification of fluorescence signals from five independent areas showed a 14-fold increase in signal intensity after the $_{SLC}$CUR treatment compared to $_{F}$CUR.

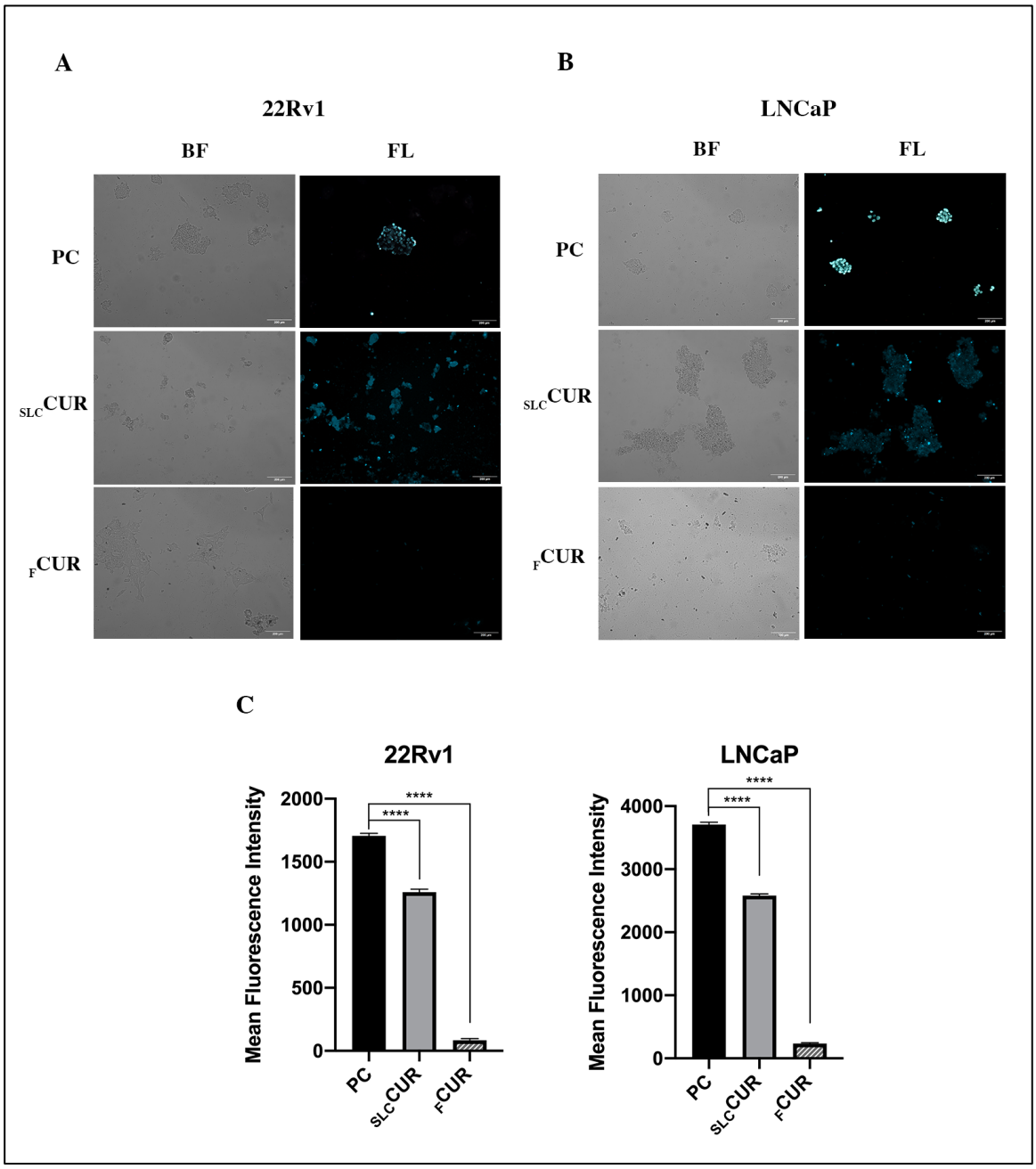

Figure 5.13. Apoptotic cell death triggered by $_{SLC}$CUR. Bright-field and fluorescence images. (a) 22Rv1 and (b) LNCaP cells were subjected to treatment with 25 µg/mL $_{SLC}$CUR or 8.33 µg/mL $_{F}$CUR for 48 hours. The images were obtained with a 20X objective under both bright-field and fluorescence. Scale bar is 200 µm. (c) Quantitative analysis of mean fluorescence intensity in 22Rv1 and LNCaP cells. PC indicates the positive control, where apoptosis was caused by 5 µg/mL of staurosporine for 90 minutes, as detected by TUNEL assay. ****$p \leq 0.0001$.

5.5. *IN VIVO* THE THERAPEUTIC POTENTIAL OF $_{SLC}$CUR

5.5.1. Effects of $_{SLC}$CUR on Tumor Progression and Body Weight

To assess the antitumor activity of $_{SLC}$CUR and $_{F}$CUR *in vivo*, prostate cancer xenografts were generated by the subcutaneous implanting of 22Rv1 cells into the dorsal flank of Foxn1^{nu}/Foxn1^{nu} nude mice. The drugs were administered intraperitoneally at specific doses every three days. Throughout the 25-day observation time, any significant changes in the average body weight of the mice were detected, suggesting that the provided treatment doses were well tolerated (Figure 5.14). Two mice from the treatment group died during the experiment and were excluded from further analyses. The cause of death was shown to be independent of the treatment method, and changes were made in the statistical analysis to ensure data accuracy. At the end of the study, control group demonstrated 953 mm^3 of average tumor volume and 870 mg of average tumor weight (Figure 5.15). In the SLC-treated group, the average tumor volume decreased to 450 mm^3 and the average tumor weight to 595 mg. $_{F}$CUR treatment showed a 695 mm^3 of tumor volume and 415 mg of tumor weight, indicating an approximate 50% reduction in the tumor weight (455 mg) relative to the control group. Although a decrease was detected, it was not statistically significant ($p=0.08$). On the other hand, the $_{SLC}$CUR-treated group showed a marked reduction in tumor volume and weight, which decreased to 43 mm^3 and 54 mg, respectively. The results demonstrate the significant anticancer effect of $_{SLC}$CUR in the xenograft model, showing greater efficacy than both $_{F}$CUR and SLC, and indicating that $_{SLC}$CUR improves the bioavailability and therapeutic potential of curcumin *in vivo*.

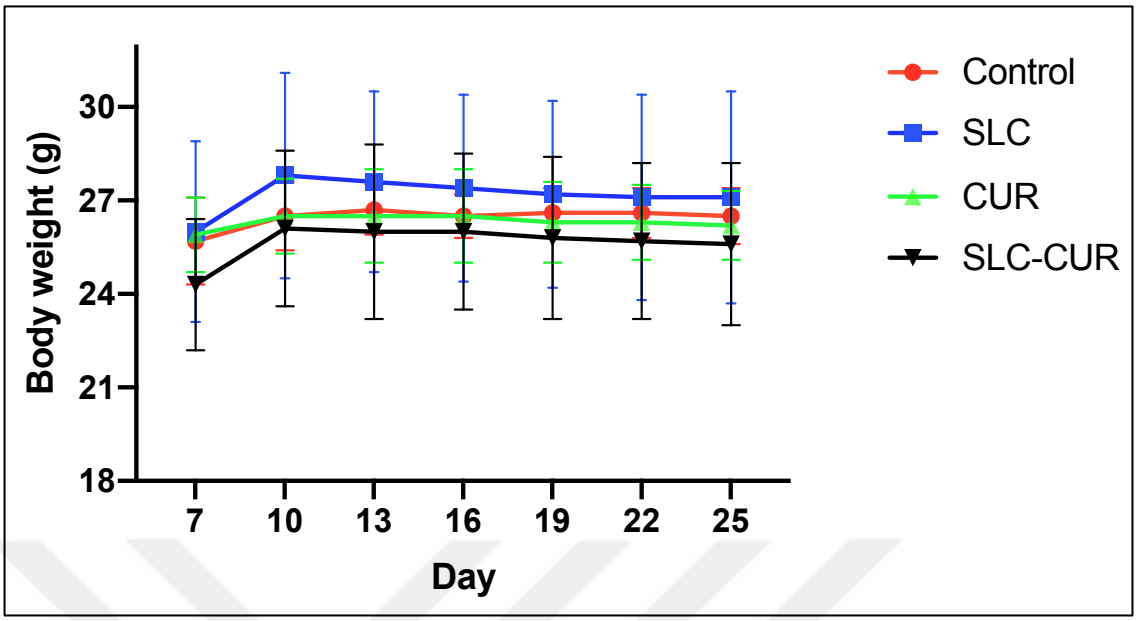

Figure 5.14. Changes in the body weight of homozygous nude (Foxn1^{nu}/Foxn1^{nu}) male mice. The animals (n=5) were received vehicle control, soy lecithin (SLC), free curcumin ($_{F}$CUR), and soy lecithin-based encapsulated curcumin ($_{SLC}$CUR) treatments.

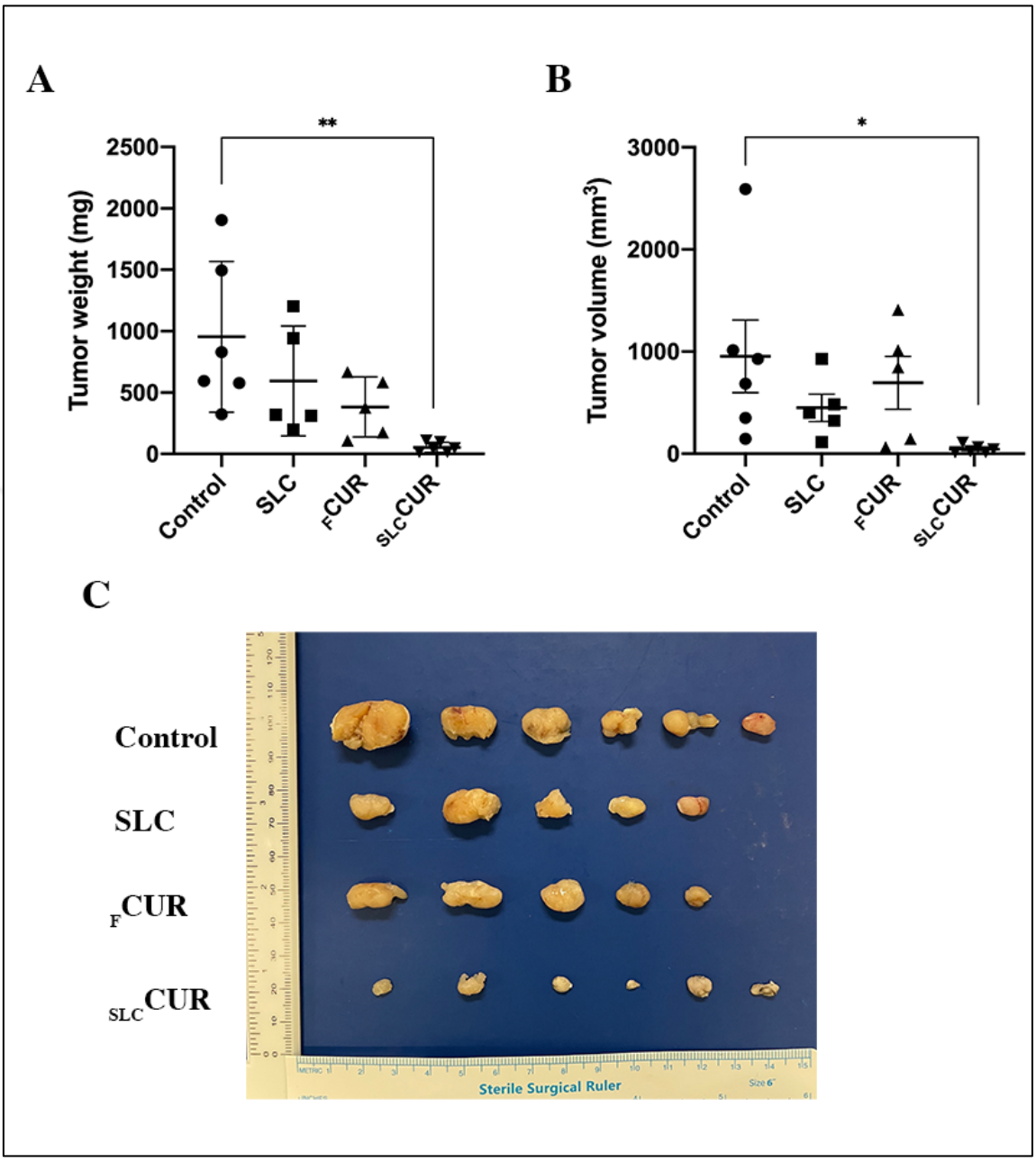

Figure 5.15. Tumor weight and volume changes in animals. (a) Tumor weight and (b) tumor volume of homozygous nude ($Foxn1^{nu}/Foxn1^{nu}$) male mice ($n \geq 5$) following vehicle control, soy lecithin (SLC), free curcumin ($_{F}$CUR), and soy lecithin-based encapsulated curcumin ($_{SLC}$CUR) treatments. (c) Tumors excised from each mouse ($n \geq 5$). *$p \leq 0.05$, **$p \leq 0.01$.

5.5.2. Histopathological Assessment of Tumor and Organ Tissues

Histopathological examination validated that all tumors were prostate carcinoma with a Gleason score (GS), confirming the successful generation of the 22Rv1 prostate cancer xenograft mouse model (Figure 5.16). The mean necrosis scores were 1.5 for the control group, 0.5 for the SLC group, 1.0 for the $_{F}$CUR group, and 1.5 for the $_{SLC}$CUR group. The average inflammation score was around 0.5 for all experimental groups, while the average fibrosis score was 0. Analysis of sections from the heart, liver, kidney, spleen, and lung exhibited no evidence of toxicity (Figure 5.17). The findings demonstrate that $_{SLC}$CUR therapy led to less necrosis, inflammation, and fibrosis in tumor tissues, implying decreased systemic toxicity.

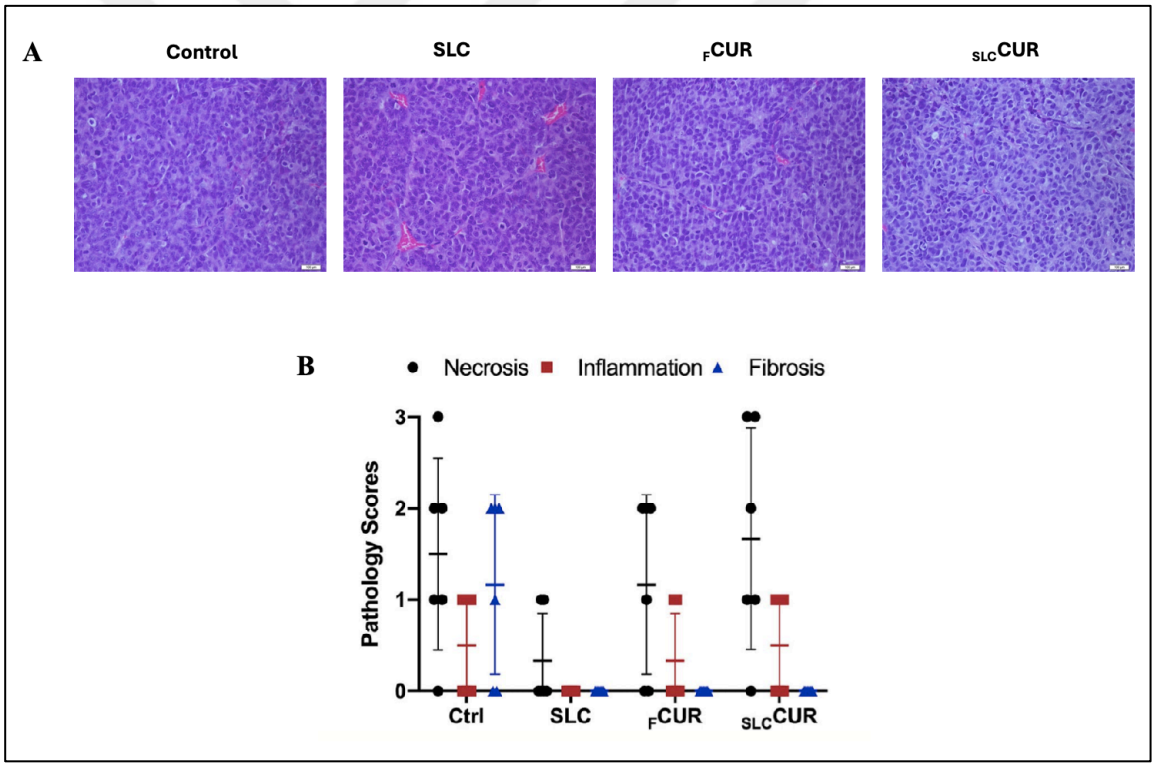

Figure 5.16. The histopathological assessment of tumor and organs. (a) Illustrative H&E-stained pictures of tumor tissue slices from the vehicle control, soy lecithin (SLC), free curcumin ($_{F}$CUR), and soy lecithin-based curcumin ($_{SLC}$CUR) groups. The scale bar: 100 µm. (b) Pathology scores for necrosis, inflammation, and fibrosis in the control (Ctrl), SLC, $_{F}$CUR, and $_{SLC}$CUR groups. Scoring scale: 0:absent, 1:mild, 2:moderate, and 3:severe.

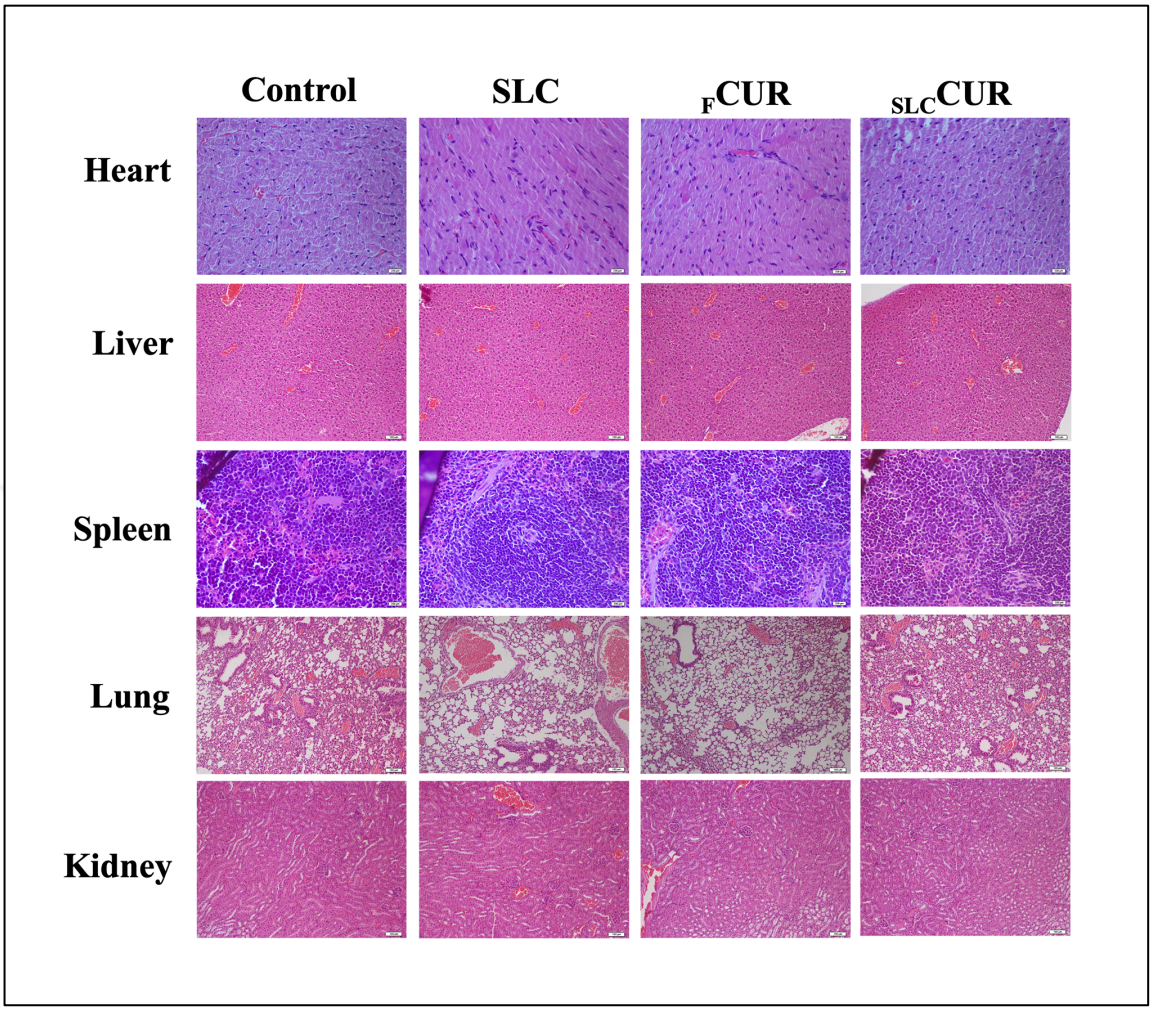

Figure 5.17. Illustrative H&E-stained pictures of the tissue slices. The images were obtained from control, soy lecithin (SLC), free curcumin ($_{F}$CUR), and soy lecithin-based curcumin ($_{SLC}$CUR) groups. Scale bar: 100 µm.

6. DISCUSSION

Prostate cancer continues to be one of the most commonly diagnosed cancers in males and continues to present considerable challenges in clinical practice, primarily due to the appearance of resistance against standard treatment approaches and the associated systemic side effects [175]. These limitations have stimulated interest in natural substances having anticancer potential as adjunctive or alternative therapeutic strategies. Among these, curcumin, a polyphenol extracted from *Curcuma longa*, has arisen as a particularly favorable agent due to its well-documented antioxidant, anti-inflammatory, anti-mutagenic, and antiproliferative features [164]. Curcumin mediates its antitumor properties via many cellular and molecular mechanisms, including the inhibition of pro-survival signaling molecules such as Bcl-2, EGFR, and VEGFR, and the activation of pro-apoptotic proteins like Bax, Bak, and IκBα [176]. Moreover, the ability of curcumin to modulate these pathways with minimal toxicity to normal cells has been widely reported [108]. However, its therapeutic utility is constrained because to inadequate water solubility, poor oral bioavailability, rapid metabolism, and systemic clearance [177]. In recent years, nanotechnology-driven delivery methods have been created to meet these pharmacokinetic limitations [178]. Several studies have demonstrated that curcumin-loaded nanoparticles, such as PLGA-based or liposomal systems, significantly enhance its stability, bioavailability, and therapeutic performance in cancer models [179]. For instance, PLGA-CUR nanoparticles were shown to suppress tumor growth and modulate oncogenic signaling by downregulating AR, β-catenin, AKT, and STAT3 expression, while simultaneously promoting apoptosis through PARP cleavage [158].

In this context, our study focused on the development and evaluation of $_{SLC}$CUR nanoformulation. It provided a comprehensive assessment of its physicochemical properties, cellular uptake, cytotoxicity, pro-apoptotic effects, and *in vivo* tumor-suppressive activity. To establish the suitability of $_{SLC}$CUR as a nanocarrier for systemic anticancer therapy, its physicochemical characteristics were first carefully examined. Nanoparticles engineered for continuous circulation in the bloodstream should optimally measure between 30 and 200 nm to target tumor tissues successfully [180]. The $_{SLC}$CUR formulation's physicochemical analysis was performed to validate its efficacy as a nanocarrier for curcumin administration. The $_{SLC}$CUR formulation demonstrated an optimal particle size (~120 nm), narrow

distribution of size (PDI: 0.3), and ZP of −20.25 ± 1.2 mV, displaying distinct particles with homogeneous distribution and consistent dispersion, which are all indicative of a stable colloidal system well-suited for systemic administration. Nanoparticles of this size are recognized for their potential to enable passive targeting of tumor tissues through the increased permeability and retention (EPR) effect, therefore enhancing treatment efficacy [181]. Also, in nanoparticle drug delivery, PDI values under 0.5 signify a uniform and restricted size range, consistent with our findings [182]. The zeta potential explains electrostatic repulsive factors influencing the colloidal stability of the carriers in conjunction with van der Waals forces, and steric interactions [183]. The observed zeta potential of −20.25 ± 1.2 mV indicates considerable colloidal stability, as particles exhibiting a ZP value exceeding ±20 mV are typically regarded as stable due to adequate electrostatic repulsion. This stability is essential for avoiding aggregation of the formulation during storage and systemic circulation [184]. The high encapsulation efficiency (78.3% ± 0.1%) not only confirms successful drug loading but also offers the potential for sustained release and reduced dosing frequency features that are highly desirable for clinical translation. Collectively, these pharmacokinetic findings highlight the $_{SLC}$CUR formulation as a reliable and effective drug delivery system that can significantly increase the pharmacokinetic profile of curcumin.

To further support the structural integrity and uniformity of the formulation, morphological analyses were conducted using TEM and SEM. These techniques provided valuable complementary insights into the nanoparticle surface characteristics, beyond what was revealed by DLS and zeta potential measurements. TEM imaging confirmed that $_{SLC}$CUR particles possessed a spherical morphology, were uniformly dispersed, and remained within the nanometric size range previously observed, thereby validating the consistency of the formulation. Spherical nanoparticles have been reported to offer significant advantages in drug delivery, including improved cellular internalization and prolonged circulation time, largely due to reduced recognition and clearance through mononuclear phagocyte system (MPS) [185]. The distinct and well-dispersed particle structures visualized via TEM align with the colloidal stability determined from the zeta potential data, supporting the stability of the $_{SLC}$CUR formulation. SEM imaging further validated the spherical shape of the particles, though slight aggregation and minor heterogeneity in particle size were observed. This observation may indicate partial aggregation occurring during the drying process

essential to SEM sample preparation, as observed in similar lipid-based nanocarriers [186]. Minor polydispersity and agglomeration in SEM pictures are frequently observed and typically have no impact on the overall efficacy of the nanoparticles, particularly when the PDI is maintained within an acceptable range, as shown here [187]. Maintaining the structural integrity and nanoparticle surface characteristics is critical for their stability, biodistribution, and eventual cellular interactions [188]. The consistency in shape and size observed in both TEM and SEM images suggests that the $_{SLC}$CUR formulation preserves its architecture under both hydrated and dehydrated conditions, which is essential for ensuring predictable biological performance. Together, these findings strengthen the physicochemical characterization of $_{SLC}$CUR and provide additional validation of its potential as a stable and effective nanocarrier for curcumin delivery.

Following the TEM and SEM examinations, AFM confirmed the spherical form and nanoscale dimensions of the $_{SLC}$CUR particles. The size distribution measured by AFM, between 150 and 180 nm, was slightly greater than the values acquired from DLS and TEM, which was related to acknowledged methodological differences, including sample hydration and probe-surface interaction during imaging [189]. AFM allows high-resolution three-dimensional measurement of surface topography, which is essential in modeling nanoparticle behavior in biological systems [190]. The smooth surface texture and spherical morphology shown in AFM pictures correlate with less protein corona formation and extended systemic circulation, which are advantageous characteristics for effective in vivo drug delivery [191]. Furthermore, the confirmed nanoscale dimensions align with the ideal range for utilizing the EPR effect, therefore enhancing the passive tumor targeting potential shown by previous DLS and TEM results. Collectively, these morphological and topographical evaluations validate the claim that $_{SLC}$CUR provides the required physicochemical characteristics, namely colloidal stability, optimal shape, and biocompatible surface properties, which are essential for effective biological application. The findings indicate that the soy lecithin-based carriers effectively pack and stabilize the curcumin within a nanostructured vehicle, demanding additional biological investigation.

To complement these structural and morphological assessments, FT-IR analysis was performed to verify the successful encapsulation of curcumin within the $_{SLC}$CUR formulation and to explore potential molecular interactions between curcumin and the lipid-

based carrier matrix. This technique is particularly effective for identifying functional group interactions and verifying the molecular integrity of components following formulation [192]. The FT-IR spectra of the $_{SLC}$CUR formulation exhibited characteristic absorption bands belonging to both curcumin and soy lecithin, suggesting that the structural integrity of both components was largely maintained, while the presence of specific interactions indicated successful encapsulation. Notably, the appearance of curcumin-specific peaks—such as those observed at approximately 1627 cm^{-1} (C=C aromatic stretching) and 1516 cm^{-1} (combined C=O and C=C vibrations), alongside lecithin-associated peaks at around 2926 and 2855 cm^{-1} (CH_2 stretching), strongly supports the conclusion that curcumin was effectively integrated into the liposomal bilayer rather than only mixed in a physical blend. The detailed variations in peak intensities and minor shifts further point to weak intermolecular interactions, such as hydrogen bonding, particularly between the phenolic OH group of curcumin and the polar headgroups of the phospholipids, potentially enhancing encapsulation efficiency and stabilizing the cargo [193]. Supporting this, the disappearance of the phenolic OH stretching peak at 3508 cm^{-1} in the spectrum of the curcumin-loaded liposomes, as compared to free curcumin, suggests a potential hydrogen bonding interaction with lecithin, which may aid in stabilizing the encapsulated molecule. Additionally, the slight shifts in the primary curcumin absorption bands after encapsulation imply that the curcumin molecules are successfully embedded within the liposomal structure, thereby masking their spectral "signature", which is a hallmark of efficient entrapment. These findings align with previous reports in the literature where curcumin's incorporation into lipid-based nanocarriers was confirmed by similar spectral behaviors, indicating non-destructive interactions for curcumin but stabilizing interactions that support curcumin's bioavailability and sustained delivery profile [194]. Consequently, FT-IR analysis provided strong evidence for the successful formation of a structurally stable $_{SLC}$CUR nanoformulation with preserved chemical characteristics and favorable encapsulation properties.

After confirming molecular integrity, it was crucial to evaluate the formulation's behavior in biologically relevant environments, specifically its stability in serum-containing environments, which directly affects its *in vivo* efficacy. The stability of nanoparticles in serum is important for affecting the behavior of nanoparticles in systemic circulation, particularly due to the development of a "protein corona", which is a dynamic layer of

consumed serum proteins that can strongly change the physicochemical characteristics of nanoparticles and induce immune responses, resulting in immediate removal from the bloodstream [195]. The durability of the $_{SLC}$CUR nanoformulation was evaluated by evaluating its colloidal stability in PBS (pH 7.4) with 10% FBS at 37°C for 24 hours. The findings revealed no significant changes in particle size, PDI, or ZP, confirming strong serum stability and a slight probability of protein-induced aggregation. The minor, insignificant increase in PDI confirms the claim that the formulation maintains homogeneity even in a protein-rich environment. Nanoparticles that maintain uniform size and surface charge in serum conditions are essential to obtain long circulation time and effective tumor accumulation through the increased EPR effect [196]. Similar results have been observed in other lipid-based nanocarriers, where maintaining stable physicochemical properties in serum-containing environments reduced the probability of the nanoparticles being recognized and cleared by the immune system, thereby improving their circulation time and therapeutic effectiveness [197]. These findings confirm that $_{SLC}$CUR nanoparticles showed required stability for systemic administration and provide an acceptable structure for effective administration of curcumin in anticancer usage.

Based on these favorable physicochemical and morphological characteristics, the next step was to examine the cellular responses to $_{SLC}$CUR, particularly its cytotoxic profile in both normal and prostate cancer cell lines. Before investigating the therapeutic potential of the $_{SLC}$CUR formulation, it was required to analyze the cytotoxicity of the unloaded soy lecithin carrier (SLC). This process ensured that any detected biological reactions in further testing could be linked to the active substance rather than the carrier matrix. Initial cytotoxicity assessments confirmed that the SLC was biocompatible at 25 µg/mL, with minimal effects on both prostate cancer (22Rv1, LNCaP) and normal epithelial (PNT1A) cells across 72 hours. However, higher concentrations (50-75 µg/mL) led to dose-dependent cytostatic and cytotoxic responses, particularly at 72 hours, consistent with previous studies reporting potential membrane disruption or oxidative stress at elevated lipid-based carrier levels. These findings highlight the importance of optimizing nanocarrier dosage, even for GRAS materials such as lecithin [198]. Based on these results, 25 µg/mL was identified as the maximum safe dose and used for subsequent $_{SLC}$CUR treatments to ensure that observed biological effects could be attributed to the active compound. When $_{SLC}$CUR was compared to $_{F}$CUR, it exhibited markedly enhanced and sustained cytotoxic effects in 22Rv1 and

LNCaP cells in a time- and dose-dependent manner, while neither formulation significantly affected the viability of PNT1A cells. $_{F}$CUR caused only transient reductions in cell viability that reversed by 72 hours, likely due to its low solubility, poor cellular uptake, and fast degradation, as previously reported. In contrast, $_{SLC}$CUR maintained its cytotoxic efficacy at 12.5 and 25 μg/mL throughout the treatment window, suggesting improved intracellular stability and retention. These results support earlier findings that lecithin-based nanocarriers enhance curcumin's membrane permeability and promote endocytic uptake, contributing to prolonged biological activity [199]. Collectively, these findings highlight the importance of lecithin-based nanoencapsulation in increasing curcumin's intracellular stability, selective cytotoxicity, and overall therapeutic efficacy. In line with earlier data, $_{SLC}$CUR not only improved the antitumor effects of curcumin but also reduced non-specific toxicity in normal prostate epithelial cells, confirming its biocompatibility and safety profile. Nevertheless, further mechanistic investigations, such as cellular uptake analysis, apoptosis assays, or endocytic pathway tracking, are necessary to comprehensively clarify the underlying reasons for this selectivity.

To clarify the processes underlying its selective cytotoxicity, intracellular uptake investigations were conducted in PNT1A, 22Rv1, and LNCaP cells by measuring curcumin-associated fluorescence. The findings indicated that $_{SLC}$CUR significantly enhanced cellular absorption in a concentration-dependent manner in cancer cell lines, whereas $_{F}$CUR exhibited minimal internalization at all administered doses. Specifically, $_{SLC}$CUR administration led to as much as a 29-fold increase in fluorescence intensity in 22Rv1 and LNCaP cells, while PNT1A cells demonstrated significantly reduced levels of absorption. This different absorption allows the selective accumulation of curcumin in cancer cells. The increased absorption is possibly caused by various physicochemical features of the nanocarriers. The nanoscale size of $_{SLC}$CUR (~120 nm) is within the ideal range for endocytosis, a crucial internalization mechanism for nanoparticle systems [160]. The amphiphilic characteristics of soy lecithin enhance membrane contact, enabling both passive diffusion and vesicle-mediated cellular entrance [200]. Literature indicates that phospholipid-based systems enhance intracellular transport, retention, and bioavailability of lipophilic drugs such as curcumin [201]. The observed selective uptake pattern may be related to changes in membrane structure and endocytic activity between malignant and normal cells. Cancer cells frequently demonstrate increased membrane fluidity, altered

cholesterol levels, and enhanced rates of receptor-mediated endocytosis, all of which facilitate nanoparticle internalization [202]. This biological differentiation enables $_{SLC}$CUR to preferentially accumulate in tumor cells, consistent with our cytotoxicity and apoptosis findings that demonstrate enhanced anticancer effects with no effects on non-malignant cells. The findings provide strong evidence that lecithin-based nanoformulation stabilizes curcumin and enables its selective and effective intracellular delivery. This feature obviously contributes significantly to the greater anticancer efficacy of $_{SLC}$CUR, supporting earlier findings about the enhanced therapeutic potential of nanocurcumin systems related to their prolonged release, increased drug loading, and improved bioavailability [203].

Considering the major increase in intracellular absorption of $_{SLC}$CUR observed in prostate cancer cells, the following aim was to determine whether this enhanced accumulation resulted in the activation of apoptotic pathways. A TUNEL assay was conducted, demonstrating a significant rise in DNA fragmentation as well as distinct apoptotic morphology in $_{SLC}$CUR-treated cells. Fluorescence intensity was up to 14-fold higher with $_{SLC}$CUR compared to $_{F}$CUR, indicating a significantly enhanced apoptotic response. Curcumin is recognized for its pro-apoptotic behaviors in cancer cells, facilitated via both p53-dependent and p53-independent pathways. It modulates intrinsic apoptosis by upregulating pro-apoptotic Bcl-2 family proteins, comprising Bak, Bax, Bim, Puma, and Noxa, while suppressing anti-apoptotic proteins including as Bcl-xL, Bcl-2, XIAP, and surviving. These processes result in the mitochondrial outer membrane permeabilization (MOMP), the releasing cytochrome c, and the activation of caspase-9, which subsequently initiates the executioner caspases (e.g., caspase-3/7), leading to PARP cleavage and DNA degradation [204]. Consistent with this mechanistic framework, our data revealed that $_{SLC}$CUR application resulted in significant activation of both cleaved PARP and cleaved caspase-9, as validated by western blot analysis. $_{SLC}$CUR induced a 1- to 2.5-fold enhancement in PARP cleavage relative to $_{F}$CUR in both 22Rv1 and LNCaP cells, which exhibited minimal response to $_{F}$CUR. The molecular findings validate the TUNEL assay results and support the idea that enhanced intracellular transport via $_{SLC}$CUR promotes mitochondrial-mediated apoptosis. This pro-apoptotic response was specifically selective to cancer cells, as PNT1A normal prostate epithelial cells did not demonstrate notable PARP activation or DNA damage after treatment. This finding further confirms the selectivity and safety of the lecithin-based formulation. The enhanced apoptotic efficiency of $_{SLC}$CUR is

likely due to a combination of physicochemical features, such as increased solubility, stability at physiological pH, and extended intracellular retention, along with the targeting capabilities of lecithin-based nanocarriers. These carriers may enhance the lysosomal or mitochondrial transport of curcumin, thereby improving its interaction with apoptotic regulators [205]. Furthermore, prostate cancer is acknowledged for its capacity to develop resistance to apoptosis via overexpression of the anti-apoptotic proteins, such as Bcl-2 and XIAP [140]. $_{SLC}$CUR's capacity to overcome this resistance and reactivate apoptotic signaling highlights a significant therapeutic benefit compared to $_{F}$CUR. These findings identify $_{SLC}$CUR as a feasible nanocarrier system for re-sensitizing apoptosis-resistant prostate cancer cells and require further investigation along with chemotherapeutics or pathway-specific inhibitors.

To confirm the in vitro findings and evaluate the therapeutic significance of $_{SLC}$CUR in a physiological context, a prostate cancer xenograft model was developed employing 22Rv1 cells in immunodeficient nude mice. The intraperitoneal administration of $_{SLC}$CUR during a 25-day treatment period led to a significant decrease in tumor size, with final average tumor volume and weight observed at 43 mm^3 and 54 mg, respectively. These data demonstrate a significant therapeutic advantage over the control group (953 mm^3, 870 mg) and significantly beat the effects of both $_{F}$CUR and SLC treatments, which produced only minimal decreases. The $_{F}$CUR group demonstrated an approximate 50% reduction in tumor weight; however, statistical significance was not achieved for this result ($p = 0.08$), possibly related to curcumin's inadequate solubility and fast metabolism in systemic circulation [97]. No significant changes in body weight were noted among treatment groups, suggesting that $_{SLC}$CUR was well tolerated. The combination of efficacy and safety is crucial for translational applicability [105]. These findings correlate with previous studies indicating that lecithin-based nanoformulations can accelerate the pharmacokinetics of curcumin, increase tumor accumulation through the increased EPR effect, and prolong its bioactivity *in vivo* [206]. The minor tumor suppression noted in the SLC group indicates a possible additional advantage of soy lecithin, either via its effects on lipid metabolism or anti-inflammatory mechanisms, requiring further research. Histopathological evaluations were conducted on excised tumor tissue and important organs to verify the tumor-suppressive effects and analyze potential systemic toxicity. Microscopic analysis validated the prostate tumor morphology in accordance with Gleason score patterns, confirming the successful

development of the 22Rv1 xenograft model. In comparison to the untreated group, tumors from the $_{SLC}$CUR-treated group had decreased necrosis (score: 1.5), inflammation (score: 0.5), and an absence of fibrosis. The histological improvements paralleled with an absence of tissue injury in essential organs, like heart, liver, kidneys, lungs, and spleen, signifying an effective systemic safety profile. The decrease in tumor necrosis and inflammation may result from curcumin's recognized anti-inflammatory and antioxidant properties [207]. Moreover, the lack of fibrosis, commonly an indicator of chronic toxicity, strengthens the biocompatibility of the lecithin-based formulation [208]. These results align with previous lipid-based nanocarriers, recognized for their advantageous toxicity profiles related to their natural phospholipid structure and capacity to deliver hydrophobic drugs while minimizing off-target accumulation [209]. The histological data verify that $_{SLC}$CUR facilitates efficient tumor targeting while reducing systemic toxicity, consequently confirming its potential as a safe and selective nanotherapeutic agent for further preclinical improvement in prostate cancer.

7. CONCLUSION

Overall, this study demonstrates that $_{SLC}$CUR presents a favorable therapeutic strategy for prostate cancer by addressing the recognized limitations of free curcumin, such as inadequate aqueous solubility, low oral bioavailability, and fast systemic clearance. This study provides an extensive evaluation of $_{SLC}$CUR as a potential nanotherapeutic approach for prostate cancer. The $_{SLC}$CUR formulation demonstrated great physicochemical characteristics, including nanoscale particle size, colloidal stability, and high encapsulation efficiency, confirming its suitability for systemic delivery. Morphological and spectroscopic investigations verified structural integrity and effective drug incorporation, whereas serum stability assays showed its performance in physiologically relevant conditions. Biological assessments demonstrated that $_{SLC}$CUR preferentially induced cytotoxicity and apoptosis in prostate cancer cell types while preserving normal prostate epithelial cells. Improved intracellular absorption and increased absorption of curcumin enhanced the activation of the mitochondrial-mediated apoptotic pathways, leading to notable activation of caspase-9 and PARP. *In vivo*, $_{SLC}$CUR dramatically reduced tumor burden in a xenograft mouse without causing systemic toxicity, therefore supporting its therapeutic potential. These findings collectively demonstrate that $_{SLC}$CUR eliminates the major pharmacokinetic limitations of free curcumin and markedly improves its anticancer efficiency and selectivity.

REFERENCES

1. Frick J, Aulitzky W. Physiology of the prostate. *Infection*. 1991;19 Suppl 3: S115-118. https://doi.org/10.1007/BF01643679.

2. Gilroy AM, Voll M, Wesker K. *Anatomy - An Essential Textbook*. 3. Auflage. Stuttgart: Thieme Medical Publishers; 2021.

3. Lee CH, Akin-Olugbade O, Kirschenbaum A. Overview of Prostate Anatomy, Histology, and Pathology. *Endocrinology and Metabolism Clinics of North America*. 2011;40(3): 565–575.

4. Aaron L, Franco OE, Hayward SW. Review of Prostate Anatomy and Embryology and the Etiology of Benign Prostatic Hyperplasia. *Urologic Clinics of North America*. 2016;43(3): 279–288.

5. Viliers A, Steg A, Boccon-Gibod L. Anatomy of the Prostate: Review of the Different Models. *European Urology*. 1991;20(4): 261–268.

6. Carson C, Rittmaster R. The role of dihydrotestosterone in benign prostatic hyperplasia. *Urology*. 2003;61(4): 2–7.

7. Toivanen R, Shen MM. Prostate organogenesis: tissue induction, hormonal regulation and cell type specification. *Development*. 2017;144(8): 1382–1398.

8. Xu Y, Chen SY, Ross KN, Balk SP. Androgens Induce Prostate Cancer Cell Proliferation through Mammalian Target of Rapamycin Activation and Post-transcriptional Increases in Cyclin D Proteins. *Cancer Research*. 2006;66(15): 7783–7792.

9. Goldenberg L, So A, Fleshner N, Rendon R, Drachenberg D, Elhilali M. The role of 5-alpha reductase inhibitors in prostate pathophysiology: Is there an additional advantage to inhibition of type 1 isoenzyme? *Canadian Urological Association Journal*. 2013;3(3-S2): 109.

10. Liu AY, True LD. Characterization of Prostate Cell Types by CD Cell Surface Molecules. *Am J Pathol.* 2002;160(1).

11. Nacusi LP, Tindall DJ. Targeting 5α-reductase for prostate cancer prevention and treatment. *Nature Reviews Urology*. 2011;8(7): 378–384.

12. Hudak SJ, Hernandez J, Thompson IM. Role of 5 alpha-reductase inhibitors in the management of prostate cancer. *Clinical Interventions in Aging*. 2006;1(4):425-31.

13. White CW, Xie JH, Ventura S. Age-related changes in the innervation of the prostate gland: Implications for prostate cancer initiation and progression. *Organogenesis*. 2013;9(3): 206–215.

14. Zhu ML, Kyprianou N. Androgen receptor and growth factor signaling cross-talk in prostate cancer cells. *Endocrine Related Cancer*. 2008;15(4): 841–849.

15. Lawrentschuk N, Ptasznik G, Ong S. Benign Prostate Disorders. In: Feingold KR, Ahmed SF, Anawalt B, Blackman MR, Boyce A, Chrousos G, et al. (eds.) *Endotext*. South Dartmouth (MA): MDText.com, Inc.; 2000.

16. Berry SJ, Coffey DS, Walsh PC, Ewing LL. The Development of Human Benign Prostatic Hyperplasia with Age. *Journal of Urology*. 1984;132(3): 474–479. https://doi.org/10.1016/S0022-5347(17)49698-4.

17. McLaughlin PW, Troyer S, Berri S, Narayana V, Meirowitz A, Roberson PL, et al. Functional anatomy of the prostate: Implications for treatment planning. *International Journal of Radiation Oncology*Biology*Physics*. 2005;63(2): 479–491.

18. Cannarella R, Condorelli RA, Barbagallo F, La Vignera S, Calogero AE. Endocrinology of the Aging Prostate: Current Concepts. *Frontiers in Endocrinology*. 2021;12: 554078.

19. Testa U, Castelli G, Pelosi E. Cellular and Molecular Mechanisms Underlying Prostate Cancer Development: Therapeutic Implications. *Medicines*. 2019 Jul 30;6(3):82.

20. Henry GH, Malewska A, Joseph DB, Malladi VS, Lee J, Torrealba J, et al. A Cellular Anatomy of the Normal Adult Human Prostate and Prostatic Urethra. *Cell Reports*. 2018;25(12): 3530-3542.

21. Zhang D, Zhao S, Li X, Kirk JS, Tang DG. Prostate Luminal Progenitor Cells in Development and Cancer. *Trends in Cancer*. 2018;4(11): 769–783.

22. Arman T, Nelson PS. Endocrine and paracrine characteristics of neuroendocrine prostate cancer. *Frontiers in Endocrinology*. 2022;13: 1012005.

23. Pérez-Ibave DC, Burciaga-Flores CH, Elizondo-Riojas MÁ. Prostate-specific antigen (PSA) as a possible biomarker in non-prostatic cancer: A review. *Cancer Epidemiology*. 2018;54: 48–55.

24. Rybak AP, Bristow RG, Kapoor A. Prostate cancer stem cells: deciphering the origins and pathways involved in prostate tumorigenesis and aggression. *Oncotarget*. 2015;6(4): 1900–1919.

25. Balk SP, Ko YJ, Bubley GJ. Biology of prostate-specific antigen. *Journal of Clinical Oncology: Official Journal of the American Society of Clinical Oncology*. 2003;21(2): 383–391.

26. Archer M, Dogra N, Kyprianou N. Inflammation as a Driver of Prostate Cancer Metastasis and Therapeutic Resistance. *Cancers*. 2020;12(10): 2984.

27. Bray F, Ferlay J, Soerjomataram I, Siegel RL, Torre LA, Jemal A. Global cancer statistics 2018: GLOBOCAN estimates of incidence and mortality worldwide for 36 cancers in 185 countries. *CA: A Cancer Journal for Clinicians*. 2018;68(6): 394–424.

28. Bray F, Laversanne M, Sung H, Ferlay J, Siegel RL, Soerjomataram I. Global cancer statistics 2022: GLOBOCAN estimates of incidence and mortality worldwide for 36 cancers in 185 countries. *CA: A Cancer Journal for Clinicians*. 2024;74(3): 229–263.

29. Schafer EJ, Laversanne M, Sung H, Soerjomataram I, Briganti A, Dahut W, et al. Recent Patterns and Trends in Global Prostate Cancer Incidence and Mortality: An Update. *European Urology*. 2025;87(3): 302–313.

30. Leslie SW, Soon-Sutton TL, Skelton WP. Prostate Cancer. In: *StatPearls*. Treasure Island (FL): StatPearls Publishing; 2025. PMID: 29261872.

31. Jeong CW. Prostate-Specific Antigen-Based Prostate Cancer Screening: One for All or Individualized for Each Race? – A Narrative Review. *Journal of Urologic Oncology*. 2024;22(1): 4–10.

32. Sekhoacha M, Riet K, Motloung P, Gumenku L, Adegoke A, Mashele S. Prostate Cancer Review: Genetics, Diagnosis, Treatment Options, and Alternative Approaches. *Molecules*. 2022;27(17): 5730.

33. Dai Y, DeSano J, Qu Y, Tang W, Meng Y, Lawrence TS. Natural IAP inhibitor Embelin enhances therapeutic efficacy of ionizing radiation in prostate cancer. *Am J Cancer Res.* 2011;1(2):128-43.

34. Brawley S, Mohan R, Nein CD. Localized Prostate Cancer: Treatment Options. *Am Fam Physician.* 2018 Jun 15;97(12):798-805.

35. Miller DC, Sanda MG, Dunn RL, Montie JE, Pimentel H, Sandler HM, et al. Long-Term Outcomes Among Localized Prostate Cancer Survivors: Health-Related Quality-of-Life Changes After Radical Prostatectomy, External Radiation, and Brachytherapy. *Journal of Clinical Oncology*. 2005;23(12): 2772–2780.

36. Rawla P. Epidemiology of Prostate Cancer. *World Journal of Oncology*. 2019;10(2): 63–89.

37. Wallis CJD, Nam RK. Prostate cancer genetics: a review. *EJIFCC*, 26(2), 79–91.

38. Rafikova G, Gilyazova I, Enikeeva K, Pavlov V, Kzhyshkowska J. Prostate Cancer: Genetics, Epigenetics and the Need for Immunological Biomarkers. *International Journal of Molecular Sciences*. 2023;24(16): 12797.

39. Pernar CH, Ebot EM, Wilson KM, Mucci LA. The Epidemiology of Prostate Cancer. *Cold Spring Harbor Perspectives in Medicine*. 2018;8(12): a030361.

40. Asmann YW, Kosari F, Wang K, Cheville JC, Vasmatzis G. Identification of differentially expressed genes in normal and malignant prostate by electronic profiling of expressed sequence tags. *Cancer Research*. 2002;62(11): 3308–3314.

41. Coussens LM, Werb Z. Inflammation and cancer. *Nature*. 2002;420(6917): 860–867.

42. Cansino Alcaide JR, Martínez-Piñeiro L. Molecular biology in prostate cancer. *Clinical & Translational Oncology: Official Publication of the Federation of Spanish Oncology Societies and of the National Cancer Institute of Mexico*. 2006;8(3): 148–152.

43. Jacob A, Raj R, Allison DB, Myint ZW. Androgen Receptor Signaling in Prostate Cancer and Therapeutic Strategies. *Cancers*. 2021;13(21): 5417.

44. Brawer MK. Prostatic Intraepithelial Neoplasia: An Overview. *Rev Urol.* 2005;7 Suppl 3(Suppl 3):11-8.

45. Schulz WA. Molecular biology of prostate cancer. *Molecular Human Reproduction*. 2003;9(8): 437–448.

46. De Visser KE, Joyce JA. The evolving tumor microenvironment: From cancer initiation to metastatic outgrowth. *Cancer Cell*. 2023;41(3): 374–403.

47. Bostwick DG, Shan A, Qian J, Darson M, Maihle NJ, Jenkins RB, et al. Independent origin of multiple foci of prostatic intraepithelial neoplasia: Comparison with matched foci of prostate carcinoma. *Cancer*. 1998;83(9): 1995–2002.

48. Maekawa S, Takata R, Obara W. Molecular Mechanisms of Prostate Cancer Development in the Precision Medicine Era: A Comprehensive Review. *Cancers*. 2024;16(3): 523.

49. St. John J, Powell K, -LaComb MKC. TMPRSS2-ERG Fusion Gene Expression in Prostate Tumor Cells and Its Clinical and Biological Significance in Prostate Cancer Progression. *Journal of Cancer Science & Therapy*. 2012;04(04).

50. Tomlins SA, Laxman B, Dhanasekaran SM, Helgeson BE, Cao X, Morris DS, et al. Distinct classes of chromosomal rearrangements create oncogenic ETS gene fusions in prostate cancer. *Nature*. 2007;448(7153): 595–599.

51. Jamaspishvili T, Berman DM, Ross AE, Scher HI, De Marzo AM, Squire JA, et al. Clinical implications of PTEN loss in prostate cancer. *Nature Reviews Urology*. 2018;15(4): 222–234.

52. Luongo F, Colonna F, Calapà F, Vitale S, Fiori ME, De Maria R. PTEN Tumor-Suppressor: The Dam of Stemness in Cancer. *Cancers*. 2019;11(8): 1076.

53. Phin S, Moore MW, Cotter PD. Genomic Rearrangements of PTEN in Prostate Cancer. *Frontiers in Oncology*. 2013;3.

54. Ofner H, Kramer G, Shariat SF, Hassler MR. TP53 Deficiency in the Natural History of Prostate Cancer. *Cancers*. 2025;17(4): 645.

55. Teroerde M, Nientiedt C, Duensing A, Hohenfellner M, Stenzinger A, Duensing S. Revisiting the Role of p53 in Prostate Cancer. In: Bott SR, Ng KL (eds.) *Prostate Cancer*. Brisbane (AU): Exon Publications; 2021.

56. McKay RR, Feng FY, Wang AY, Wallis CJD, Moses KA. Recent Advances in the Management of High-Risk Localized Prostate Cancer: Local Therapy, Systemic Therapy, and Biomarkers to Guide Treatment Decisions. *American Society of Clinical Oncology Educational Book. American Society of Clinical Oncology. Annual Meeting*. 2020;40: 1–12.

57. Pospihalj B. Staging of prostate cancer: a review with reference for further refinement. *Analytical and Quantitative Cytopathology and Histopathology*. 2015;37(1): 69–74.

58. Munjal A, Leslie SW. Gleason Score. In: *StatPearls*. Treasure Island (FL): StatPearls Publishing; 2025. PMID: 31985971.

59. Barakzai MA. Prostatic Adenocarcinoma: A Grading from Gleason to the New Grade-Group System: A Historical and Critical Review. *Asian Pacific Journal of Cancer Prevention*. 2019;20(3): 661–666.

60. Epstein JI, Zelefsky MJ, Sjoberg DD, Nelson JB, Egevad L, Magi-Galluzzi C, et al. A Contemporary Prostate Cancer Grading System: A Validated Alternative to the Gleason Score. *European Urology*. 2016;69(3): 428–435.

61. Tagai EK, Miller SM, Kutikov A, Diefenbach MA, Gor RA, Al-Saleem T, et al. Prostate Cancer Patients' Understanding of the Gleason Scoring System: Implications for Shared Decision-Making. *Journal of Cancer Education*. 2019;34(3): 441–445.

62. Ambrogi MC, Aprile V, Lenzini A, Bacchin D, Mastromarino MG, Korasidis S, et al. TNM Staging System in Thymoma: A Critical Appraisal? *Journal of Clinical Medicine*. 2024;13(2): 610.

63. Chang AJ, Autio KA, Roach M, Scher HI. High-risk prostate cancer—classification and therapy. *Nature Reviews Clinical Oncology*. 2014;11(6): 308–323.

64. Humphrey PA. Gleason grading and prognostic factors in carcinoma of the prostate. *Modern Pathology*. 2004;17(3): 292–306.

65. Baydar DE, Epstein JI. Gleason grading system, modifications and additions to the original scheme. *Turkish Journal of Pathology*. 2009;25(3): 59.

66. Feng Q, He B. Androgen Receptor Signaling in the Development of Castration-Resistant Prostate Cancer. *Frontiers in Oncology*. 2019;9: 858.

67. Seruga B, Ocana A, Tannock IF. Drug resistance in metastatic castration-resistant prostate cancer. *Nature Reviews. Clinical Oncology*. 2011;8(1): 12–23.

68. Bellmunt J, Oh WK. Castration-resistant prostate cancer: new science and therapeutic prospects. *Therapeutic Advances in Medical Oncology*. 2010 May;2(3):189-207.

69. Bukowski K, Kciuk M, Kontek R. Mechanisms of Multidrug Resistance in Cancer Chemotherapy. *International Journal of Molecular Sciences*. 2020;21(9): 3233.

70. Zhang J, Wang L, You X, Xian T, Wu J, Pang J. Nanoparticle Therapy for Prostate Cancer: Overview and Perspectives. *Current Topics in Medicinal Chemistry*. 2019;19(1): 57–73.

71. Kita K, Dittrich C. Drug delivery vehicles with improved encapsulation efficiency: taking advantage of specific drug-carrier interactions. *Expert Opinion on Drug Delivery*. 2011;8(3): 329–342.

72. Kvízová J, Pavlíčková V, Kmoníčková E, Ruml T, Rimpelová S. Quo Vadis Advanced Prostate Cancer Therapy? Novel Treatment Perspectives and Possible Future Directions. *Molecules*. 2021;26(8): 2228.

73. Klein EA, Kupelian PA. Localized prostate cancer: radiation or surgery? *Urologic Clinics of North America*. 2003;30(2): 315–330.

74. Yuan X, Cai C, Chen S, Chen S, Yu Z, Balk S. Androgen receptor functions in castration-resistant prostate cancer and mechanisms of resistance to new agents targeting the androgen axis. *Oncogene*. 2014 May 29;33(22):2815-25.

75. Fujita K, Nonomura N. Role of Androgen Receptor in Prostate Cancer: A Review. *The World Journal of Men's Health*. 2019;37(3): 288.

76. Maitland N. Resistance to Antiandrogens in Prostate Cancer: Is It Inevitable, Intrinsic or Induced? *Cancers*. 2021;13(2): 327.

77. Sun M, Choueiri TK, Hamnvik OPR, Preston MA, De Velasco G, Jiang W, et al. Comparison of Gonadotropin-Releasing Hormone Agonists and Orchiectomy: Effects of Androgen-Deprivation Therapy. *JAMA oncology*. 2016;2(4): 500–507.

78. Schrecengost RS, Knudsen KE. Molecular Pathogenesis and Progression of Prostate Cancer. *Seminars in oncology*. 2013;40(3): 244–258.

79. Gurel B, Ali TZ, Montgomery EA, Begum S, Hicks J, Goggins M, et al. NKX3.1 as a Marker of Prostatic Origin in Metastatic Tumors. *American Journal of Surgical Pathology*. 2010;34(8): 1097–1105.

80. Ohtsu H, Xiao Z, Ishida J, Nagai M, Wang HK, Itokawa H, et al. Antitumor Agents. 217. Curcumin Analogues as Novel Androgen Receptor Antagonists with Potential as Anti-Prostate Cancer Agents. *Journal of Medicinal Chemistry*. 2002;45(23): 5037–5042.

81. Aggarwal BB, Sundaram C, Malani N, Ichikawa H. CURCUMIN: THE INDIAN SOLID GOLD. In: Aggarwal BB, Surh YJ, Shishodia S (eds.) *The Molecular Targets and Therapeutic Uses of Curcumin in Health and Disease*. Boston, MA: Springer US; 2007. p. 1–75.

82. Miyamoto DT, Lee RJ, Stott SL, Ting DT, Wittner BS, Ulman M, et al. Androgen Receptor Signaling in Circulating Tumor Cells as a Marker of Hormonally Responsive Prostate Cancer. *Cancer Discovery*. 2012;2(11): 995–1003.

83. Karantanos T, Corn PG, Thompson TC. Prostate cancer progression after androgen deprivation therapy: mechanisms of castrate resistance and novel therapeutic approaches. *Oncogene*. 2013;32(49): 5501–5511.

84. Inderjeeth AJ, Topp M, Sanij E, Castro E, Sandhu S. Clinical Application of Poly(ADP-ribose) Polymerase (PARP) Inhibitors in Prostate Cancer. *Cancers*. 2022;14(23): 5922.

85. Park J, Kim J. CRISPR/Cas9 Technology Providing the Therapeutic Landscape of Metastatic Prostate Cancer. *Pharmaceuticals*. 2024;17(12): 1589.

86. Randhawa M, Institute of Cancer Sciences, University of Glasgow, Glasgow, UK, Jones R, Institute of Cancer Sciences, University of Glasgow, Glasgow, UK. Immunotherapy in Advanced Prostate Cancer. *European Oncology & Haematology*. 2020;16(1): 44.

87. Chopra H, Dey PS, Das D, Bhattacharya T, Shah M, Mubin S, et al. Curcumin Nanoparticles as Promising Therapeutic Agents for Drug Targets. *Molecules (Basel, Switzerland)*. 2021;26(16): 4998.

88. Gurib-Fakim A. Medicinal plants: Traditions of yesterday and drugs of tomorrow. *Molecular Aspects of Medicine*. 2006;27(1): 1–93.

89. Hassanzadeh K, Buccarello L, Dragotto J, Mohammadi A, Corbo M, Feligioni M. Obstacles against the Marketing of Curcumin as a Drug. *International Journal of Molecular Sciences*. 2020;21(18): 6619.

90. Moon DO. Curcumin in Cancer and Inflammation: An In-Depth Exploration of Molecular Interactions, Therapeutic Potentials, and the Role in Disease Management. *Int J Mol Sci*. 2024 Mar 2;25(5):2911.

91. Fu YS, Chen TH, Weng L, Huang L, Lai D, Weng CF. Pharmacological properties and underlying mechanisms of curcumin and prospects in medicinal potential. *Biomedicine & Pharmacotherapy*. 2021;141: 111888.

92. Maiti P, Dunbar G. Use of Curcumin, a Natural Polyphenol for Targeting Molecular Pathways in Treating Age-Related Neurodegenerative Diseases. *International Journal of Molecular Sciences*. 2018;19(6): 1637.

93. Goel A, Kunnumakkara AB, Aggarwal BB. Curcumin as '"Curecumin"': From kitchen to clinic. *Biochem Pharmacol.* 2008 Feb 15;75(4):787-809.

94. Aggarwal BB, Kumar A, Bharti AC. Anticancer potential of curcumin: preclinical and clinical studies. *Anticancer Research*. 2003;23(1A): 363–398.

95. Karatayli E, Sadiq SC, Schattenberg JM, Grabbe S, Biersack B, Kaps L. Curcumin and Its Derivatives in Hepatology: Therapeutic Potential and Advances in Nanoparticle Formulations. *Cancers*. 2025;17(3): 484.

96. Ucisik MH, Küpcü S, Schuster B, Sleytr UB. Characterization of CurcuEmulsomes: nanoformulation for enhanced solubility and delivery of curcumin. *Journal of Nanobiotechnology*. 2013;11(1): 37.

97. Tabanelli R, Brogi S, Calderone V. Improving Curcumin Bioavailability: Current Strategies and Future Perspectives. *Pharmaceutics*. 2021;13(10): 1715.

98. Hewlings S, Kalman D. Curcumin: A Review of Its Effects on Human Health. *Foods*. 2017;6(10): 92.

99. Wong KE, Ngai SC, Chan KG, Lee LH, Goh BH, Chuah LH. Curcumin Nanoformulations for Colorectal Cancer: A Review. *Frontiers in Pharmacology*. 2019;10: 152.

100. Bertoncini-Silva C, Vlad A, Ricciarelli R, Giacomo Fassini P, Suen VMM, Zingg JM. Enhancing the Bioavailability and Bioactivity of Curcumin for Disease Prevention and Treatment. *Antioxidants*. 2024;13(3): 331.

101. Wahnou H, El Kebbaj R, Liagre B, Sol V, Limami Y, Duval RE. Curcumin-Based Nanoparticles: Advancements and Challenges in Tumor Therapy. *Pharmaceutics*. 2025;17(1): 114.

102. Mundekkad D, Cho WC. Applications of Curcumin and Its Nanoforms in the Treatment of Cancer. *Pharmaceutics*. 2023;15(9): 2223.

103. Prasad S, Tyagi AK, Aggarwal BB. Recent Developments in Delivery, Bioavailability, Absorption and Metabolism of Curcumin: the Golden Pigment from Golden Spice. *Cancer Research and Treatment*. 2014;46(1): 2–18.

104. Sharifi-Rad J, Rayess YE, Rizk AA, Sadaka C, Zgheib R, Zam W, et al. Turmeric and Its Major Compound Curcumin on Health: Bioactive Effects and Safety Profiles for Food, Pharmaceutical, Biotechnological and Medicinal Applications. *Frontiers in Pharmacology*. 2020;11: 01021.

105. Hegde M, Girisa S, BharathwajChetty B, Vishwa R, Kunnumakkara AB. Curcumin Formulations for Better Bioavailability: What We Learned from Clinical Trials Thus Far? *ACS Omega*. 2023;8(12): 10713–10746.

106. Zhai K, Brockmüller A, Kubatka P, Shakibaei M, Büsselberg D. Curcumin's Beneficial Effects on Neuroblastoma: Mechanisms, Challenges, and Potential Solutions. *Biomolecules*. 2020;10(11): 1469.

107. Sohn SI, Priya A, Balasubramaniam B, Muthuramalingam P, Sivasankar C, Selvaraj A, et al. Biomedical Applications and Bioavailability of Curcumin—An Updated Overview. *Pharmaceutics*. 2021;13(12): 2102.

108. Giordano A, Tommonaro G. Curcumin and Cancer. *Nutrients*. 2019;11(10): 2376.

109. Singh S, Khar A. Biological effects of curcumin and its role in cancer chemoprevention and therapy. *Anti-Cancer Agents in Medicinal Chemistry*. 2006;6(3): 259–270.

110. Farghadani R, Naidu R. Curcumin: Modulator of Key Molecular Signaling Pathways in Hormone-Independent Breast Cancer. *Cancers*. 2021;13(14): 3427.

111. Zhou H, Beevers CS, Huang S. The targets of curcumin. *Current Drug Targets*. 2011;12(3): 332–347.

112. Amaroli A, Panfoli I, Bozzo M, Ferrando S, Candiani S, Ravera S. The Bright Side of Curcumin: A Narrative Review of Its Therapeutic Potential in Cancer Management. *Cancers (Basel)*. 2024 Jul 18;16(14):2580.

113. Cacciola NA, Cuciniello R, Petillo GD, Piccioni M, Filosa S, Crispi S. An Overview of the Enhanced Effects of Curcumin and Chemotherapeutic Agents in Combined Cancer Treatments. *International Journal of Molecular Sciences*. 2023;24(16): 12587.

114. Liu Z, Huang P, Law S, Tian H, Leung W, Xu C. Preventive Effect of Curcumin Against Chemotherapy-Induced Side-Effects. *Frontiers in Pharmacology*. 2018;9: 1374.

115. Setiawan PYB, Kertia N, Nurrochmad A, Wahyuono S. Curcumin in combination: Review of synergistic effects and mechanisms in the treatment of inflammation. *Journal of Applied Pharmaceutical Science*. 2021;11(2): 001–011.

116. Pandya SK, Pandya A, Larsen A, Gowin K. A Review of The Synergistic Effects of Curcumin with Proteasome Inhibitors in Multiple Myeloma Preclinical Models. *Integrative Cancer Therapies*. 2023;22: 15347354231159322.

117. Hossain DMS, Bhattacharyya S, Das T, Sa G. Curcumin: the multi-targeted therapy for cancer regression. *Frontiers in Bioscience (Scholar Edition)*. 2012;4(1): 335–355.

118. Shanmugam MK, Rane G, Kanchi MM, Arfuso F, Chinnathambi A, Zayed ME, et al. The Multifaceted Role of Curcumin in Cancer Prevention and Treatment. *Molecules*. 2015;20(2): 2728–2769.

119. Pavan A, Silva G, Jornada D, Chiba D, Fernandes G, Man Chin C, et al. Unraveling the Anticancer Effect of Curcumin and Resveratrol. *Nutrients*. 2016;8(11): 628.

120. Schmidt KT, Figg WD. The potential role of curcumin in prostate cancer: the importance of optimizing pharmacokinetics in clinical studies. *Translational Cancer Research*. 2016;5(S6): S1107–S1110.

121. Mbese Z, Khwaza V, Aderibigbe BA. Curcumin and Its Derivatives as Potential Therapeutic Agents in Prostate, Colon and Breast Cancers. *Molecules*. 2019;24(23): 4386.

122. Vue B, Zhang S, Chen QH. Synergistic Effects of Dietary Natural Products as Anti-Prostate Cancer Agents. *Natural Product Communications*. 2015;10(12): 2179–2188.

123. Hosseini-Zare MS, Sarhadi M, Zarei M, Thilagavathi R, Selvam C. Synergistic effects of curcumin and its analogs with other bioactive compounds: A comprehensive review. *European Journal of Medicinal Chemistry*. 2021;210: 113072.

124. Lin L, Li C, Zhang D, Yuan M, Chen CH, Li M. Synergic Effects of Berberine and Curcumin on Improving Cognitive Function in an Alzheimer's Disease Mouse Model. *Neurochemical Research*. 2020;45(5): 1130–1141.

125. Kundur S, Prayag A, Selvakumar P, Nguyen H, McKee L, Cruz C, et al. Synergistic anticancer action of quercetin and curcumin against triple-negative breast cancer cell lines. *Journal of Cellular Physiology*. 2019;234(7): 11103–11118.

126. Eom DW, Lee JH, Kim YJ, Hwang GS, Kim SN, Kwak JH, et al. Synergistic effect of curcumin on epigallocatechin gallate-induced anticancer action in PC3 prostate cancer cells. *BMB reports*. 2015;48(8): 461–466.

127. Teiten MH, Eifes S, Dicato M, Diederich M. Curcumin—The Paradigm of a Multi-Target Natural Compound with Applications in Cancer Prevention and Treatment. *Toxins*. 2010;2(1): 128–162.

128. Aggarwal BB. Prostate cancer and curcumin: add spice to your life. *Cancer Biology & Therapy*. 2008;7(9): 1436–1440.

129. Hu S, Xu Y, Meng L, Huang L, Sun H. Curcumin inhibits proliferation and promotes apoptosis of breast cancer cells. *Exp Ther Med.* 2018 Aug;16(2):1266-1272.

130. Talib WH, Al-hadid SA, Wild Ali MB, AL-Yasari IH, Abd Ali MR. Role of curcumin in regulating p53 in breast cancer: an overview of the mechanism of action. *Breast Cancer: Targets and Therapy*. 2018;10:207–217.

131. Anto RJ, Mukhopadhyay A, Denning K, Aggarwal BB. Curcumin (diferuloylmethane) induces apoptosis through activation of caspase-8, BID cleavage and cytochrome c release: its suppression by ectopic expression of Bcl-2 and Bcl-xl. *Carcinogenesis*. 2002;23(1): 143–150.

132. Marsden VS, Ekert PG, Van Delft M, Vaux DL, Adams JM, Strasser A. Bcl-2–regulated apoptosis and cytochrome *c* release can occur independently of both caspase-2 and caspase-9. *The Journal of Cell Biology*. 2004;165(6): 775–780.

133. Mustafa M, Ahmad R, Tantry IQ, Ahmad W, Siddiqui S, Alam M, et al. Apoptosis: A Comprehensive Overview of Signaling Pathways, Morphological Changes, and Physiological Significance and Therapeutic Implications. *Cells*. 2024;13(22): 1838.

134. Kumar S. Caspase function in programmed cell death. *Cell Death & Differentiation*. 2007;14(1): 32–43.

135. Dai X, Zhang J, Arfuso F, Chinnathambi A, Zayed M, Alharbi SA, et al. Targeting TNF-related apoptosis-inducing ligand (TRAIL) receptor by natural products as a potential therapeutic approach for cancer therapy. *Exp Biol Med (Maywood)*. 2015 Jun;240(6):760-73.

136. Dorai T, Gehani N, Katz A. Therapeutic potential of curcumin in human prostate cancer-I. curcumin induces apoptosis in both androgen-dependent and androgen-independent prostate cancer cells. *Prostate Cancer and Prostatic Diseases*. 2000;3(2): 84–93.

137. Pae HO, Jeong SO, Jeong GS, Kim KM, Kim HS, Kim SA, et al. Curcumin induces pro-apoptotic endoplasmic reticulum stress in human leukemia HL-60 cells. *Biochemical and Biophysical Research Communications*. 2007;353(4): 1040–1045.

138. Sa G, Das T. Anti-cancer effects of curcumin: cycle of life and death. *Cell Division*. 2008;3: 14.

139. Zielinski RR, Eigl BJ, Chi KN. Targeting the apoptosis pathway in prostate cancer. *Cancer Journal (Sudbury, Mass.)*. 2013;19(1): 79–89.

140. McKenzie S, Kyprianou N. Apoptosis evasion: The role of survival pathways in prostate cancer progression and therapeutic resistance. *Journal of Cellular Biochemistry*. 2006;97(1): 18–32.

141. Guo H, Xu YM, Ye ZQ, Yu JH, Hu XY. Curcumin induces cell cycle arrest and apoptosis of prostate cancer cells by regulating the expression of IkappaBalpha, c-Jun and androgen receptor. *Die Pharmazie*. 2013;68(6): 431–434.

142. Termini D, Den Hartogh DJ, Jaglanian A, Tsiani E. Curcumin against Prostate Cancer: Current Evidence. *Biomolecules*. 2020;10(11): 1536.

143. Perrone D, Ardito F, Giannatempo G, Dioguardi M, Troiano G, Lo Russo L, et al. Biological and therapeutic activities, and anticancer properties of curcumin. *Experimental and Therapeutic Medicine*. 2015;10(5): 1615–1623.

144. Ide H, Lu Y, Noguchi T, Muto S, Okada H, Kawato S, et al. Modulation of AKR1C2 by curcumin decreases testosterone production in prostate cancer. *Cancer Science*. 2018;109(4): 1230–1238.

145. Wahab NAA, Lajis NH, Abas F, Othman I, Naidu R. Mechanism of Anti-Cancer Activity of Curcumin on Androgen-Dependent and Androgen-Independent Prostate Cancer. *Nutrients.* 2020 Mar 2;12(3):679.

146. Ameer SF, Mohamed MY, Elzubair QA, Sharif EAM, Ibrahim WN. Curcumin as a novel therapeutic candidate for cancer: can this natural compound revolutionize cancer treatment? *Frontiers in Oncology*. 2024;14: 1438040.

147. Selvam C, Prabu SL, Jordan BC, Purushothaman Y, Umamaheswari A, Hosseini Zare MS, et al. Molecular mechanisms of curcumin and its analogs in colon cancer prevention and treatment. *Life Sciences*. 2019;239: 117032.

148. Aggarwal BB, Harikumar KB. Potential therapeutic effects of curcumin, the anti-inflammatory agent, against neurodegenerative, cardiovascular, pulmonary, metabolic, autoimmune and neoplastic diseases. *The International Journal of Biochemistry & Cell Biology*. 2009;41(1): 40–59.

149. Johnson SM, Gulhati P, Arrieta I, Wang X, Uchida T, Gao T, et al. Curcumin inhibits proliferation of colorectal carcinoma by modulating Akt/mTOR signaling. *Anticancer Research*. 2009;29(8): 3185–3190.

150. Talib WH, Awajan D, Hamed RA, Azzam AO, Mahmod AI, AL-Yasari IH. Combination Anticancer Therapies Using Selected Phytochemicals. *Molecules*. 2022;27(17): 5452.

151. Subramaniam D, Ramalingam S, Houchen CW, Anant S. Cancer Stem Cells: A Novel Paradigm for Cancer Prevention and Treatment. *Mini reviews in medicinal chemistry*. 2010;10(5): 359–371.

152. Mohanty C, Sahoo SK. The in vitro stability and in vivo pharmacokinetics of curcumin prepared as an aqueous nanoparticulate formulation. *Biomaterials*. 2010;31(25): 6597–6611.

153. Yakubu J, Pandey AV. Innovative Delivery Systems for Curcumin: Exploring Nanosized and Conventional Formulations. *Pharmaceutics*. 2024;16(5): 637.

154. Chen Y, Lu Y, Lee RJ, Xiang G. Nano Encapsulated Curcumin: And Its Potential for Biomedical Applications. *International Journal of Nanomedicine*. 2020;15:3099–3120.

155. Nsairat H, Khater D, Sayed U, Odeh F, Al Bawab A, Alshaer W. Liposomes: structure, composition, types, and clinical applications. *Heliyon*. 2022;8(5): e09394.

156. Ghalandarlaki N, Alizadeh AM, Ashkani-Esfahani S. Nanotechnology-Applied Curcumin for Different Diseases Therapy. *BioMed Research International*. 2014;2014: 1–23.

157. Kroon J, Metselaar JM, Storm G, Van Der Pluijm G. Liposomal nanomedicines in the treatment of prostate cancer. *Cancer Treatment Reviews*. 2014;40(4): 578–584.

158. Yallapu MM, Khan S, Maher DM, Ebeling MC, Sundram V, Chauhan N, et al. Anti-cancer activity of curcumin loaded nanoparticles in prostate cancer. *Biomaterials*. 2014;35(30): 8635–8648.

159. Azandeh SS, Abbaspour M, Khodadadi A, Khorsandi L, Orazizadeh M, Heidari-Moghadam A. Anticancer Activity of Curcumin-Loaded PLGA Nanoparticles on PC3 Prostate Cancer Cells. *Iran J Pharm Res*. 2017 Summer;16(3):868-879.

160. Hafez Ghoran S, Calcaterra A, Abbasi M, Taktaz F, Nieselt K, Babaei E. Curcumin-Based Nanoformulations: A Promising Adjuvant towards Cancer Treatment. *Molecules*. 2022;27(16): 5236.

161. Boroughani M, Moaveni AK, Hatami P, Mansoob Abasi N, Seyedoshohadaei SA, Pooladi A, et al. Nanocurcumin in cancer treatment: a comprehensive systematic review. *Discover Oncology*. 2024;15(1): 515.

162. Keshavarz Shahbaz S, Koushki K, Izadi O, Penson PE, Sukhorukov VN, Kesharwani P, et al. Advancements in curcumin-loaded PLGA nanoparticle delivery systems: progressive strategies in cancer therapy. *Journal of Drug Targeting*. 2024;32(10): 1207–1232.

163. de Oliveira CR, Droppa-Almeida D, Padilha FF, de Souza RR, de Albuquerque-Júnior RLC. Polymeric Nanoparticles for the Treatment of Prostate Cancer- Technological Prospecting and Critical Analysis. *Recent Patents on Nanotechnology*. 2023;17(1): 8–14.

164. El-Saadony MT, Yang T, Korma SA, Sitohy M, Abd El-Mageed TA, Selim S, et al. Impacts of turmeric and its principal bioactive curcumin on human health: Pharmaceutical, medicinal, and food applications: A comprehensive review. *Frontiers in Nutrition*. 2022;9: 1040259.

165. Gutiérrez-Méndez N, Chavez-Garay DR, Leal-Ramos MY. Lecithins: A comprehensive review of their properties and their use in formulating microemulsions. *Journal of Food Biochemistry*. 2022;46(7): e14157.

166. Jin HH, Lu Q, Jiang JG. Curcumin liposomes prepared with milk fat globule membrane phospholipids and soybean lecithin. *Journal of Dairy Science*. 2016;99(3): 1780–1790.

167. Yanasarn N, Sloat BR, Cui Z. Nanoparticles engineered from lecithin-in-water emulsions as a potential delivery system for docetaxel. *International Journal of Pharmaceutics*. 2009;379(1): 174–180.

168. Hu K, Feng, Cao. Enhanced oral bioavailability of docetaxel by lecithin nanoparticles: preparation, in vitro, and in vivo evaluation. *International Journal of Nanomedicine*. 2012; 3537.

169. Chen LC, Chen YC, Su CY, Wong WP, Sheu MT, Ho HO. Development and Characterization of Lecithin-based Self-assembling Mixed Polymeric Micellar (saMPMs) Drug Delivery Systems for Curcumin. *Scientific Reports*. 2016;6(1): 37122.

170. Rommasi F, Esfandiari N. Liposomal Nanomedicine: Applications for Drug Delivery in Cancer Therapy. *Nanoscale Research Letters*. 2021;16(1): 95.

171. Radha R, Paul V, Anjum S, Bouakaz A, Pitt WG, Husseini GA. Enhancing Curcumin's therapeutic potential in cancer treatment through ultrasound mediated liposomal delivery. *Scientific Reports*. 2024;14(1): 10499.

172. Nezir AE, Bolat ZB, Ozturk N, Kocak P, Zemheri E, Gulyuz S, et al. Targeting prostate cancer with docetaxel-loaded peptide 563-conjugated PEtOx-co-PEI30%-b-PCL polymeric micelle nanocarriers. *Amino Acids*. 2023;55(8): 1023–1037.

173. Nayman AH, Siginc H, Zemheri E, Yencilek F, Yildirim A, Telci D. Dual-Inhibition of mTOR and Bcl-2 Enhances the Anti-tumor Effect of Everolimus against Renal Cell Carcinoma In Vitro and In Vivo. *Journal of Cancer*. 2019;10(6): 1466–1478.

174. Faustino-Rocha A, Oliveira PA, Pinho-Oliveira J, Teixeira-Guedes C, Soares-Maia R, da Costa RG, et al. Estimation of rat mammary tumor volume using caliper and ultrasonography measurements. *Lab Animal*. 2013;42(6): 217–224.

175. Rebello RJ, Oing C, Knudsen KE, Loeb S, Johnson DC, Reiter RE, et al. Prostate cancer. *Nature Reviews Disease Primers*. 2021;7(1): 1–27.

176. Kong WY, Ngai SC, Goh BH, Lee LH, Htar TT, Chuah LH. Is Curcumin the Answer to Future Chemotherapy Cocktail? *Molecules*. 2021;26(14): 4329.

177. Li C, Naeem A, Shen J, Zha W, Zeng Q, Zhang P, et al. Advances in the pharmaceutical research of curcumin for oral administration. *Open Chemistry*. 2023;21(1).

178. Sun Q, Lv M, Li Y. Nanotechnology-based drug delivery systems for curcumin and its derivatives in the treatment of cardiovascular diseases. *Journal of Functional Foods*. 2024;122: 106476.

179. Yakubu J, Natsaridis E, du Toit T, Barata IS, Tagit O, Pandey AV. Nanoparticles with curcumin and piperine modulate steroid biosynthesis in prostate cancer. *Scientific Reports*. 2025;15(1): 13613.

180. Albanese A, Tang PS, Chan WCW. The effect of nanoparticle size, shape, and surface chemistry on biological systems. *Annual Review of Biomedical Engineering*. 2012;14: 1–16.

181. Vagena IA, Malapani C, Gatou MA, Lagopati N, Pavlatou EA. Enhancement of EPR Effect for Passive Tumor Targeting: Current Status and Future Perspectives. *Applied Sciences*. 2025;15(6): 3189.

182. Hoseini B, Jaafari MR, Golabpour A, Momtazi-Borojeni AA, Karimi M, Eslami S. Application of ensemble machine learning approach to assess the factors affecting size and polydispersity index of liposomal nanoparticles. *Scientific Reports*. 2023;13(1): 18012.

183. Diga G. Investigation of bio-physical interaction between Nanoparticles, Colloids, and biomolecules: Pharmaco-medical application. *Research & Reviews:Journal of Physics.* 2025;13(03):6-17.

184. Sultana S, Alzahrani N, Alshamrani R, Aloufi W, Ali W,Amena A, et al. Stability issues and approaches to stabilised nanoparticles based drug delivery system. *Journal of Drug Targeting*. 2020;28(5): 468–486.

185. Ly PD, Ly KN, Phan HL, Nguyen HHT, Duong VA, Nguyen HV. Recent advances in surface decoration of nanoparticles in drug delivery. *Frontiers in Nanotechnology*. 2024;6.

186. Kąkol M, Tagliasacchi E, Borkowski A, Słowakiewicz M. Influence of different sample preparation techniques on imaging viruses and virus-like particles by scanning electron and scanning transmission electron microscopes. *Frontiers in Microbiology*. 2023;14: 1279720.

187. Bai Y, Wang Y, Qiang D, Yuan X, Wu J, Chen W, et al. Identification of nanocomposites agglomerates in scanning electron microscopy images based on semantic segmentation. *IET Nanodielectrics*. 2022;5(2): 93–103.

188. Mu Q, Jiang G, Chen L, Zhou H, Fourches D, Tropsha A, et al. Chemical Basis of Interactions Between Engineered Nanoparticles and Biological Systems. *Chemical reviews*. 2014;114(15): 7740–7781.

189. Hoo CM, Starostin N, West P, Mecartney ML. A comparison of atomic force microscopy (AFM) and dynamic light scattering (DLS) methods to characterize nanoparticle size distributions. *Journal of Nanoparticle Research*. 2008;10(1): 89–96.

190. Grobelny J, DelRio FW, Pradeep N, Kim DI, Hackley VA, Cook RF. Size Measurement of Nanoparticles Using Atomic Force Microscopy. In: McNeil SE (ed.) *Characterization of Nanoparticles Intended for Drug Delivery*. Totowa, NJ: Humana Press; 2011. p. 71–82.

191. Pinals RL, Chio L, Ledesma F, Landry MP. Engineering at the Nano-Bio Interface: Harnessing the Protein Corona Towards Nanoparticle Design and Function. *The Analyst*. 2020;145(15): 5090–5112.

192. Kassem A, Abbas L, Coutinho O, Opara S, Najaf H, Kasperek D, et al. Applications of Fourier Transform-Infrared spectroscopy in microbial cell biology and environmental microbiology: advances, challenges, and future perspectives. *Frontiers in Microbiology*. 2023;14: 1304081.

193. Karewicz A, Bielska D, Gzyl-Malcher B, Kepczynski M, Lach R, Nowakowska M. Interaction of curcumin with lipid monolayers and liposomal bilayers. *Colloids and Surfaces. B, Biointerfaces*. 2011;88(1): 231–239.

194. Gonçalves RFS, Vicente AA, Pinheiro AC. Incorporation of curcumin-loaded lipid-based nano delivery systems into food: Release behavior in food simulants and a case study of application in a beverage. *Food Chemistry*. 2023;405(Pt A): 134740.

195. Huang W, Xiao G, Zhang Y, Min W. Research progress and application opportunities of nanoparticle–protein corona complexes. *Biomedicine & Pharmacotherapy*. 2021;139: 111541.

196. Vagena IA, Malapani C, Gatou MA, Lagopati N, Pavlatou EA. Enhancement of EPR Effect for Passive Tumor Targeting: Current Status and Future Perspectives. *Applied Sciences*. 2025;15(6): 3189.

197. Waheed I, Ali A, Tabassum H, Khatoon N, Lai WF, Zhou X. Lipid-based nanoparticles as drug delivery carriers for cancer therapy. *Frontiers in Oncology*. 2024;14: 1296091.

198. Hsu CY, Wang PW, Alalaiwe A, Lin ZC, Fang JY. Use of Lipid Nanocarriers to Improve Oral Delivery of Vitamins. *Nutrients*. 2019;11(1): 68.

199. Jardim KV, Siqueira JLN, Báo SN, Sousa MH, Parize AL. The role of the lecithin addition in the properties and cytotoxic activity of chitosan and chondroitin sulfate nanoparticles containing curcumin. *Carbohydrate Polymers*. 2020;227: 115351.

200. Ahmed SA, Salama AA, Gaber MH, Ali SA. Development and Characterization of Soy Lecithin Liposome as Potential Drug Carrier Systems for Doxorubicin. *Journal of Pharmaceutical Innovation*. 2023;18(3): 1415–1426.

201. Lens M. Phospholipid-Based Vesicular Systems as Carriers for the Delivery of Active Cosmeceutical Ingredients. *International Journal of Molecular Sciences*. 2025;26(6): 2484.

202. Bompard J, Rosso A, Brizuela L, Mebarek S, Blum LJ, Trunfio-Sfarghiu AM, et al. Membrane Fluidity as a New Means to Selectively Target Cancer Cells with Fusogenic Lipid Carriers. *Langmuir*. 2020;36(19): 5134–5144.

203. Karthikeyan A, Senthil N, Min T. Nanocurcumin: A Promising Candidate for Therapeutic Applications. *Frontiers in Pharmacology*. 2020;11: 487.

204. Shankar S, Chen Q, Sarva K, Siddiqui I, Srivastava RK. Curcumin enhances the apoptosis-inducing potential of TRAIL in prostate cancer cells: molecular mechanisms of apoptosis, migration and angiogenesis. *Journal of Molecular Signaling*. 2007;2: 10.

205. Hao M, Chu Y, Lei J, Yao Z, Wang P, Chen Z, et al. Pharmacological Mechanisms and Clinical Applications of Curcumin: Update. *Aging and Disease*. 2023;14(3): 716–749.

206. Maeda H, Nakamura H, Fang J. The EPR effect for macromolecular drug delivery to solid tumors: Improvement of tumor uptake, lowering of systemic toxicity, and distinct tumor imaging in vivo. *Advanced Drug Delivery Reviews*. 2013;65(1): 71–79.

207. Peng Y, Ao M, Dong B, Jiang Y, Yu L, Chen Z, et al. Anti-Inflammatory Effects of Curcumin in the Inflammatory Diseases: Status, Limitations and Countermeasures. *Drug Design, Development and Therapy*. 2021;15: 4503–4525.

208. Khan S, Sharma A, Jain V. An Overview of Nanostructured Lipid Carriers and its Application in Drug Delivery through Different Routes. *Advanced Pharmaceutical Bulletin*. 2023;13(3): 446–460.

209. Mehta M, Bui TA, Yang X, Aksoy Y, Goldys EM, Deng W. Lipid-Based Nanoparticles for Drug/Gene Delivery: An Overview of the Production Techniques and Difficulties Encountered in Their Industrial Development. *ACS Materials Au*. 2023;3(6): 600–619.

APPENDIX A: ETHICAL APPROVAL FORM

YEDİTEPE ÜNİVERSİTESİ HAYVAN DENEYLERİ YEREL ETİK KURULU	HAYVAN DENEYLERİ YEREL ETİK KURULU KARAR FORMU	Doküman No : FR83 Yayın Tarihi : 06.12.2022 Revizyon No : 00 Revizyon Tarihi : 00.00.0000 Sayfa : 1 / 1

ETİK KURUL KARARI

Protokol No	Toplantı Tarihi	Toplantı Sayısı	Karar No	Proje Yürütücüsü
2023-17	18.04.2023	2023/04	2023/04-01	Prof.Dr.Dilek Telci

'Prostat Kanserinde Soya Lesitin Bazlı Lipozomal Kurkuminin Anti-Kanser Aktivitesinin TRAMP-C2 in vivo Modelinde İncelenmesi'isimli proje oy birliğiyle etik açıdan uygun görülmüştür.

Hayvan Türü / Irkı	Toplam Hayvan Sayısı	Hayvan Cinsiyeti
Fare/C57BL-6	24	Erkek

Görevi	Adı Soyadı	Onay/Ret Durumu	Katılım Durumu
Başkan	Prof. Dr. Bayram YILMAZ	☑ Onay ☐ Ret	
Başkan Vekili	Prof. Dr. Erdem YEŞİLADA	☐ Onay ☐ Ret	
Üye	Dr. Engin SÜMER	☑ Onay ☐ Ret	
Üye	Prof. Dr. M. Ece GENÇ	☑ Onay ☐ Ret	
Üye	Prof. Dr. Rukset ATTAR	☑ Onay ☐ Ret	
Üye	Prof. Dr. Gamze TORUN KÖSE	☑ Onay ☐ Ret	
Üye	Prof. Dr. Özlem MALKONDU	☑ Onay ☐ Ret	
Üye	Prof. Dr. Aylin YABA UÇAR	☑ Onay ☐ Ret	
Üye	Prof. Dr. Burcu GEMİCİ BAŞOL	☑ Onay ☐ Ret	
Üye	Atakan Mücahit YAVUZ	☑ Onay ☐ Ret	
Üye	Ahmet ŞENKARDEŞLER	☑ Onay ☐ Ret	

Hazırlayan YÜDETAM SORUMLU YÖNETİCİ	Sistem Onayı YÜDETAM MÜDÜRÜ	Yürürlük Onayı YÜDETAM MÜDÜRÜ

This page is intentionally left blank